

NORTHWESTERN UNIVERSITY

**Properties of Retinal Ganglion Cell Receptive Fields at the
Lower Limit of Visual Sensitivity**

A DISSERTATION

**SUBMITTED TO THE GRADUATE SCHOOL IN PARTIAL
FULFILLMENT OF THE REQUIREMENTS**

For the degree

DOCTOR OF PHILOSOPHY

Neuroscience Institute Graduate Program

By

JIE CHEN

EVANSTON, ILLINOIS

June 2007

©Copyright by Jie Chen 2007

All Rights Reserved

ABSTRACT**Properties of retinal ganglion cell receptive fields at the lower limit of visual sensitivity****JIE CHEN**

The goal of this study was to investigate the properties of the retinal ganglion cell receptive field at low light levels. There has been considerable interest in whether the surround of a ganglion cell receptive field disappears and the center expands in size under scotopic conditions. The previous data from our laboratory had shown that, while antagonism between center and surround is reduced for ON-center Y-cell receptive fields within the scotopic range, the surround remains very much present. In addition, expansion of the receptive field center is quite modest (only 30% greater radius). We have now extended this work to focus on a range of scotopic light levels not explored by us previously. This is the range from where each rod would be expected to capture a photon once every 10 seconds down to a light level where each rod would be expected to capture a photon once every 5 minutes.

A more significant expansion has occurred by the lowest light level we studied with the radius of the center summing area increasing to 250% its photopic dimension for ON-center X cells (170% greater radius for ON-Y cells). Over the same range, the responsivity of the center falls dramatically, as one might expect were the responses of ON-center cells to reflect simple summation of photons captured by rods within the center. Although the presence of a surround mechanism was less evident in the range studied than under photopic

or higher scotopic light levels, our data suggest that a receptive field surround persists even to the lowest scotopic levels studied. The delay between center and surround signals increases progressively from photopic levels, with the result that center and surround signals are more nearly in phase at these low scotopic levels than they are under photopic conditions, where they are antagonistic. As a result of this phase “synchrony” both mechanisms are mobilized by the X- and Y-cells to sum photons, helping to preserve the cell’s responsivity and maximize the signal to noise ratio.

ACKNOWLEDGEMENTS

I would like to acknowledge many people for helping and encouraging me during my research and writing up of this dissertation. First and foremost I want to thank my thesis advisor, Dr. John Troy, for his guidance, patience and commitment. During my doctoral work he continually helped with my experiments, stimulated my analytical thinking and greatly assisted me with thesis writing. He also helped me a lot with my life in general. I will never forget that he picked me up at airport and accommodated me on my first day arriving US. He is one of the rare advisors that students dream that they will find. Meanwhile, I want to give my special thanks to Mrs. Guang Yu, my advisor's wife. Her friendship and care made me feel at home and never troubled by homesickness. Unfortunately, she passed away one month ago, after suffering from cancer for one year, and will never see my thanks to her. However, her kindness and encouragement to me will never be forgotten.

I am also very grateful for having an exceptional doctoral committee and want to thank Drs. Robert Linsenmeier, Mitra Hartmann, and Steven DeVries for their generous time and continual support.

I wish to thank Dr. Christina Enroth-Cugell for her help with those animal surgeries, sharing her invaluable experience and the delicious food for seminars. Thank you, Grandma!

I would like to thank Dr. Christopher Passaglia for his patience and encouragement whilst teaching me all the experiment procedures and data analysis. I also want to thank Drs Xiaoli Guo and Chao Sun. Without their help during these crazy over night experiments, I would never have completed my data collection.

I extend many thanks to my current lab members, Donald Robinson Cantrell and Samsoun Inayat for their support and making the lab an enjoyable place.

Finally, I would like to thank my family. My father extended his passion for eyes and science to me. His advice and encouragement has led me all the way through my studies. My mother has been a constant source of support, from the very beginning of my life, and never

has any complaint. I'm especially grateful to my beloved husband Jianfeng, for his patience and unwavering faith in me. He has helped me keep my life in balance and happiness. I also want to thank my brother and sister in law for their support. It was because they were looking after our parents, that I could have studied abroad without being troubled back at home.

TABLE OF CONTENTS

ABSTRACT.....	3
ACKNOWLEDGEMENTS.....	5
TABLE OF CONTENTS.....	7
LIST OF FIGURES.....	10
I. INTROUDUCTION.....	12
II. BACKGROUND.....	14
2.1 Eye anatomy.....	14
2.2 Retina	15
2.2.1 Retinal structure.....	15
1. Photoreceptors.....	17
2. Horizontal cells.....	18
3. Bipolar cells.....	19
4. Amacrine cells.....	20
5. Ganglion cells.....	23
2.2.2 Retinal signaling	23
1. ON and OFF retinal pathways.....	23
2. Scotopic and photopic retinal pathways.....	25
3. Inhibitory circuitry in the retina.....	29
2.3 Retinal ganglion cell.....	31
2.3.1 Morphological types of retinal ganglion cell.....	31
2.3.2 Physiological types of retinal ganglion cell.....	33
2.3.3 Receptive fields of retinal ganglion cells.....	34
1. Center-surround receptive field.....	34
2. Mathematical models.....	36
2.4 Effect of illuminance on the retina.....	38
2.4.1 Visual performance as a function of mean light level.....	39
1. Linear range (L).....	40

	8
2. DeVries-Rose Law range (DeV-R).....	41
3. Weber Law range (W).....	41
2.4.2 Receptive field properties of ganglion cell as a function of mean light level.....	42
1. Receptive field center.....	43
2. Receptive field surround.....	43
2.5 Motivation.....	44
III. EXPERIMENTAL METHODS AND DATA ANALYSIS.....	46
3.1 Experimental Techniques.....	46
3.1.1 Cat Preparation.....	46
3.1.2 Recording with microelectrodes.....	48
3.1.3 Visual stimulation.....	50
1. Contrast-reversing bipartite field.....	51
2. Contrast-reversing sinusoidal gratings.....	51
3. Uniform field.....	52
4. Drifting sinusoidal gratings.....	52
5. Surround isolating stimulus.....	53
6. Center spot stimulus.....	54
3.1.4 Dark adaptation.....	55
3.1.5 Data collection.....	56
3.2 Data analysis.....	58
IV. RESULTS.....	61
4.1 Spatial –frequency responses to gratings at different light levels.....	62
4.2 Fits of Gaussian center-surround model with gratings.....	64
4.2.1 Dependence of center radius on light level.....	67
4.2.2 Dependence of surround radius on light level.....	70
4.2.3 Dependence of center responsivity on light level.....	71
4.2.4 Dependence of surround responsivity on light level.....	75
4.2.5 Dependence of center and surround phase on light level.....	77

4.2.6 Phase difference between center and surround.....	9
4.3 Frequency responses and Gaussian center-surround model fits for surround-isolating stimulus.....	79
4.3 Frequency responses and Gaussian center-surround model fits for surround-isolating stimulus.....	81
V. DISCUSSION.....	85
5.1 Expansion of receptive field center at low scotopic levels.....	85
5.2 Presence of surround under low scotopic conditions.....	88
5.3 Significance of changes in the receptive field center and surround under low scotopic conditions.....	96
5.4 Retinal circuitry underlying scotopic vision.....	99
VI. REFERENCES.....	105

LIST OF FIGURES

Figure 2.1: Structure of the human eye.....	14
Figure 2.2: Structure of the retina.....	16
Figure 2.3: ON and OFF retinal pathways.....	24
Figure 2.4: Convergence of rod and cone pathways.....	26
Figure 2.5: Rod pathways.....	28
Figure 2.6: Morphological types of retinal ganglion cells.....	32
Figure 2.7: Difference of Gaussian center-surround model.....	35
Figure 2.8: Hochstein & Shapley's (1976) model of the Y-cell receptive field.....	37
Figure 2.9: Gaussian center-surround model.....	38
Figure 2.10: Increment threshold and contrast sensitivity as function of light level.....	40
Figure 3.1: Scanning electron microscope image of a microelectrode.....	47
Figure 3.2: Use of a commercial sewing machine in an electrolytic etching set up.....	49
Figure 3.3: Record discharge of retinal ganglion cell from the optic tract.....	50
Figure 3.4: Drifting sinusoidal gratings.....	52
Figure 3.5: Surround isolating stimulus.....	53
Figure 3.6: Center spot stimulus.....	54
Figure 4.1: Peri-stimulus histograms of spikes.....	63
Figure 4.2: Frequency responses for sinusoidal gratings of different spatial frequencies of an ON-center X cell measured at three light levels.....	65
Figure 4.3: Frequency responses for sinusoidal gratings of different spatial frequencies of an ON-center Y cell measured at three light levels.....	67
Figure 4.4: Dependence of normalized center radius upon retinal illuminance.....	68
Figure 4.5: Expansion in scotopic center radius is independent of eccentricity.....	69
Figure 4.6: Dependence of normalized surround radius upon retinal illuminance.....	70
Figure 4.7: The ratio of normalized surround radius to normalized center radius vs. retinal illuminance.....	71
Figure 4.8: Dependence of normalized center responsivity upon retinal illuminance.....	73
Figure 4.9: Dependence of normalized peak center responsivity upon retinal illuminance...	75
Figure 4.10: Dependence of normalized surround responsivity upon retinal illuminance.....	76

	11
Figure 4.11: The ratio of surround to center responsivity as function of retinal illuminance.....	76
Figure 4.12: Dependence of center phase upon retinal illuminance.....	77
Figure 4.13: Dependence of surround phase upon retinal illuminance.....	78
Figure 4.14: Dependence of phase difference between center and surround upon retinal illuminance.....	79
Figure 4.15: Sets of responsivity and phase measurements for spatial-frequency response and responses to the surround-isolating stimuli of an ON-Y cell measured at 2.58 log cat td.....	80
Figure 4.16: Sets of responsivity and phase measurements for spatial-frequency response and responses to the surround-isolating stimuli of an ON-Y cell measured at -1.92 log cat td.....	82
Figure 4.17: Comparison of center and surround phase measured with gratings and surround-isolating stimuli.....	83
Figure 4.18: Comparison of phase difference between center and surround measured with gratings and surround-isolating stimuli.....	84
Figure 5.1: Comparison of fits with single Gaussian model and Gaussian center-surround model.....	91
Figure 5.2: Two models that explain the phase change in the surround.....	93
Figure 5.3: Receptive field center and surround responses of dark-adapted AII amacrine cells.....	94
Figure 5.4: Comparison of normalized center responsivity with and without center expansion.....	95
Figure 5.5: Optimal solution of Atick & Redlich's model at different values of S/N.....	98
Figure 5.6: Summary of some of the major findings of this and earlier studies and the functional relevance of different light levels for the cat.....	99
Figure 5.7: Retinal circuitries underlies scotopic vision (I).....	102
Figure 5.8: Retinal circuitries underlies scotopic vision (II).....	103
Figure 5.9: Retinal circuitries underlies scotopic vision (III).....	104

I. INTRODUCTION

The operational range for the retinal ganglion cell is from $\sim 10^{-4.5}$ cd m⁻² (dark light) to $\sim 10^5$ cd m⁻² (bright sunlight). A complete description of the receptive field properties of retinal ganglion cells over their full range of operation is essential for understanding their function in perception.

The models of the visual information processing performed by X- and Y- retinal ganglion cells have been well established under photopic condition. However, the properties of receptive fields of these cells under scotopic (especially lower scotopic) conditions are controversial. For example, Andrews and Hammond (1970) found that the radius of the rod-driven receptive field center of retinal ganglion cells is two times larger than the radius of the cone-driven center while a number of other studies indicated there is little or no change in the size of receptive field center when going from photopic to scotopic illuminance (Barlow et al., 1957; Cleland & Enroth-Cugell, 1968; Enroth-Cugell et al., 1977a, b; Troy et al., 1993; Troy et al., 1999). Also there is controversy on the issue whether the surround of a ganglion cell receptive field disappears under scotopic illuminance (For: Barlow et al., 1957; Rodieck & Stone, 1965; Barlow & Levick, 1976; Kaplan et al., 1979; Peichl & Wässle, 1983; Against: Lennie & Enroth-cugell, 1975; Chan et al., 1992; Troy et al., 1993; Troy et al., 1999).

In previous work (Troy et al., 1993; Troy et al., 1999), it was found that, while antagonism between center and surround is reduced for X- and Y-cell receptive fields within the scotopic range, the surround remains very much present. In addition, expansion of the receptive field center is quite modest. The work contained in this thesis is an extension of this

earlier work focusing on a range of scotopic light levels unexplored in the earlier investigation. This is the range from where each rod would be expected to capture a photon once every 10 seconds down to a light level where each rod would be expected to capture a photon once every 5 minutes. By doing so, we intend to characterize the spatial and to a limited extent temporal properties of the X- and Y- center and surround receptive field mechanisms as a function of mean retinal illuminance over their full operational range.

II. BACKGROUND

2.1 Eye anatomy

Most of our knowledge about the world we live in comes from our visual experience. Our eyes are the organs that allow us to see. Figure 2-1 shows the structure of the human eye. The cat eye we studied is similar to the human eye except that the cat's eye has a tapetum, a larger lens and an area centralis instead of a fovea. The eye is divided into 3 chambers: the anterior chamber which is between the cornea and the iris, the posterior chamber which is between the iris, the zonule fibers and the lens and the vitreous chamber which is between the lens and the retina. The first two chambers contain a watery material called aqueous humor whereas the vitreous chamber is filled with a gel-like fluid, the vitreous humor. The iris, a circular muscle, controls the size of the pupil in the eye, lines the back two-thirds of the inside

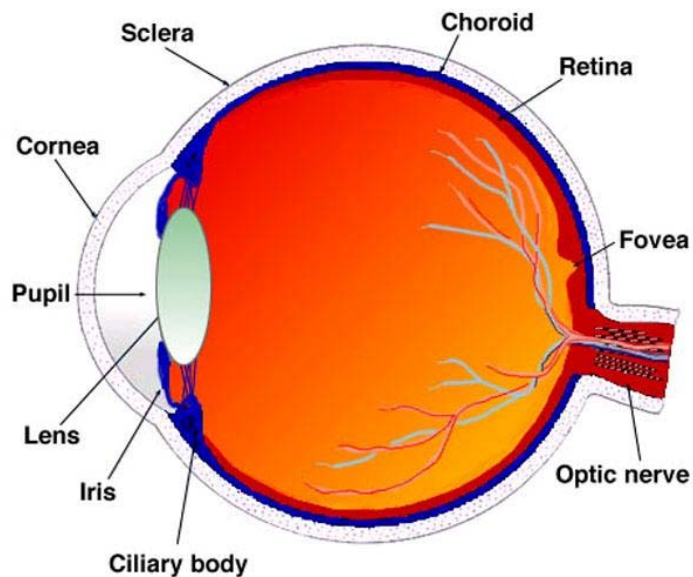


Figure 2.1: Structure of the human eye (from <http://webvision.med.utah.edu/>). so that more or less light is allowed to enter the eye. The retina, the most vital layer for vision

wall of the eye, with an approximate thickness of 180-240 μm in the cat. The neuronal output of the eye is sent to the higher vision centers in the brain via the optic nerve.

2.2 Retina

Communication between the retina and the brain is a particularly attractive subject for experimental study for many reasons. Firstly, we know exactly what is presented to the retina: it is the image projected onto the retinal surface by the optics of the eye. Secondly, the retina can be directly stimulated with its natural input (patterns of light and dark) and the output monitored with relative ease by *in vivo* extracellular recording from ganglion cells, optic nerve or tract fibers, or their terminals in the lateral geniculate nucleus. Thirdly, the retina performs a significant amount of information processing, compressing the visual signal distributed across a population of $\sim 5 \times 10^7$ photoreceptors into just $\sim 170,000$ optic nerve fibers in cat. Moreover, the retina is unusual in that an isolated preparation preserves most of the functionality present *in vivo*. There is believed to be little or no neural feedback to the retina from higher levels of the visual system. These advantages make the retina an attractive model system for studying neural information processing.

2.2.1 Retinal structure

The retina (Fig. 2-2) is a thin layer of neural tissue that lines the inner surface of the eye. There are six basic categories of retinal neuron, although most categories have several sub-types. The major categories of retinal neuron are distinguished by the location of their cell bodies, dendritic trees, and axon terminals. There are three layers of cell bodies. The first of

these is farthest from the center of the eye and thus called the outer nuclear layer. It contains the cell bodies of the photoreceptors (rods and cones). Outside of this layer lie the outer and inner segments of rods and cones. The second cell layer is the inner nuclear layer and it contains the cell bodies of the retina's interneurons, including horizontal, bipolar, and amacrine. Finally, the ganglion cell layer contains the the retinal ganglion cell bodies and some displaced amacrine cells. Interposed between three cell body layers are two layers of cell processes, the outer and inner plexiform layers. The synaptic terminals of the photoreceptors make contact with the dendritic trees of the bipolar cells and horizontal cells as well as the axon terminals of the interplexiform cells in the outer plexiform layer. Both the dendrites and the branching axon terminals of the horizontal cells make connections with cells of the outer nuclear layer. The bipolar cells, however, make connections onto the dendrites of the ganglion cells and amacrine cells within the inner plexiform layer. The dendrites of the amacrine cells make connections with the axons of the bipolar cells, dendrites of the ganglion

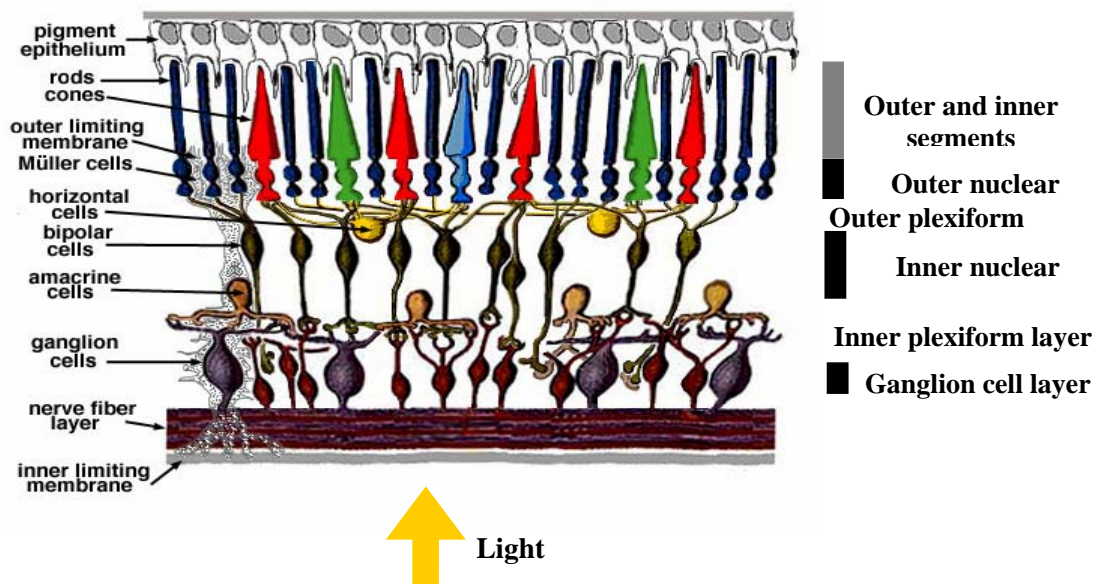


Figure 2.2: Structure of the retina (modified from <http://webvision.med.utah.edu/>).

cells and interplexiform cells in the inner plexiform layer. The ganglion cell axons comprise the optic nerve (optic tract), and exit the retina at a single location called the optic disk.

1. Photoreceptors

Photoreceptor cells are the first order neurons of the visual system capturing quanta of light, evoking an electrical message from this that is passed onto the next stage of processing through chemical neurotransmission. Vertebrate retinas generally possess two types of photoreceptors, called rods and cones, after the shapes of their outer segments. The outer segment is a structure filled entirely with discs of folded double membranes in which are embedded with the light sensitive visual pigment molecules. Upon absorption of a photon of light, these photopigments are activated and in turn activate the G-protein transducin and a further cascade of events that hyperpolarize the photoreceptor (reviewed by Hargrave & McDowell, 1992; Archer, 1995). Both photoreceptors' synaptic endings are filled with synaptic vesicles and exhibit synaptic ribbons pointing to the postsynaptic invaginated processes.

Cones are sensitive to different wavelengths of light depending on the structure of the opsin molecule (visual pigment) they contain. Most mammalian species including cats are dichromatic, which contain middle wavelength (green light) and short wavelength (blue light) sensitive cones in their retina. Primates and humans, birds, reptiles and fish are trichromatic, tetrachromatic and some even pentachromatic. The spectral variety of cones provides the ability to encode color. Cones also provide the substrate for visual acuity.

Rods have rhodopsin as their visual pigment and are sensitive to blue-green light with peak sensitivity around 500 nm wavelength of light. There is only one type of rod photoreceptor. Rods are so sensitive to light that they provide a measurable response to a single quantum of light (Schneeweis & Schnapf, 1995), and convey the ability to see under conditions of very dim illuminance.

2. Horizontal cells

Horizontal cells (HCs) are second order neurons interconnecting photoreceptors laterally across the plane of the outer plexiform layer of the retina. They make contacts with photoreceptors (cone pedicles or rod spherules) at presynaptic ribbons. The horizontal cell shows a slow hyperpolarization in response to light, which is called an S-potential (Svaetichin, 1953).

Two morphological types of horizontal cells have been identified in most vertebrate retinas, A-type HCs that are axonless and B-type HCs with axons. The A-type horizontal cell of mammals is pure cone connecting without any rod connection. The A-type horizontal cell has large expanded dendrites covering a field of 150~250 μm . The dendrites of B-type horizontal cells in mammalian retinas are smaller (70~150 μm) and bushy, contacting all cones in their dendritic field. The B-type horizontal cell's axon travels 300 μm or more and collects signals from large numbers of rods with a big expansive terminal. The cone connecting dendritic field and rod connecting axon terminal field for each B-type horizontal cell are electrically believed to be relatively independent of each other.

Two physiological types of horizontal cell, luminosity (L-type) and chromaticity (C-type), have been identified by their photo responses to chromatic light stimuli. The L-type horizontal cells always respond with hyperpolarization to light stimuli of any wavelength within the visible range of the spectrum, while the C-type horizontal cells respond with different polarity to light stimuli of different wavelengths (Svaetichin & MacNichol, 1958). The L-type horizontal cells are found in all vertebrates that have been studied however C-type horizontal cells have only been found in cold-blooded vertebrates such as turtle and fish.

Horizontal cells are electrical coupled to one another via gap junctions. These junctions are very selective, with cells only connected to their homologous neighbors, and only formed dendrite to dendrite, axon terminal to axon terminal, and cell body to cell body (Kaneko, 1971; Mills & Massey, 1994). The conductance of these gap junctions seems to be regulated by dopamine through a c-AMP-mediated cascade which can be modulated by the ambient light level (Witkovsky & Dearry, 1992; Xin & Bloomfield, 1999).

3. Bipolar cells

Bipolar cells are the second order neurons that connect photoreceptors vertically with ganglion cells, amacrine cells and interplexiform cells. Anatomical investigation of bipolar cells reveals a variety of different morphological types (Kolb et al., 1981; Euler et al., 1996; Connaughton and Nelson, 2000; Wu et al., 2000). In human retina eleven different bipolar cell types are revealed by Golgi staining (Boycott and Wassle, 1991; Kolb et al., 1992; Mariani, 1984, 1985). Ten are for cones and one type is for rods. Seven of the cone bipolar cell types

receive signals from many cones, and thus are known as diffuse cone bipolar cells. Two of the cone bipolar types only make contact with a single cone in a one-to-one relationship. They are known as midget bipolar cells. The last one only makes contacts with S-cone pedicles and is known as S-cone (or blue-cone) bipolar cells.

Bipolar cells have two fundamental physiological varieties: ON-center or OFF-center bipolar cells. The ON-center bipolar cells respond to light with a depolarization and are thought to be driven by metabotropic glutamate receptors, specifically mGluR6 (Masu et al., 1995; Nawy, 1999). The OFF-center bipolar cells respond to light by hyperpolarizing and are stimulated via ionotropic AMPA-kainate glutamate channels (Slaughter & Miller, 1983; DeVries & Schwartz, 1999). Recent studies show that the different AMPA or kainate receptors transmit signals in different morphological types of OFF cone bipolar cells (DeVries, 2000). The ON-center bipolar cells make invaginating contacts with cone pedicles or rod spherules at presynaptic ribbons while most OFF-center bipolar cells only make synapses with cones at basal junctions.

4. Amacrine cells

Amacrine cells are interneurons that interact in the inner plexiform layer (IPL) and serve to integrate and modulate the visual message presented to the ganglion cells. Amacrine cells are so named because they are thought to lack an axon (Ramón Y Cajal, 1892). However later studies found that certain large field amacrine cells of the vertebrate retina can have long "axon-like" processes that run in different strata of the IPL, in the ganglion cell layer and sometimes into the outer plexiform layer (OPL) but that never leave the retina (Kolb et al.,

1981, 1992; Mariani, 1990). Amacrine cells have many subtypes according to their shape, size and stratification pattern. Presently, about 40 different subtypes of amacrine cell have been identified.

The AII cell is a narrow field (dendritic tree diameter typically 30-70 μm), bistratified amacrine cell. It has a round or oval cell body located in the proximal inner nuclear layer and gives off two distinct dendritic trees. Just below the cell body, in *sublamina a*, is the first dendritic tree composed of a cluster of lobular appendages arising from the main dendrite (Famiglietti & Kolb, 1975; Famiglietti & Kolb, 1976; Vaney et al., 1991). The thinner arboreal dendrites penetrate down into sublamina b to form the second dendritic tree, which is called its distal dendrites (Vaney, 1985; Kolb et al., 1992; Wassle et al., 1993; Wassle et al., 1995; Mills & Massey, 1999). The distribution of AII cell bodies forms a regular mosaic (Vaney, 1985; Mills & Massey, 1991). And AII dendritic trees are reported to be more regularly distributed than their cell bodies, with their processes filling in gaps between adjacent cell bodies to get full coverage of the IPL (Vaney et al., 1991a; Wassle et al., 1995). The AII cell density decreases with increasing eccentricity, while fields of both dendritic trees enlarge proportionally (Kolb et al., 1981; Mills & Massey, 1991; Vaney et al., 1991; Wassle et al., 1993).

The AII cells receive glutamatergic inputs directly from rod bipolar cells at synapses in *sublamina b* of the IPL (Kolb & Famiglietti, 1974; Famiglietti & Kolb, 1975; Strettoi et al., 1990) and also receive chemical inputs from other amacrine cells (Kolb et al., 1990; Strettoi et al., 1992). In *sublamina b* the AII cells are electrically coupled to ON-center cone bipolar cells

(Kolb and Famiglietti, 1974; Famiglietti and Kolb, 1975; Kolb, 1979; Strettoi et al., 1992)

and to other AII cells (Strettoi et al., 1992) through gap junctions. The homologous gap junctions formed between AII and AII cells are modulated by dopamine, while the heterologous gap junctions formed between AII cells and ON-center cone bipolar cells are regulated by nitric oxide and cGMP (Mills & Massey, 1995). The lobular appendages in *sublamina a* are the primary chemical synaptic output sites of AII cells. AIIs make reciprocal, inhibitory synapses with OFF-center cone bipolar cells. These synapses account for 90% of the chemical output from AII cells in the rabbit (Strettoi et al., 1992). AII amacrine cells in rabbit rarely synapses directly onto OFF ganglion cells whereas in cat and monkey synapses to OFF ganglion cells are common (Kolb, 1979).

The A17 cell is a wild-field diffusely branching amacrine cell of cat. The equivalent cell of rabbit is called S1. In contrast to the AII cell's small dendritic tree field, the A17 cell's dendritic tree can span as far as one millimeter. Most of the A17 cell's dendrites branch in *sublamina b* of IPL. Along these dendrites, over 1000 pronounced beads have been found on each A17 cell in the cat (Nelson and Kolb, 1985), where reciprocal synapses with rod bipolar cells are formed (Sandell et al., 1989). The A17 cells are driven predominantly by rod-dominant signals and send their output exclusively to rod bipolar cells through reciprocal synapses.

The A18 cell is another type of wild-field amacrine cell. It is known to be a dopamine containing cell. This cell stratifies almost exclusively in *stratum a* of the IPL, just below the amacrine cell bodies. Its fine terminals surround cell bodies and dendrites of other amacrine

cells, particularly the AII and A17 cells, and make synapses with these amacrine cells (Kolb et al., 1990; Voigt and Wässle, 1987). It is thought that the dopaminergic A18 cell can modulate the AII-AII cell coupling (Hampson et al., 1992).

5. Ganglion cell

The ganglion cell is the final output neuron of the retina. It receives and integrates signals from the two layers of cells preceding it in the retinal network and, sends messages to higher visual centers of the brain in the form of a spike train via its long axon.

2.2.2 Retinal signaling

A representation of the visual scene is created in the retina through a series of optical and neural transformations. Patterns of light and dark (visual scenes) arriving at the eye are transformed by the cornea and lens, focusing an optical image on the retina. The optical image is then transformed into neural responses by the light-sensitive elements of the eye, the photoreceptors. The photoreceptors' responses are transformed into the ganglion cell responses by the neural network within the retina that is composed of four types of interneurons (bipolar, horizontal, interplexiform and amacrine cells). Finally, the ganglion cells, the only output neurons of the retina, send visual information to higher level visual structures through trains of action potentials traveling in the axons of the optic nerve and tract.

1. ON and OFF retinal pathways

Within the retinal circuitry, visual information is transmitted through two parallel pathways, the ON- and OFF-pathways (Fig 2.3). The segregation into two pathways is

initiated at the cone photoreceptor to cone bipolar cell contacts in the outer plexiform layer, or the AII amacrine cell to cone bipolar synapse in the inner plexiform layer.

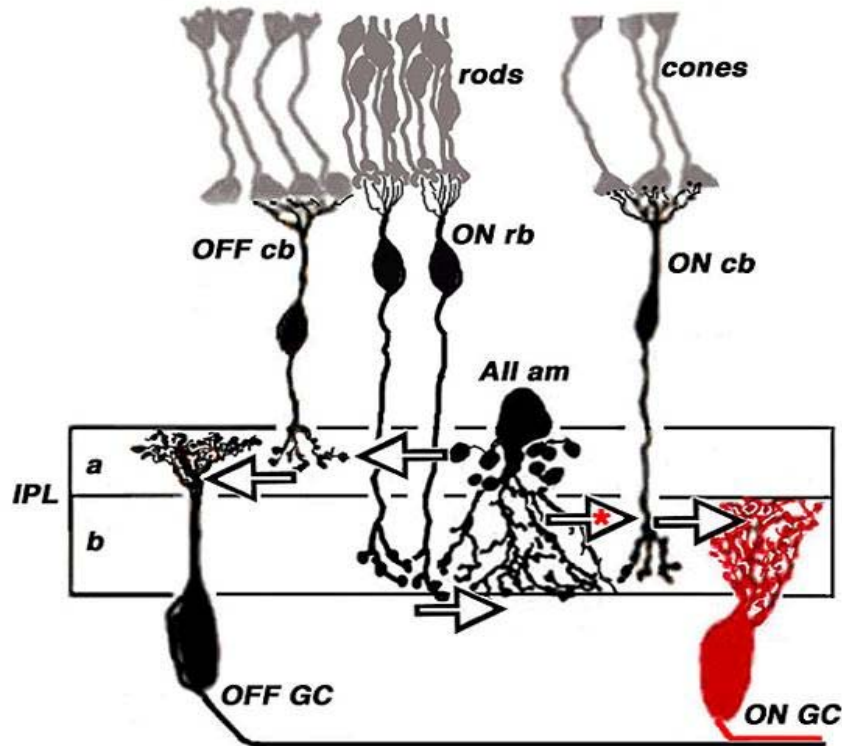


Figure 2.3: ON and OFF retinal pathways (Modified from Kolb & Famiglietti, 1974). *cb*: cone bipolar; *rb*: rod bipolar; *GC*: ganglion cell; *am*: amacrine cell; *IPL*: inner plexiform layer. The red asterisk indicates that the synapses are connected with gap junctions.

In response to light stimulation, the photoreceptor (rod or cone) is hyperpolarized and neurotransmitter release is inhibited. The postsynaptic cone bipolar cells (CB cells) have two different responses, either hyperpolarization or depolarization, to light stimulation. These CB cells are called OFF (hyperpolarizing) or ON-center (depolarizing) CB cells respectively (Werblin and Dowling, 1969; Werblin, 1991). The axons of ON-center CB cells terminate at

sublamina b of IPL and make ribbon synapses with dendrites of retinal ganglion cells (RGCs) while the axons of OFF-center CB cells make ribbon synapses with ganglion cells at *sublamina a*. Since the synapses between both type of cone bipolar cells and ganglion cells are excitatory synapses, the sign of signals in the ganglion cell are determined by the nature of its preceding CB cell (ON or OFF). Thus the visual signals transmitted from cones are passed to the ON- and OFF-center ganglion cells by transferring signals either to ON- or OFF-center CB cells.

The rod bipolar cells (RB cells) only respond with depolarization of their membranes to light stimulation. The separation of rod signals into ON and OFF pathways happens when the rod signals are transferred from AII cells to cone bipolar cells in the IPL. In the IPL, the axon terminals of rod bipolar cells form excitatory synapses with AII cells, which, in turn, make sign-conserving electrical synapses (gap junctions) with ON-center CB cells axon terminals in *sublamina b*, and sign-inverting chemical synapses with OFF-center CB cells (Nelson et al., 1978; Strettoi et al., 1990) or with OFF-center ganglion cells (in cat and monkey) (Kolb, 1979) in *sublamina a*. By this means, the visual signals transmitted from rods are passed to ON- and OFF-center ganglion cells through ON- and OFF CB cells.

2. Scotopic and photopic retinal pathways

As noted earlier, the photoreceptors are composed of two types of cells: rods and cones. According to their different sensitivities to light, rod and cone activated vision is referred to as scotopic and photopic respectively. In cat and human, the retina is known to operate over a wide range of illuminances from $\sim 10^{-4.5}$ cd m⁻² to $\sim 10^5$ cd m⁻². The bottom 3 ~ 4 log units of

luminance constitute the domain of rod (scotopic) vision, in which only rods are active; while the top 3 ~ 4 log units of luminance is the domain of cone (photopic) vision, in which only the cone-driven pathway is active. The middle range, where both pathways are active, is called mesopic vision.

Rods convey the ability to see under very dim illumination conditions because of their high sensitivity to light (they can be activated by a single photon) (Baylor et al., 1980; Schneeweis and Schnapf, 1995) and a high degree of convergence (signals from many rods converge on one retinal ganglion cell, Fig 2.4A). However, there are trade offs. Rods are slower in response to light stimulation than cones and, because many rod signals converge on a single cell, rod vision provides poor spatial resolution.

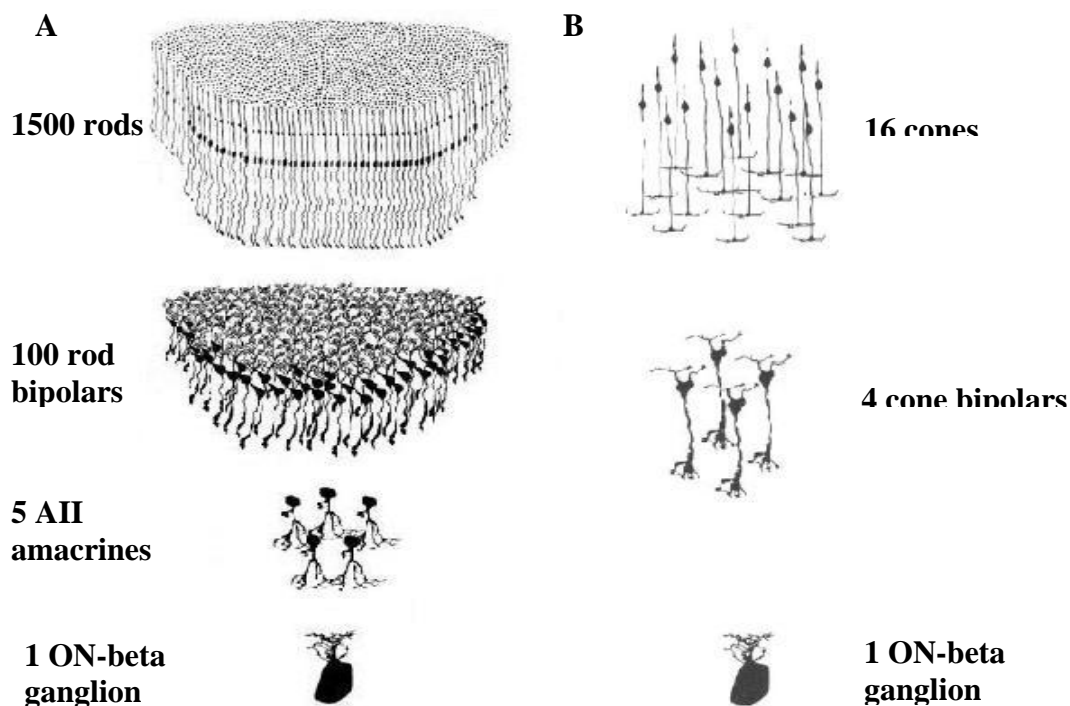


Figure 2.4: Convergence of rod and cone pathways (Modified from Sterling et al., 1988)

To date, it has been found that rod-driven signals can be transmitted to ganglion cells through 3 pathways. In the first (primary) pathway (Fig 2.5A), rod-driven signals travel through RB cells and AII cells, then use the cone bipolar cell circuitry to reach ON or OFF ganglion cells as described earlier. In the second pathway (Fig 2.5B), rod spherules and cone pedicles are connected with gap junctions (Raviola and Gilula, 1973). Thus the rod signals are transmitted directly to cones and then to ganglion cells via the CB cells (Nelson, 1977). It is thought that the primary pathway carries slow, low-threshold signals while the second pathway carries faster, higher-threshold signals (Blakemore & Rushton, 1965a, b; Völgyi et al., 2004). A third pathway (Fig 2.5C) has recently been described where chemical synapses connect rods to some OFF cone bipolar cells in rodents (Hack et al., 1999) and rabbits (Li et al., 2004). However it is still unknown at this time whether this third pathway exists in the cat or primate retinas.

The cone photopic pathway is activated at high ambient light levels. A major difference between the circuitry of the cone and the rod pathways of the mammalian retina is that the cone as compared to rod bipolar cells makes direct synapses with ganglion cell dendrites, without the need for intermediate amacrine cell circuitry. Fewer cones converge onto cone bipolars than rod to rod bipolars and then only a relatively small number of cone bipolar cells converge onto ganglion cells (Fig 2.4B). Thus the cone pathway provides high spatial resolution vision. Also since cones have different wavelength sensitivity (maximally sensitive to long, medium or short wavelengths) depending on the cone opsins, the cone photopic pathway provides the basis for color coding in the visual image. Most mammalian

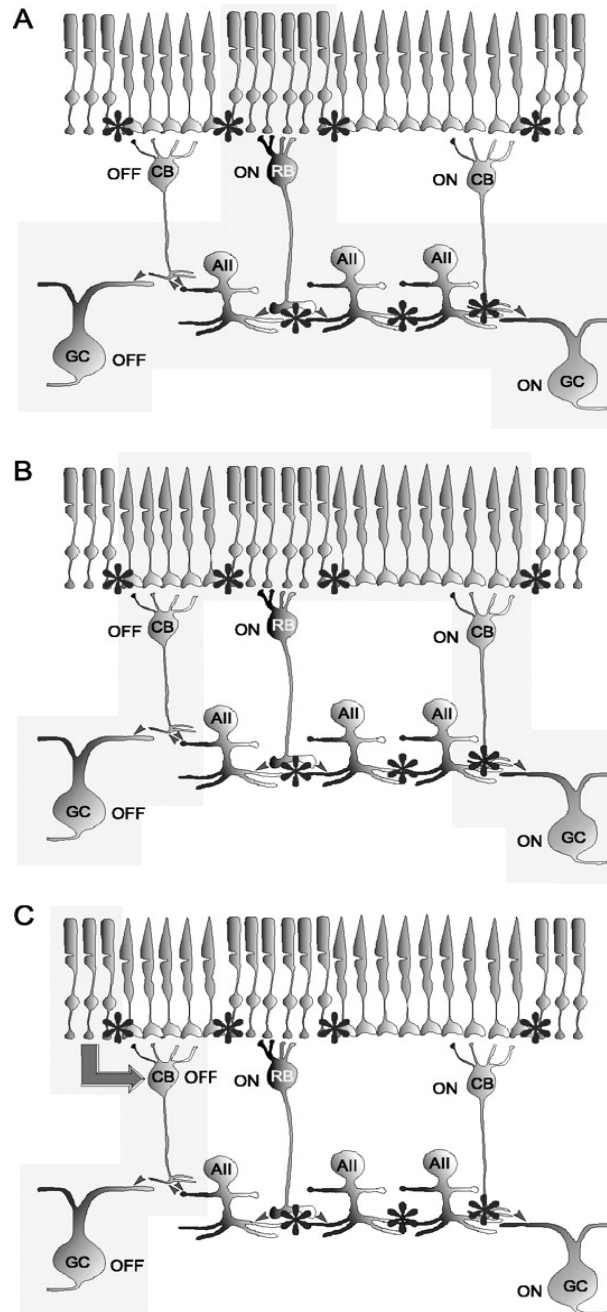


Figure 2.5: Rod pathways (From Völgyi et al., 2004). CB: cone bipolar; RB: rod bipolar; AII: AII amacrine cell; GC: ganglion cell. The asterisks indicate electrical synapses, arrowheads indicate chemical synapses, and the shaded areas mark the elements of the particular rod pathway. A: The primary rod pathway. B: The secondary rod pathway. C: A tertiary rod pathway.

species are dichromatic containing as well as rods only middle and short wavelength sensitive cones in their retinas. Primates and humans, birds, reptiles and fish are trichromatic, tetrachromatic and some even pentachromatic.

3. Inhibitory circuitry in the retina

In the outer plexiform layer, horizontal cells are the interneurons that mediate antagonistic interactions between signals from neighboring retinal areas. The photoreceptors release a transmitter, glutamate, that depolarizes horizontal cells, which, in turn, release a transmitter that hyperpolarizes neighboring cones and rods. Therefore, the hyperpolarization of some cones by light leads to the depolarization of neighboring cones by means of horizontal interneurons. Although rods don't contact the cell bodies and dendrites of horizontal cells, rod-driven signals can pass to horizontal cells through rod-cone gap junctions and to all subsequent second and third order cells in the retina (Smith et al., 1986; Sterling, 1990). The inhibitory circuitry mediated by the horizontal cell is the basis of center-surround antagonism for the subsequent neurons, such as bipolar cells and ganglion cells. Although rods also contact with axon terminals of B-type horizontal cells, there is evidence that rod bipolar cells have surround responses. Therefore, Sterling (1983) has suggested that while the visual signals pass from rods to cones to cone bipolars at high scotopic illuminance, it passes from rods to rod bipolars in the low scotopic range, and that the rod bipolar pathway contains no surround mechanism in the low scotopic range.

However, recent evidence suggests that, in the inner plexiform layer, the amacrine cells also contribute to the ganglion cell surround (Schwartz, 1973; Taylor, 1999; Roska et al., 2000). It is proposed that the degree of amacrine cell contribution to the surround is affected by differences in light level. Under photopic conditions, blocking GABAergic neurotransmission with picrotoxin showed little effect on the surrounds of retinal ganglion cells in cat (Frishman & Linsenmeier, 1982), rabbit (Daw & Ariel, 1981) and primate (McMahon et al., 2004), and blocking amacrine cell spiking with TTX also showed little effect on the center-surround spatial structure of rabbit (Bloomfield, 1996) and primate (McMahon et al., 2004) retinal ganglion cell receptive fields. These results suggested that the amacrine cells are only a minor source of surround inhibition under photopic conditions. Nevertheless, other recent studies done under lower illumination conditions showed that GABAergic amacrine cells do make a major contribution to the classical receptive field surround of some mammalian ganglion cells. Flores-Herr et al. (2001) measured substantial surround inhibition in the excitatory signal arriving from bipolar cells that was attenuated by picrotoxin and TTX. They also isolated direct inhibitory input from amacrine cells and found that it was blocked by picrotoxin and TTX in most ganglion cells in rabbit. Likewise, Taylor (1999) showed that TTX produced a large attenuation of rabbit ON-center brisk-transient ganglion cell surrounds. Both Flores-Herr et al. (2001) and Taylor (1999) made their measurements at mesopic light levels. Also there are a number of previous studies which have shown that GABA antagonists attenuate the ganglion cell surround in cat (Kirby & Schweitzer-Tong, 1981) and rabbit (Daw & Ariel, 1981), but only under scotopic conditions. At low scotopic conditions, rod signals are relayed to ganglion cells by AII amacrine cells (Bloomfield and Dacheux, 2000), whose surrounds are blocked by picrotoxin in rabbit (Völgyi

et al., 2002), and it is proposed that the surround receptive field of AII cells is generated by lateral, inhibitory signals derived from neighboring GABAergic, on-center amacrine cells (the S1 amacrine cell in rabbit, and the A17 amacrine cell in cat) via inhibitory, feedback circuitry to the axon terminals of rod bipolar cells (Bloomfield & Xin, 2000).

2.3 Retinal ganglion cell

Since the electrical spikes conveyed by ganglion cell axons are the basis of our visual experience, to understand how visual information is encoded in the activity of the ganglion cells is a principal goal of vision research. Unlike the other classes of retinal interneuron (bipolar, horizontal, interplexiform and amacrine cells), the activity of ganglion cells can be measured relatively easily by recording their action potential discharges with extracellular electrodes.

2.3.1 Morphological types of retinal ganglion cell

As early as the 1890s, Ramón Y Cajal was able to classify many different varieties of ganglion cell based on form (dendritic morphology), extent (cell body and dendritic tree size), and number of sublayers in which they arborize (stratification levels in the inner plexiform layer) by studying Golgi stained cross-sections of vertebrate retina. Boycott and Wassle in their work on whole-mount cat retina proposed a successful morphological classification scheme in which four main morphological classes were defined as alpha, beta, gamma and delta ganglion cells (Fig. 2-6) (Boycott and Wassle, 1974). Both alpha and beta cells of the cat retina are arranged in regular, superimposed bi-level mosaics across the whole retina (Wassle et al., 1981a,b). Both varieties can be subdivided into separate subtypes depending on whether

they branch in sublamina a (OFF-center) or b (ON-center) of the inner plexiform layer (Famiglietti and Kolb, 1976). The major morphological difference between these two types of ganglion cells is that alpha ganglion cells have a much larger dendritic tree than beta ganglion cells. It has been estimated that alpha cells form 3% and beta cells 40-50% of all ganglion cells in the cat retina (Fukuda and Stone, 1974; Stone and Fukuda, 1974). The non-alpha/non-beta cell classes (including gamma and delta cells) have been classified into more than 20 different morphological types (Kolb, et al., 1981).

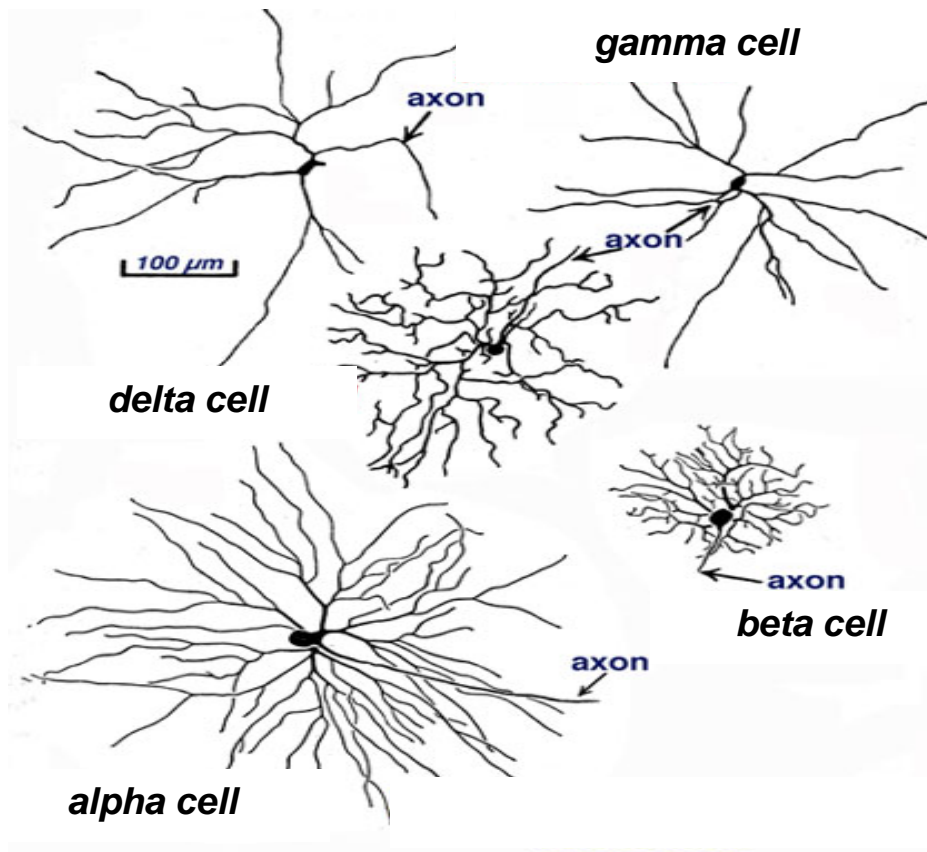


Figure 2-6: Morphological types of retinal ganglion cells. (modified from Boycott & Wassle, 1974)

2.3.2 Physiological types of retinal ganglion cell

The nature of the cell's response to light flashed within the receptive field immediately points to the existence of three very different cell types. ON-center/OFF-surround cells: a spot flashed near the center of the receptive field produces an increase of firing at light onset and a reduction of firing at light offset. OFF-center/ON-surround cells: the firing rate decreases at light onset and increases at light offset. For both cell types, a spot flashed at some distance from the center (the surround) has the opposite effect to stimulation with a spot in the center (Kuffler, 1953). ON/OFF cells: a brief burst of spikes is produced at both the onset and offset of light stimulation, irrespective of where the spot is flashed in the receptive field (Fukuda et al. 1984). Quantitative analysis has classified the cat's retinal ganglion cells into X, Y (Enroth-Cugell & Robson, 1966; Hochstein & Shapley, 1976a, b) and W cells (Cleland & Levick, 1974a, b; Stone & Fukuda, 1974). The physiological X, Y and W types are considered to be the equivalents of beta, alpha, non-alpha/beta morphological ganglion cell types (Boycott and Wässle, 1974; Enroth-Cugell and Robson, 1966; Cleland and Levick, 1974, Levick and Thibos, 1983, Troy and Shou, 2002). The X-cell integrates light from different points in space by simple weighted summation; i.e., linear spatial summation. The Y-cell's receptive field is several times larger than that of a nearby X cell. Besides the conventional (linear) center and surround, the Y-cell receptive field also contains many small rectifying spatial subunits overlapping both the center and surround. These rectifying subunits cause the Y-cell to exhibit a nonlinear response. The Y-cell conveys a fast but coarse neural image to the brain because it has a shorter visual latency (Troy & Lennie, 1987), a more transient response (Cleland et al., 1973), lower cell density (Wässle et al., 1981a, b) and a larger receptive field (Linsenmeier et al., 1982) while the X-cell provides a somewhat slower, but

sustained and higher resolution image. The term W-cell stands for the many ganglion cell-types other than the X- and Y-cell. As indicated from the variety of morphological types, the W-cell has diverse physiological properties (Troy & Shou, 2002).

2.3.3 Receptive fields of retinal ganglion cells

Each ganglion cell responds to light directed to a specific area of the retina. This area is called the receptive field of the cell. Hartline (1940) used 'spot mapping' to define such fields, a technique still widely employed, and concluded that ganglion cell receptive fields were fixed in retinal space and immobile.

1. Center-surround receptive field

The classical center-surround receptive field (Fig. 2-7, left) was described by Kuffler (1952; 1953) fifty years ago. Visual stimulation in the center or peripheral areas of the receptive field elicits opposite responses. For example, an ON-center cell, which is excited at stimulus onset by central stimulation, has regions in the peripheral receptive field where offset excitation is evoked. It has been shown that the center mechanism has a higher spatial frequency resolution while the surround has a wider temporal frequency response (Frishman et al., 1987). The dimensions of center-surround receptive fields also increase with retinal eccentricity (Linsenmeier et al., 1982). Both X- and Y-cells have receptive fields of this type. However the receptive field center of the X-cell is much smaller than that of Y-cell, therefore the image carried by the X-cell has higher spatial frequency resolution than the one carried by the Y-cell.

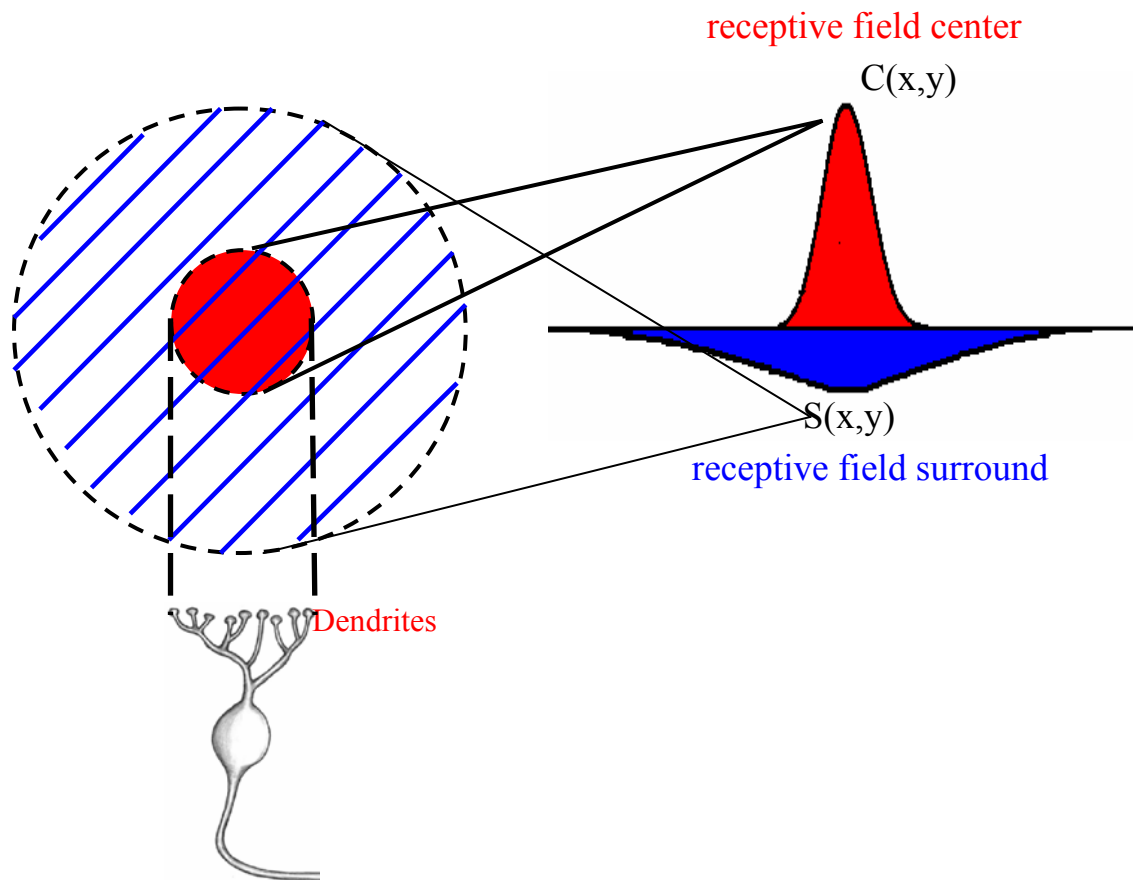


Figure 2-7: Difference of Gaussian center-surround model (Rodieck, 1965). Left panel: red area represents the spatial pool of the Gaussian center; blue strip shaded area represents the spatial pool of the surround. The receptive field center corresponds to the dendritic tree field of the ganglion cell. Right panel plots the Gaussian weighing function of the center (red) and the surround (blue) mechanisms.

The classical center was assumed to be circular, however later research has shown that the shape of the receptive field center is somewhat elongated (Hammond, 1974). The typical ellipticity of the receptive field center is ~ 1.3 .

The precise role of the center-surround receptive field in visual information processing remains uncertain. One hypothesis is that the surround pools signals from receptors over a

wide area to generate a prediction of the local average luminance. Subtracting the surround signal from that of the center-evoked signal enables the ganglion cells to report only local differences in luminance (Srinivasan et al., 1982). Another hypothesis maintains that the center-surround receptive field results from two conflicting pressures. The conflict results from the retina trying to maximize signal-to-noise while eliminating redundancy in the message transmitted (Atick & Redlich, 1992).

2. Mathematical models

The ‘difference of Gaussians receptive field model’ (Rodieck, 1965) provides a good quantitative prediction of the responses of X-cells. Retinal signals are assumed to be pooled by two mechanisms (center and surround) with the difference of the signals generating the ganglion cell’s response (Fig. 2-7, right). The spatial pools of the center and surround mechanisms are concentric and overlapping. Both mechanisms integrate visual signals with Gaussian weighting.

The ‘difference of Gaussians’ model assumes linear summation of light-evoked signals over space, an assumption that is mostly valid for X-cells, but not for Y-cells. Thus to give a satisfying prediction of the responses of Y-cells, another model was proposed by Hochstein & Shapley (1976), which combines the difference of Gaussian receptive field with a pool of subunits whose signals are rectified prior to summation. In this model, the individual subunits sum light over a smaller field than the classical receptive field center (Fig. 2-8). As a result, when the visual stimulus is rich in high spatial frequencies, the responses of Y-cells are

heavily influenced by these nonlinear subunits. However, when low spatial frequencies dominate the stimulus, the responses of Y-cells are primarily determined by the linear center-surround component of the receptive field.

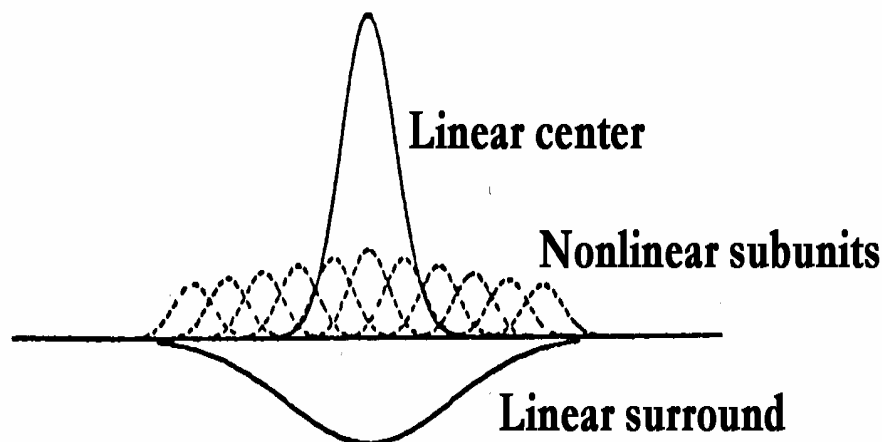


Figure 2-8: Hochstein & Shapley (1976) model of the Y-cell receptive field. Center and surround mechanisms sum light with Gaussian weighing, as in the Rodieck (1965) model. The nonlinear component of Y-cell responses results from the summed activity of a set of nonlinear subunits that individually sum light over a region smaller in area than the linear center.

In the two models described above, it was assumed that the time-course of signals evoked by the center and surround mechanisms were the same, an assumption that was shown to be invalid by subsequent work. To account for the difference between the time-courses of center and surround responses, a new model known as the ‘Gaussian center-surround model’ has been employed in preference to the difference of Gaussians model since the early 1980s. In this model, the spatial integration of retinal signals by the center and surround is the same as in the difference of Gaussians model, but the time-courses of the center and surround responses are permitted to differ (Fig. 2-9).

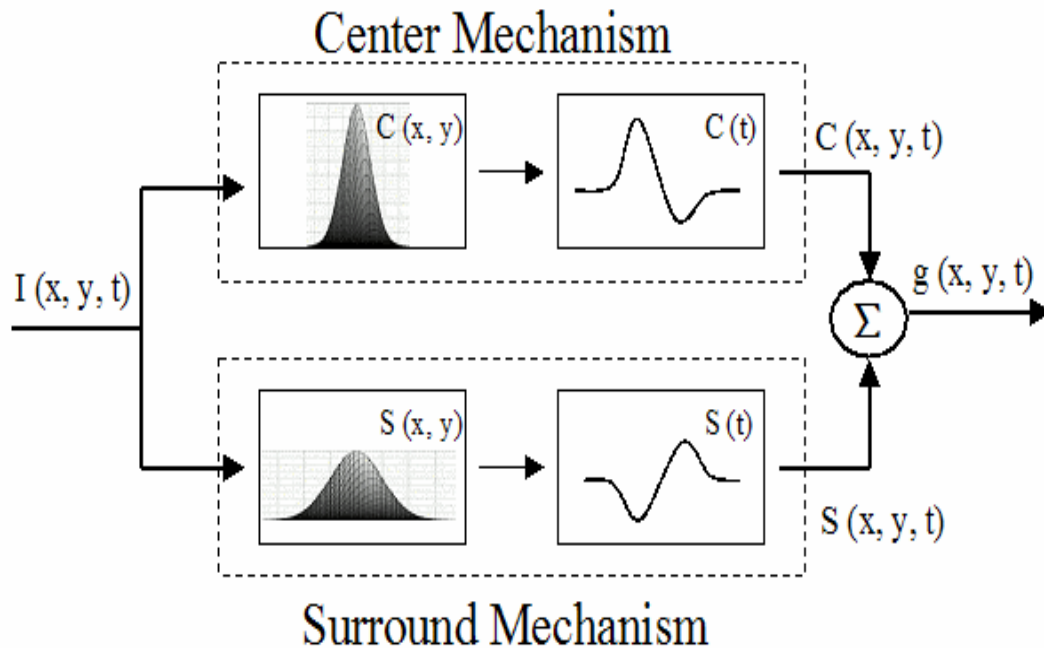


Figure 2-9. Gaussian center-surround model. $I(x, y, t)$: input signals as a function of space (x, y) and time (t); $C(x, y)$: Gaussian weighing for the spatial integration of signals for the center mechanism; $S(x, y)$: Gaussian weighing for the spatial integration of signals for the surround mechanism. $C(t)$: time course of the center; $S(t)$: time course of the surround. $C(x, y, t)$: center responses as a function of space and time; $S(x, y, t)$: surround responses as a function of space and time. $g(x, y, t)$: ganglion cell's responses result from the difference between the center and the surround.

2.4 Effects of illumination on the retina

The eye operates over a very wide range of light levels as the lighting conditions change from a bright sunlit noon to a dark night. As early as 1865, Aubert found that the sensitivity of the eye to light increased 35 times after some time in the dark. Yet the dynamic range of neurons is far too small to encode illuminance. Thus adaptation occurs in the retina to adjust to changing conditions of illuminance. The adaptation resets the operating range to the

current space-time-average light level, allowing good discrimination of variation near that average level.

The duplex nature of the visual system results in a division of the range of illuminance. Above a certain luminance level (about 0.03 cd/m²), the cone pathway is involved in mediating vision. Below this level, the rod pathway comes into play providing scotopic (night) vision (see previous chapter 2.2.2). With dark adaptation, there is a progressive increase in sensitivity with time in dark, which is thought to be a result of photopigment regeneration. However, bleaching of cone photopigment has a smaller effect on cone thresholds. Further retinal processing and retinal 'rewiring' (switching between retinal pathways) are also involved in adaptation.

2.4.1 Visual performance as a function of mean light level

In many psychophysical and physiological experiments, adaptation is explored by determining increment thresholds or contrast sensitivity. In an increment threshold experiment, a test stimulus is presented on a background of a certain luminance. The stimulus is increased in luminance until detection threshold is reached against the background. The quantity of light needed for detection is the increment threshold (Rose 1948). Contrast sensitivity is measured in terms of the threshold contrasts for detecting sinusoidal gratings. In such experiments, a field filled with a sinusoidal grating is presented. The contrast sensitivity is determined by adjusting the contrast until the gratings can be just detected by the test subject (Daitch & Green, 1969; Pasternak & Merigan, 1981) or can evoke a criterion response in a retinal ganglion cell (Enroth-Cugell & Robson, 1966; Derrington & Lennie, 1982). It has been found

that increment thresholds decrease and contrast sensitivity increases with increasing mean light level and that the rate of change is not constant. Three sections of the curve are apparent in a log-log scale plot (Fig. 2-10):

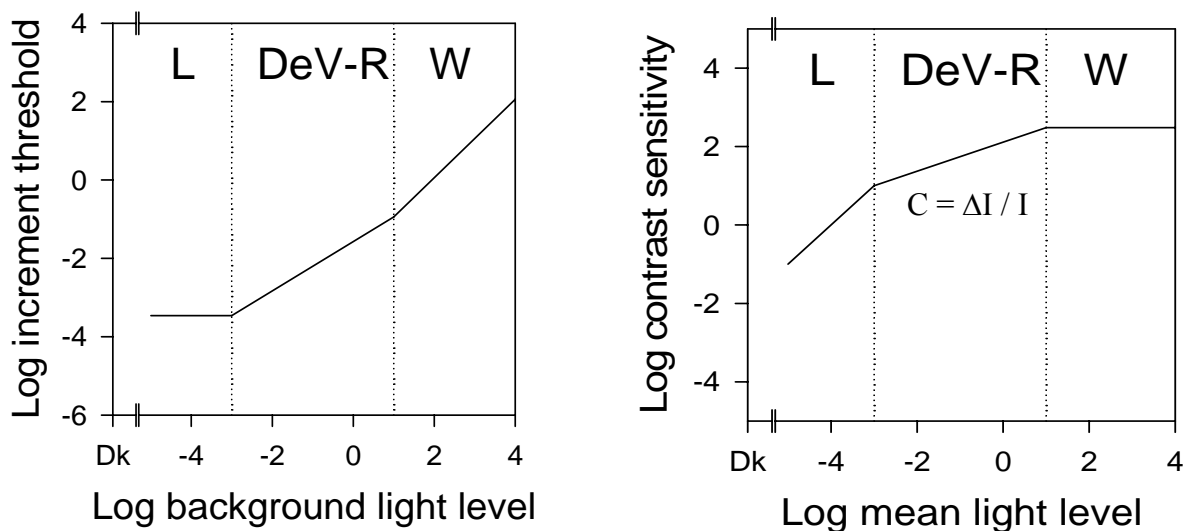


Figure 2-10. Increment threshold (left) and contrast sensitivity (right) as a function of light level. There are three ranges of sensitivity adjustment, the linear range (L), the DeVries-Rose (DeV-R) and the Weber Law (W) range. C: contrast sensitivity; ΔI : increment threshold; I: mean light level. Both axes, arbitrary units.

1. Linear range (L)

At the lowest light levels the increment threshold is independent of the background luminance because it is the inherent noise within rods under darkness (the so called dark light), which includes thermal isomerizations of photopigment, spontaneous opening of photoreceptor membrane channels and spontaneous neurotransmitter release, that limits detection of the increment. A light-evoked signal must exceed this 'dark noise' to be detected. Over the same range, contrast sensitivity increases linearly with mean light level. Because contrast equals the ratio of threshold increment (the luminance difference between the

stimulus and the background) by background luminance, when the threshold increment is constant, the contrast needed for detection decreases in direct proportion as the mean light level increases. Thus this section of the curve is referred as the linear range.

2. DeVries-Rose Law range (DeV-R)

In the middle range of light levels increment threshold and contrast sensitivity are limited by quantal fluctuation in the background. Because of the Poisson stochastic property of light, background light itself is noisy with a variance equal to the number of photons absorbed. Therefore when the luminance of the background becomes sufficiently high that the photon noise is greater than the dark noise, the photon noise becomes the main source of noise. To detect the stimulus, the discharge evoked by a stimulus must exceed that evoked by fluctuation of the background (photon noise) sufficiently. As photon noise increases as the square root of the number of photons absorbed (in proportion to background luminance) both increment threshold and contrast sensitivity increase as the square root of background luminance as mean light level increases. This gives a slope of one half on a log-log plot of contrast sensitivity or increment threshold versus background illuminance. The range of light levels over which this prevails is called the DeVries-Rose law range or square root law range.

3. Weber Law range (W)

At the highest light levels, contrast sensitivity is constant. Over the same range, the increment threshold increases proportionally to the background luminance thus having a slope

of 1 when plotted using log-log coordinates. This range is referred to as the Weber law range. This section of the curve demonstrates an important aspect of our visual system. Our visual system is designed to distinguish objects from its background. In the real world, objects have contrast, which results from the differential luminance of surfaces. Surface luminance is the product of the surface reflectance and illuminating light. Since the illuminating light for two adjacent surfaces is the same in the real world, the contrast between the surfaces results from their differential reflectance, which is constant and independent of ambient luminance. Therefore, the principle of Weber's law can be applied to contrast, which remains constant regardless of illumination changes. This is called contrast constancy or contrast invariance. It has been found that it is the retina that performs the task of establishing constant contrast sensitivity for the visual system at high light levels (Troy & Enroth-Cugell, 1993).

Barlow (1958) explored the conditions that influenced the transition from the DeVries-Rose law to Weber's law. He concluded that for brief, small test spots, increment thresholds rise as the square root of the background over the entire photopic range. Spots of large area and long duration have slopes close to Weber's law. Other spatio-temporal configurations result in different proportions for each region.

2.4.2 Receptive field properties of ganglion cell as a function of mean light level

In retinal ganglion cells, separate rod and cone pathways converge. During dark adaptation, as input signals to ganglion cells shift from cone-dominant to rod-dominant pathways, the receptive field properties of ganglion cells might be expected to change.

1. Receptive field center

The strength of the center mechanism has been found to be independent of retinal illuminance above 1.5 log cat td (corresponding to ~310 quanta absorbed/rod/sec), which corresponds to the Weber Law range. A clear transition in receptive field properties occurs at 1.5 log cat td where we believe that the ganglion cell response shifts from cone-dominant to rod-dominant. Below this transition light level, responsivity declines with retinal illuminance (Troy et al., 1993; Troy et al., 1999). Also the receptive field center size is found to be fixed at photopic light levels (Troy et al., 1993; 1999; Chan et al., 1992) and increases modestly under scotopic conditions (Barlow et al., 1957; Cleland & Enroth-Cugell, 1968; Enroth-Cugell et al., 1977; Chan et al., 1992; Troy et al., 1993; 1999). The latency of the center's signal increases as light level declines (Cleland & Enroth-Cugell, 1970; Enroth-Cugell & Lennie, 1975; Enroth-Cugell et al., 1977; Troy et al., 1993; 1999) which implies the retina has a longer integration time under scotopic conditions.

2. Receptive field surround

The results of area threshold studies (Barlow et al., 1957) were interpreted to imply the loss of surround mechanism at low light levels. Subsequent work has found that this is not true. The surround is present, but its strength is decreased and its signal less antagonistic to the center (Enroth-Cugell & Lennie, 1975; Chan et al., 1992; Troy et al., 1993; 1999). The latency of the surround signal is longer than that of the center signal, and it increases more as light level declines (Cleland & Enroth-Cugell, 1970; Enroth-Cugell & Lennie, 1975; Enroth-Cugell et al., 1977; Troy et al., 1993; 1999).

2.5 Motivation

In previous studies from our lab (Troy et al., 1993; 1999), the receptive field properties for light levels above $-2 \log \text{cat td}$ have been investigated. The lower light levels were not investigated for a number of reasons, such as lack of comparable psychophysical measurements of contrast sensitivity in the cat for these lower light levels; there have been previous studies of cat ganglion cell behavior at these very low light levels and recording at very low light levels is too time consuming.

With a new electrode etching technique, we are able to efficiently make electrodes that can more routinely make stable recording from a ganglion cell for longer times. This improvement made it possible to investigate receptive field properties at very low light levels. From some preliminary data, we found that the receptive field center expands significantly at light levels below $-2 \log \text{cat td}$, much larger than had been reported earlier for higher light levels. Also, we found the surround of receptive field, which is thought to disappear under scotopic condition, is still present under low light levels all the way down to the dark light level.

These discrepancies between our results and the traditional views of ganglion cell receptive field within the low scotopic range and recent interest in how the retina handles single photon signals (Field & Rieke, 2002) led us to re-examine the properties of X- and Y-cells for very low light levels. After carefully investigation, we found that both the center and surround of receptive field expand dramatically under low scotopic conditions. This expansion might be a result of electrical coupling between AII amacrine cells. We also found that the

surround is still present, but no longer antagonistic. The surround becomes almost synergistic with the center because the phase difference between the center and surround mechanisms changes from 180 degree to few tens of degree.

III. EXPERIMENT METHODS AND DATA ANALYSIS

3.1 Experimental techniques

3.1.1 Cat preparation.

An adult male cat weighing 2~4 kg was initially anesthetized either with a single intravenous injection of sodium thiopental (25~30 mg/kg, *i.v.*) or with a single intramuscular injection of ketamine hydrochloride (25 mg/kg, *i.m.*). After the cat lost consciousness, showing muscle relaxation and no withdrawal of extremity on deep pinch of a paw, preparatory surgery was started with the insertion of a tracheal cannula for later artificial respiration. Both femoral veins were catheterized with polyethylene tubes and the left femoral artery was catheterized with a Teflon tube. One of the venous catheters was used to deliver additional sodium thiopental (2.5%, 2.5-5mg/dose, *i.v.*) during surgery and deliver a loading dose of ethyl carbamate (200mg/kg, *i.v.*) after surgery. Then the tube was connected to a pump that continuously infused ethyl carbamate (15-50 mg/kg/hr, *i.v.*) to maintain anesthesia at a surgical level during the remainder of the experiment. The other tube was connected to another pump that continuously infused pancuronium bromide (0.2 mg/kg/hr, *i.v.* after an initial loading dose of 0.1 mg/kg, *i.v.*) or gallamine triethiodide (10 mg/kg/hr, *i.v.*) to achieve paralysis. Paralysis was induced only after anesthesia was well maintained by ethyl carbamate without administration of sodium thiopental for at least one hour. The arterial catheter was connected to a blood pressure transducer to monitor the blood pressure of the cat. EKG needles were inserted to monitor heart rate. During the period of paralysis, the cat was artificially ventilated. Ventilation was adjusted to give an end-tidal CO₂ near 4%. Core body temperature was monitored and maintained between 38.0~41.0 °C. Mean arterial blood

pressure and heart rate were monitored to assess the depth of anesthesia. End tidal CO₂ and subscapular temperature were also tracked to ensure the cat was maintained in a good physiological state. Atropine sulfate (0.2mg, *i.m.*), dexamethasone (4 mg, *i.m.*) and cefazolin sodium (100mg / 12hr, *i.m.*) were given to minimize salivation caused by the anesthetics and to inhibit inflammatory reactions and cerebral edema.

A pair of ear bars secured the cat's head to the stereotaxic frame (with the help of bite and eye bars). The pupils were dilated with atropine (1%) and nictitating membranes retracted with 2.5% phenylephrine. The cat's eyes were fitted with contact lenses with built in artificial pupils (4 mm diameter). Artificial tears were administered occasionally to prevent the corneas from drying. Spectacle lenses of appropriate power were used to provide optimal focus of images on the retina.

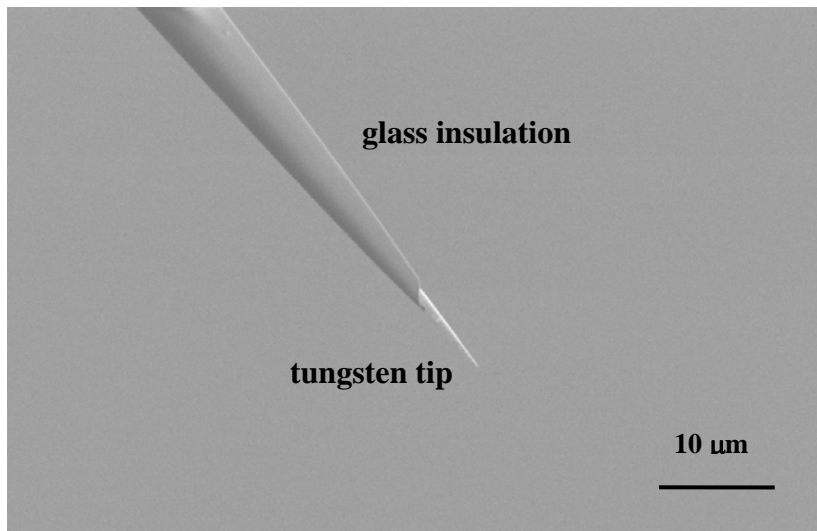


Figure 3-1: Scanning electron microscope image of a microelectrode. The exposed tip of tungsten is $\sim 7 \mu\text{m}$.

3.1.2 Recording with microelectrodes

Extracellular recordings were made with Levick (1972) microelectrodes (Fig. 3-1). Fabrication of the microelectrodes followed four steps modified from the Levick (1972) method. Firstly, a tungsten wire (127 μ m in diameter and about 8 cm in length, Small Parts, USA) was etched in a solution composed of 100 ml distilled water, 71 g sodium nitrate (NaNO₂) and 34 g potassium hydroxide (KOH). 4V DC was set up between the tungsten wire (anode) and a carbon cylinder electrode (cathode). In order to generate a sharpened cone-shaped tip, the wire was repeatedly dipped in and out of the etching solution with a maximum immersion depth of 3mm. A commercial electric sewing machine (Singer, LaVergne, Tennessee, USA) was adapted to provide a consistent up and down motion of the tungsten wire (Fig. 3-2). It took about 3~4 minutes to create a sharp cone-shaped tip. The tungsten wire was thoroughly cleaned of residual etching solution after it was sharpened. In the second step, a glass pipette (0.45 mm in diameter) was pulled with a programmable Flaming Brown Micropipette Puller (model P.80/PC, Sutter Instrument Co., Novato, California, USA) to produce a pipette tip diameter of ~1.5 μ m. Then, the sharpened tungsten was threaded into the back end of the glass pipette and advanced until its tip protruded through the opening. Finally, the tungsten wire was glued to the glass pipette at its back end with super glue.

A craniotomy was performed over the left or right optic tract. The tungsten-in-glass microelectrode, driven by a microstepper controlled by a custom program via a stepper motor controller interfaced to a Pentium computer, was advanced downward through a protective guide tube into the brain. The position and depth of the optic tract were estimated using a cat brain atlas (Fig. 3-3). Once the electrode tip reached the optic tract, it was possible to isolate

discharges from a single optic tract fiber. The discharge could be modulated by visual stimulation. Well-isolated and stable recordings of single cell spikes were achieved from retinal optic tract fibers when the length of the electrode tip was 5~7 μm .

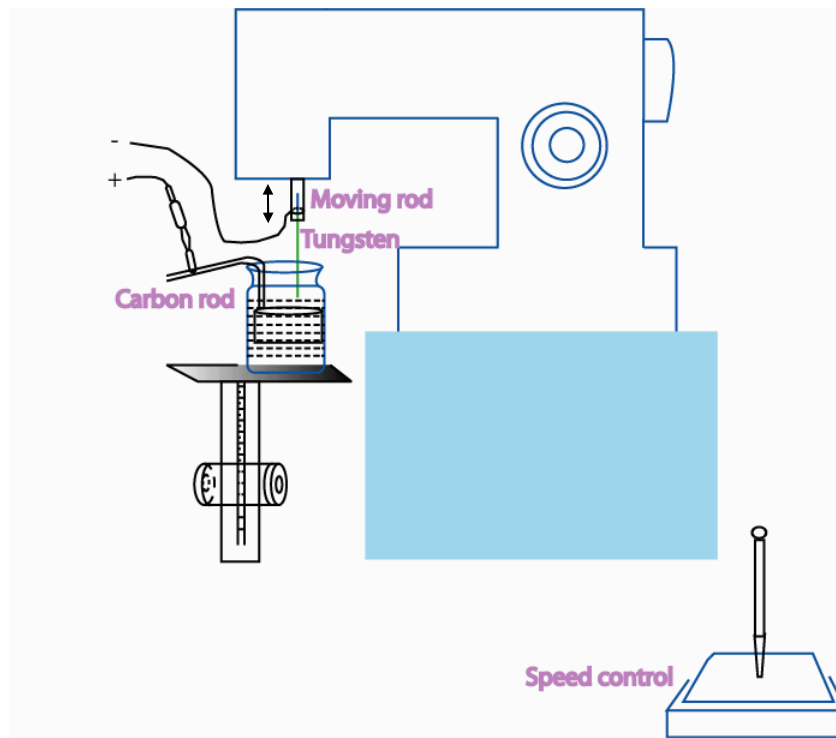


Figure 3-2: Use of a commercial sewing machine in an electrolytic etching set up. The tungsten is moved in and out of the etching solution by the up and down motion (direction shown as the vertical arrow) of the 'Moving rod' that would normally move the sewing machine needle. The speed of the movement can be controlled by adjusting a potentiometer in a foot pedal with a screwdriver, as indicated. A collar that can hold many tungsten wires can be fixed to the rod (only one tungsten wire is shown in this figure). The beaker containing the etching solution and a graphite cylinder cathode is mounted on a platform with fine vertical adjustment. The tungsten wire serves as the anode.

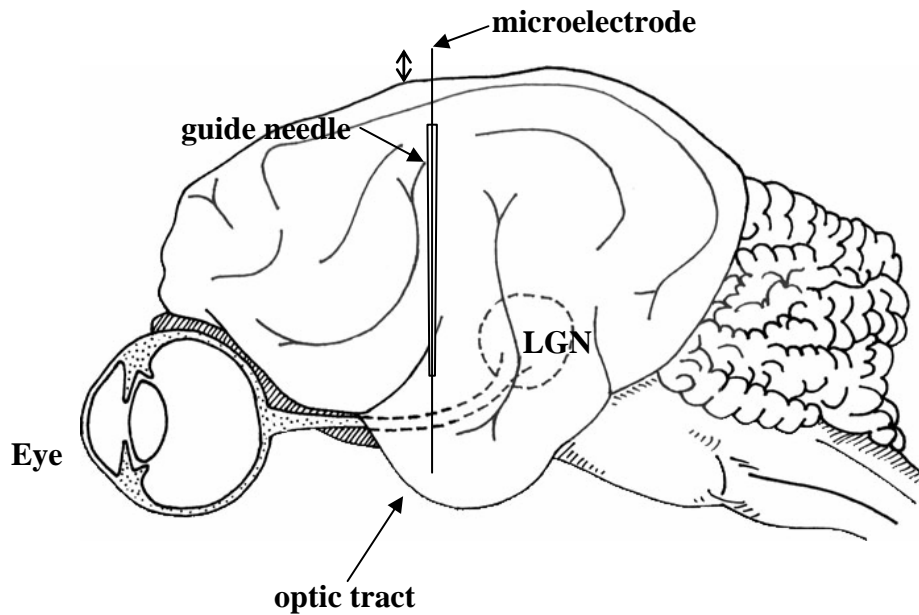


Figure 3-3: Record discharge of retinal ganglion cells from the optic tract. The microelectrode was inserted into the brain within a guide needle, and then was moved up and down by a microstepper controlled by a custom program via a stepper motor controller. LGN: lateral geniculate nucleus.

3.1.3 Visual stimulation

After isolating the discharges of a single optic tract fiber, the retinal location (retinal eccentricity) of the recorded ganglion cell was determined by mapping its receptive field center on a tangent screen, onto which the optic disk and major blood vessels surrounding the area centralis of each eye had been drawn (Pettigrew et al., 1979). The receptive field was then projected via an adjustable (horizontally and vertically) mirror onto a Sony Trinitron 17se monitor whose properties have been thoroughly characterized by Bohnsack et al. (1997). The viewing distance (the optical distance from the monitor to the eye) was ~60cm. The monitor's frame was refreshed at 150 Hz which is fast enough that X- and Y-cells cannot

respond to the raster flicker (Frishman et al., 1987). With the 4-mm diameter artificial pupils, the mean luminance (L_{mean}) of the display was equivalent to a retinal illuminance of approximately 2.5 log cat troland, which is within the low photopic range of the cat (Troy et al., 1999).

Visual stimulation presented on the Sony monitor was controlled by custom software via a stimulus generation card (VSG2/2, Cambridge Research Systems) interfaced to a Pentium computer. The following visual stimuli were used:

1. Contrast-reversing bipartite field

The contrast of a bipartite field stimulus was modulated at 1 Hz. The stimulus was oriented horizontally and then vertically. The midpoint of the receptive field was centered on the monitor (width: 27 deg, height: 20.5 deg) by rotating the mirror until the response to the stimulus at either orientation contained no component at the frequency of reversal.

2. Contrast-reversing sinusoidal gratings

The contrast of sinusoidal gratings of high spatial frequency was modulated sinusoidally at 2 Hz. These stimuli were used to differentiate X-cells and Y-cells according to the modified null test: the second harmonic component dominates the responses of Y-cells to contrast-reversing gratings of high spatial frequency (Hochstein & Shapley, 1976a, b).

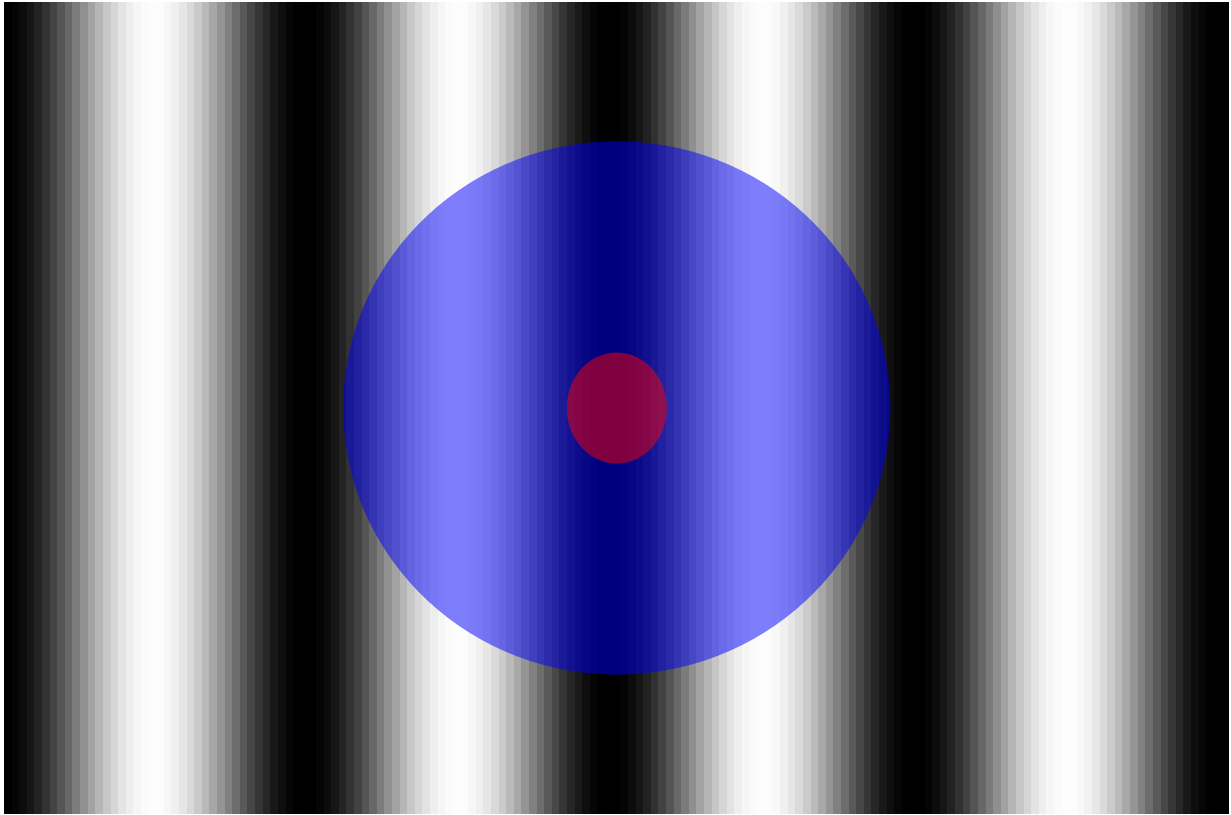


Figure 3-4: Drifting sinusoidal gratings. The receptive field of ganglion cell was centered on the screen as indicated (red: center; blue: surround). Full screen sinusoidal gratings were drifted over the receptive field in a horizontal direction.

3. *Uniform field*

A full-screen-width constant luminance field was used to measure the maintained discharge of the recorded ganglion cell.

4. *Drifting sinusoidal gratings*

Sinusoidal luminance gratings of different contrasts and spatial frequencies drifted across the receptive field of retinal ganglion cell at 2 Hz (Fig. 3-4). These stimuli were used to measure the spatial frequency transfer function of the cell.

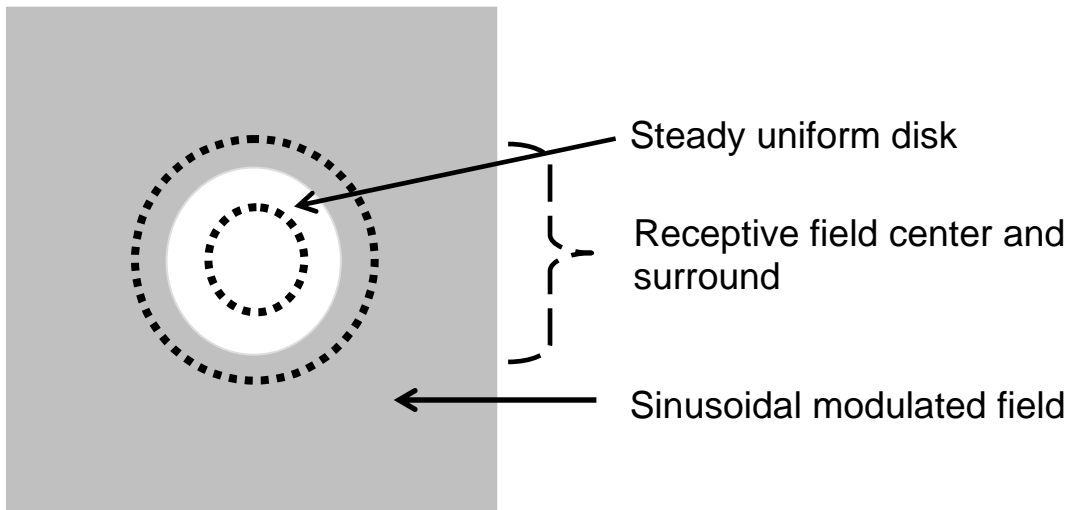


Figure 3-5: Surround isolating stimulus. The dashed circles represent the receptive field center (inner circle) and surround (outer circle) of a retinal ganglion cell. The white circle indicates the area that was held at a constant luminance. The grey region indicates that the luminance of the field that was modulated sinusoidally in time.

5. *Surround isolating stimulus*

A surround isolating stimulus was designed to preferentially stimulate the surround component of the center-surround receptive field. As shown in Fig. 3-5, the luminance of a spot within the central region is held constant at a mean level (L_{mean}) while the luminance over the rest of the screen is modulated sinusoidally about L_{mean} at 2 Hz. The diameter of the unmodulated center spot was fixed for one trial but could be varied from trial to trial so that different portions of the peripheral receptive field might be stimulated. When the center spot was sufficiently big, essentially no stimulation was applied to the center mechanism of the cell's receptive field and the cell could be considered to be driven by its surround mechanism in isolation. With this stimulus we can measure the properties (such as phase and strength) of

the surround component of the receptive field independently from those estimated from measurements made with the grating stimuli.

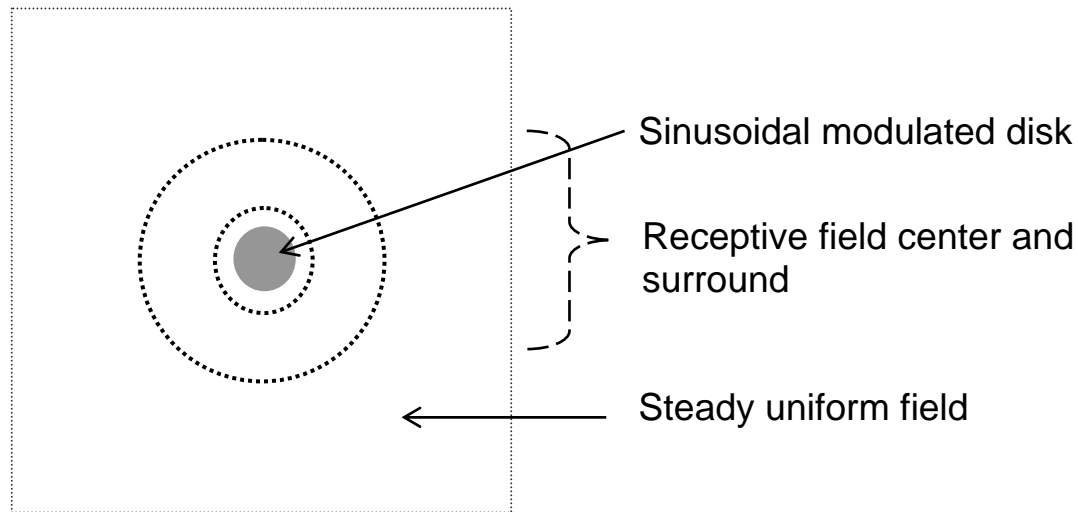


Figure 3-6: Center spot stimulus. The dashed circles represent the receptive field center (inner circle) and surround (outer circle) of a retinal ganglion cell. The white circle indicates the area that was modulated sinusoidally. The grey region indicates that the luminance of the field was held constant.

6. *Center spot stimulus*

A spot was centered on the receptive field center and its luminance was modulated sinusoidally about L_{mean} at 2 Hz. The luminance of the rest of the screen was held constant at L_{mean} (Fig. 3-6). With this stimulus, only the center mechanism contributes to the cell's response.

For all these stimuli used, the contrast, C , is defined as:

$$C = (L_{max} - L_{min}) / (L_{max} + L_{min}) \quad (1)$$

where L_{max} and L_{min} are maximum and minimum luminance of the pattern.

3.1.4 Dark adaptation

Retinal illuminance is given in terms of *cat troland* (cat td), which is the product of luminance (units of cd m^{-2}) and pupil area (units of mm^2). Here, the highest light level studied was 320 cat td ($\sim 2.5 \log \text{ cat td}$). An attempt was also made to collect data at the following lower light levels: - 1.5, - 2, - 2.5, - 3, - 3.5 log cat td and darkness. Some data were also collected at intermediate light levels to compare with data collected previously from the lab (Troy et al., 1993; Troy et al., 1999).

At the highest light level (2.5 log cat td), the receptive field location and type of the recorded cell were determined. The cell was centered on the screen and the spatial frequency transfer function of the cell measured. Then lower mean levels of luminance were obtained by placing neutral density filters between the animal and the display. The cat was placed in a light-tight box with a window at the front which could be closed with neutral density fillters. Great care was taken to ensure that stray light did not leak into the box and contribute to the illuminance experienced by the cat. Adaptation from one light level to another was tracked carefully. Steady-state adaptation at the new level was assessed by monitoring the cell's

response to a grating of the optimal spatial frequency and of a constant contrast (generally 50%) drifting at 2 Hz across the receptive field. Adaptation was assumed to be complete when the Fourier fundamental component of the cell's response amplitude stopped increasing with time and the cell's mean rate had stabilized. Usually 10 ~ 15 min were needed per log unit of dark adaptation.

3.1.5 Data collection

Extracellular recordings of the discharges of single retinal ganglion cells (X-, and Y-cells) were recorded from the optic tract with microelectrodes of the type described above. Spike times were collected with 0.1-ms precision via a data acquisition card (AS1, Cambridge Research System) interfaced to the same Pentium computer that generates the stimuli.

For each trial of response, peri-stimulus time histograms were generated with bin widths of 5 ms. Histograms were collected for as many full periods as could fit in to the recording period. The amplitudes (in impulses s^{-1}) and phase (in deg) of the fundamental (2-Hz) and second harmonic (4-Hz) components of the response were determined by performing a Fourier Transform on the histogram. Mean rate of the cell was calculated by dividing the total number of spikes by the recording duration (in seconds).

To characterize the spatial filtering properties of a retinal ganglion cell (X- or Y- cell), we measured its 2-Hz frequency responses to a set of either gratings or to the surround-isolating stimuli. To measure frequency responses, the peak contrast of the stimulus was

adjusted until the amplitude of the fundamental (2 Hz) component of response from the cell was in the range $5 \sim 10$ impulses s^{-1} . In this range, the amplitude of the fundamental component scales linearly with contrast and its phase is essentially constant (Troy & Enroth-Cugell, 1993).

The responsivity of the cell to the stimulus was calculated by dividing the fundamental amplitude by the contrast that evoked the response. Responsivity has units of impulses s^{-1} , though per unit contrast is implied. Our responsivity measure can be considered virtually equivalent to contrast sensitivity (Enroth-Cugell & Robson, 1966) and contrast gain (Chan et al., 1992) measures used by these authors. The phase of the fundamental component of response was referenced to the temporal phase of the stimulus that was always modulated at 2 Hz. The phase values given are the difference in degrees between the peak of the temporal luminance modulation of the stimulus and the peak of the 2-Hz modulation of the cell's discharge. The phase is given as positive if it leads and negative if it lags the phase of the stimulus. Phase angles separated by 360 degrees are identical.

Each fundamental response measurement was based on 10 s of discharge at the highest light level, and of increased duration for trials at lower light levels (i.e. 15-s at -1.5 and -2 log cat td; 20-s at -2.5 and -3 log cat td; 30-s at -3.5 log cat td). Each responsivity measurement was determined by the average over 3 or more fundamental response measurements of the cell to the same stimulus.

Frequency responses to drifting gratings were measured for each cell at all light levels we explored, including 2.5 log cat td and -3.5 to -1.5 log cat td, to quantitatively assess the spatial filtering properties of that cell at different light levels. Frequency responses to surround-isolating stimuli were measured at lower levels of retinal illuminance in the range of -3.5 to -1.5 log cat td, permitting properties of the surround component of the receptive field under scotopic conditions to be assessed independently from those estimated from measurements made with the grating stimuli.

3.2 Data analysis

The frequency responses of retinal ganglion cells, measured for a set of gratings of different spatial frequency and a set of surround isolating stimuli of different center spot diameters, were fitted with the Gaussian center-surround model (Enroth-Cugell et al., 1983). In the Gaussian center-surround model for ganglion cell receptive fields, center and surround mechanisms are assumed to have concentrically overlapping Gaussian spatial distributions of responsivity. And the signals from the two mechanisms are assumed to combine as vector quantities, which permits each to hold a temporal phase that can differ from each other in the range -180 to 180 deg.

The Gaussian center-surround model uses six parameters to describe the receptive field: the integrated responsivity of the center (K_c), the integrated responsivity of the surround (K_s), the radius of the Gaussian center (r_c), the radius of the surround (r_s), the phase of fundamental component (2 Hz) of the center (ρ_c) and the phase of fundamental component of

the surround (ρ_s). Fittings were performed in Matlab with a standard nonlinear optimization routine.

For grating stimuli, the mathematical expressions for the Gaussian center-surround model are:

$$R_c(\nu, f, I) = K_c(f, I) \exp(-(\pi r_c(f, I) \nu)^2) \quad (2)$$

$$R_s(\nu, f, I) = K_s(f, I) \exp(-(\pi r_s(f, I) \nu)^2) \quad (3)$$

where R_c and R_s are the responsivities of the center and surround measured at the spatial frequency ν , the temporal frequency f , and retinal illuminance I . K_c and K_s are the integrated responsivities of the center and surround, which are equivalent to the responsivities for a spatial frequency of 0 cycles deg^{-1} (full-field modulation). r_c and r_s are the characteristic radii of the Gaussian spatial responsivity profiles. To generate the model cell's frequency responses, the responsivities of the center (R_c) and surround (R_s) are added vectorially. The center and surround signals are assumed to have phases ρ_c and ρ_s . The cell's frequency response is mathematically expressed as

$$\mathbf{R}(\nu, f, I) = R_c(\nu, f, I) \exp(i2\pi \rho_c(f, I)/360) + R_s(\nu, f, I) \exp(i2\pi \rho_s(f, I)/360) \quad (4)$$

Where \mathbf{R} is the cell's frequency response, which has responsivity R and phase ρ . Since we are concerned only with measurements at one temporal frequency (2 Hz), the dependence of responsivities, radii and phase upon f can be ignored. In this work we look at the dependence of the parameters upon retinal illuminance (I).

Frequency response of a ganglion cell to surround-isolating stimuli were estimated

in a similar fashion as:

$$R_c = K_c [(1/2\pi\sigma_1^2)\int\exp(-x^2/2\sigma_1^2)dx]\int\exp(-y^2/2\sigma_1^2)dy - \int(t/\sigma_1^2)\exp(-t^2/2\sigma_1^2)dt] \quad (5)$$

$$2\sigma_1^2 = r_c^2 \quad (6)$$

$$R_s = K_s [(1/2\pi\sigma_2^2)\int\exp(-x^2/2\sigma_2^2)dx]\int\exp(-y^2/2\sigma_2^2)dy - \int(t/\sigma_2^2)\exp(-t^2/2\sigma_2^2)dt] \quad (7)$$

$$2\sigma_2^2 = r_s^2 \quad (8)$$

$$\mathbf{R} = R_c(v,f,I) \exp(i2\pi\rho_c(f, I)/360) + \mathbf{R}_s(v,f,I) \exp(i2\pi\rho_s(f, I)/360) \quad (9)$$

Where x and y are width and height ($x \in [-13.5^\circ, 13.5^\circ]$, $y \in [-10.25^\circ, 10.25^\circ]$) of the screen and t is the radius of the steady uniform disk over the center.

IV. RESULTS

To explore characteristic changes of the retinal ganglion cell's receptive field at different light levels, we made recordings from 68 ON-center cells and 25 OFF-center cells. In most respects, the ON- and OFF-center cells behaved similarly with regard to changes in receptive field properties at different light levels. The differences seen in the data from OFF-center cells were based on a low number of cells, especially at lower light levels ($-2.5 \sim -3.5$ log cat td), making conclusions unreliable. Consequently, only data from ON-center cells (32 ON-center X cells and 36 ON-center Y cells) from 28 adult cats are presented here. 15 of the cells were from the ipsilateral eye and 53 were from the contralateral eye. 10 of the cell's receptive fields were located within 10 deg of the *area centralis*, 32 had eccentricities in the range 10 ~ 20 deg, 15 had eccentricities in the range 20 ~ 35 deg and eleven had eccentricities higher than 35 deg. The median eccentricity was 16.4 deg.

For all the cells, spatial-frequency responses to drifting sinusoidal gratings were collected at 2 Hz for a set of spatial frequencies that covered the full range for which the cell's response had a significant Fourier fundamental component (2 Hz component). The lowest spatial frequency, which was limited by the monitor's size, was usually set to be 0.01 cycle / deg. The characteristic radius of the photopic center mechanism (r_c) and surround mechanism (r_s) of the cells studied ranged from 0.1 ~ 0.8 deg and 0.9 ~ 7.4 deg for the X-cells, and from 0.4 ~ 1.7 deg and 2.2 ~ 10.8 deg for the Y-cells respectively. Thus, for surround-isolating stimuli, the diameter of the central unmodulated spot was kept in the range 0.2 ~ 15 deg, which ensured that surround-evoked responses were obtained with most of the patterns. In six

cats, for 11 of the X-cells and 15 of the Y-cells, responses to surround-isolating stimuli were measured. In most of the cells (64 out of 68), one set of measurements was taken at a photopic light level (2.5 log cat td), which was used to normalize all data collected from a cell. Sets of measurements were also taken at low scotopic light levels: - 1.5 (66 cells), - 2 (40 cells), - 2.5 (48 cells), -3 (34 cells) and - 3.5 (27 cells) log cat td. The lowest light level (- 3.5 log cat td) used in this study corresponds to the dark light level if the dark light is assumed to result from thermal isomerization of photopigment, which is 0.0063 ± 0.0036 isomerization/s in the outer segment of a rod of a macaque monkey (Baylor et al., 1984) (we assume that the rate for cat and macaque rods is the same). The estimate of dark light is also consistent with the measurement of the dark light sensed by cat X- and Y- cells made by Mastronarde (1983).

Data collected previously from the lab (Troy et al., 1993; Troy et al., 1999) have been combined with new data to show the receptive field changes over the full operational range of the retinal ganglion cells.

4.1 Spatial-frequency responses to gratings at different light levels

Figure 4-1 shows peri-stimulus time histograms generated with bin width of 50ms for spikes collected at a photopic light level (2.5 log cat td) and at a low scotopic light level respectively (- 3 log cat td). As shown in the figure, the time delay between the peak of the stimulus and the peak of fundamental component of cell's responses becomes much longer when background illuminance drops from photopic level to low scotopic level.

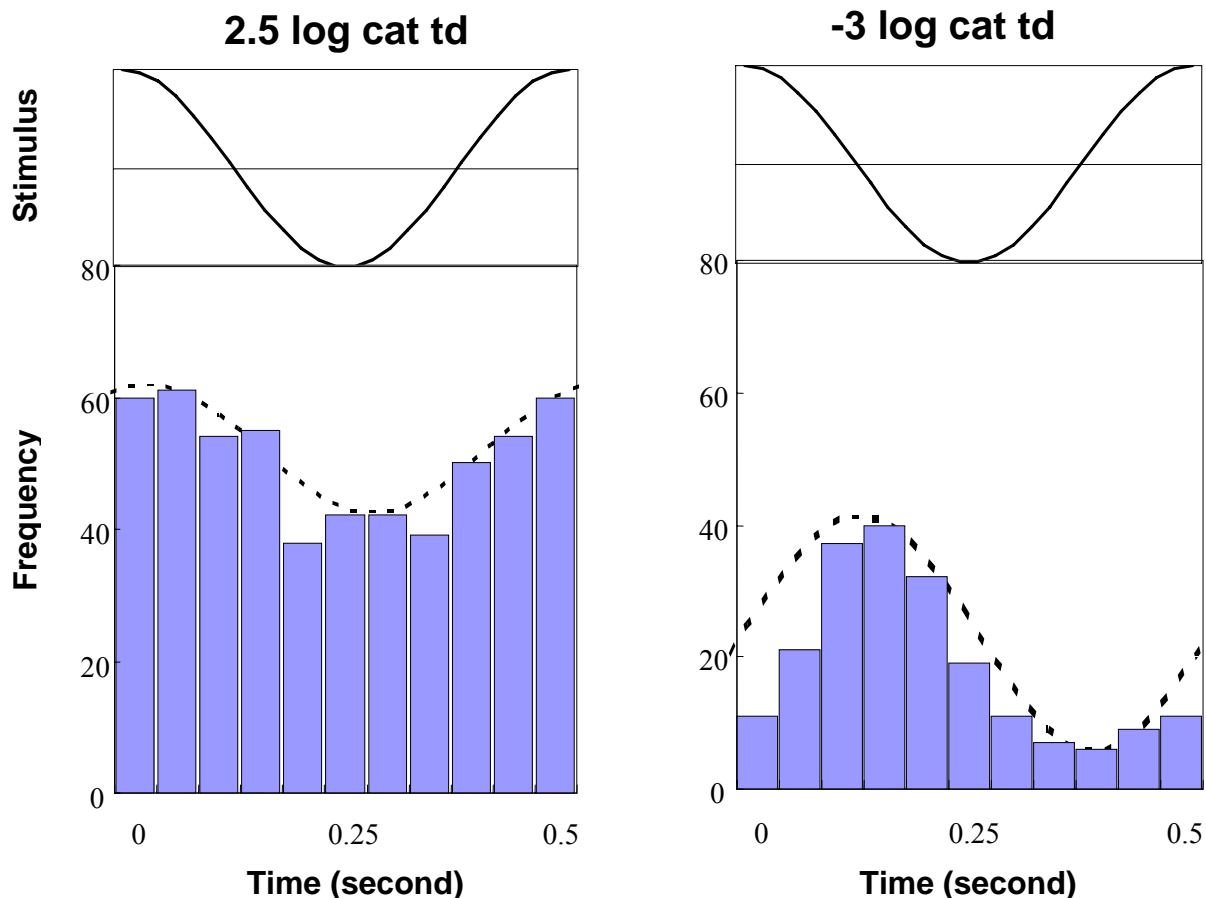


Figure 4-1: Peri-stimulus histograms of spikes. Shown are the histograms averaged over as many full periods ($T = 0.5$ sec) as could fit in a 10-s interval (2.5 log cat td) or a 20-s interval (-3 log cat td) of an ON-X cell (J1208). Each bar represents the frequency of a spike occurs at this time bin (50 ms). The solid curve on the top of each panel represents the waveform of the 2 Hz sinusoidal gratings. The dashed curve in each panel represents the fundamental (2 Hz) component of the cell responses.

Spatial-frequency responses to gratings at different light levels are illustrated in Figure 4-2 for one representative ON-center X cell (J1208) and in Figure 4-3 for one representative ON-center Y cell (J0430). Characteristic changes in receptive field filtering properties at different levels of retinal illuminance are demonstrated by the figures. As shown in the upper panels of the figures, as light level fell the peak of the cell's responsivity curve declined

dramatically. This is consistent with previous results from the lab (Troy et al., 1993; Troy et al., 1999). However the change in peak responsivity is not followed over the full spatial-frequency range. The responsivity is attenuated more severely at intermediate and high spatial frequencies than that at lower spatial frequencies, causing the shape of the responsivity versus spatial-frequency function to become more low-pass at lower light levels. The spatial frequency resolution also decreases with light level. As shown in the lower panels, it is apparent that the temporal phase of the spatial-frequency responses becomes more lagged at lower levels of retinal illuminance. At the highest light level, the temporal phase decreases with increasing spatial frequency, asymptoting at about zero degrees at high spatial frequencies, which is expected for the center mechanism of an ON-center cell. The difference in temporal phase between low spatial frequency and high spatial frequency becomes smaller at lower light levels.

4.2 Fits of Gaussian center-surround model with gratings

Figure 4-2 shows the responsivity and phase (filled circles) and the Gaussian fits (solid lines) of an ON-center X-cell's frequency responses to gratings of different spatial frequencies measured at 3 light levels (2.5, - 1.5, - 2.5 log cat td). Figure 4-3 shows the responsivity and phase (filled circles) and the Gaussian fits (solid lines) of an ON-center Y-cell's frequency responses to gratings of different spatial frequencies measured at 3 light levels (2.5, - 2, - 3 log cat td). The data were fitted with the Gaussian center-surround receptive field model (solid lines) using a standard nonlinear optimization routine in Matlab. These fits allow us to quantify the characteristic changes in receptive-field properties. As shown in the figures, the model fits successfully capture the major features of the responses at

all light levels explored. The median RMS (root mean standard error) values for all fits of this study was 0.16 ([0.11, 0.26], $n = 236$). Hence, a set of data for each cell at one light level can be reduced reliably to a description in terms of the six parameters (r_c , r_s , K_c , K_s , ρ_c and ρ_s) of the Gaussian center-surround receptive field model.

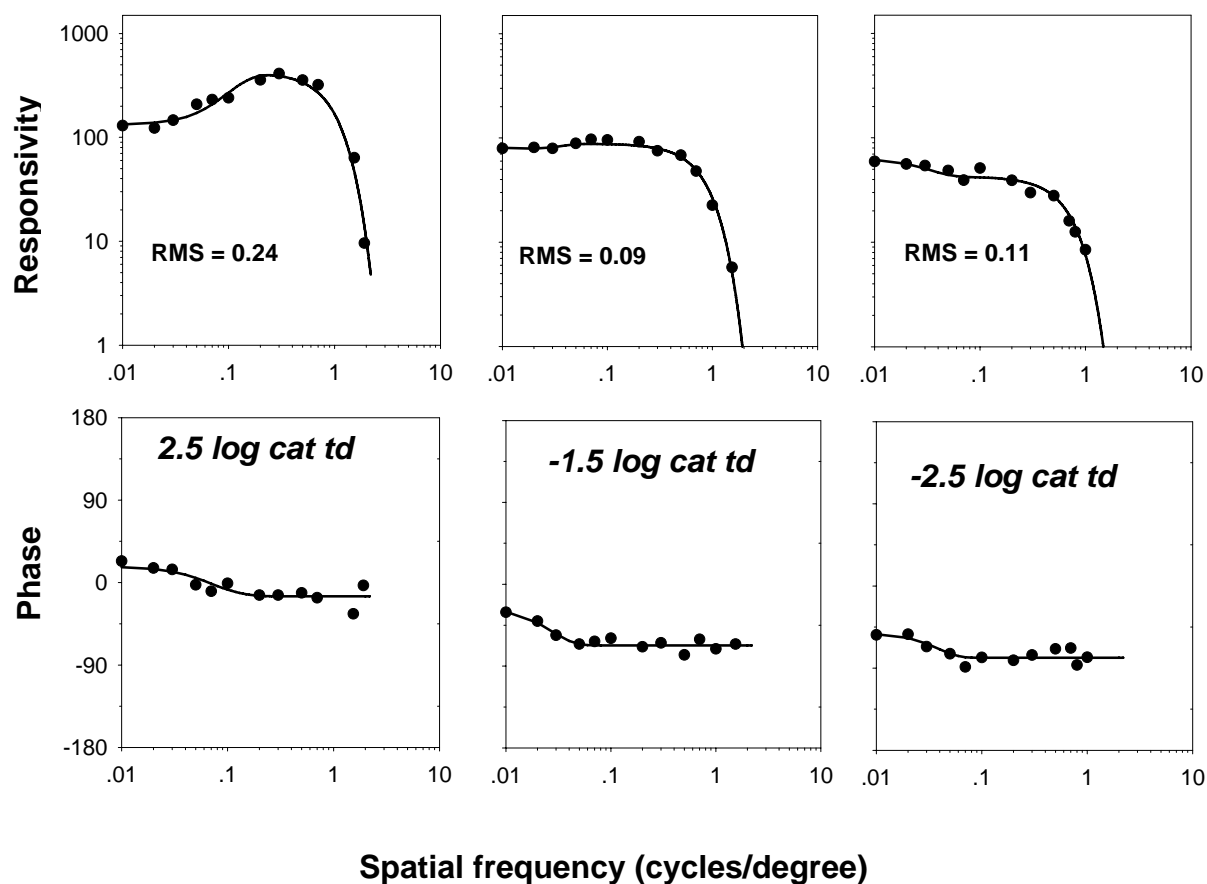


Figure 4-2: Frequency responses (solid circles: responsivity and temporal phase) for sinusoidal gratings of different spatial frequencies of an ON-center X-cell (J1208) measured at three light levels (2.5, - 1.5, - 2.5 log cat td) and fitted with the Gaussian center-surround receptive field model (solid lines). The illuminance and RMS are noted on the responsivity panel of each plot (td: troland; RMS: root mean standard error)

The Gaussian receptive field center radius (r_c) is determined primarily by the high-spatial frequency limb of the responsivity versus spatial-frequency plot (Linsenmeier et al., 1982). The radius of the surround mechanism (r_s) is determined mostly by the form of attenuation in responsivity and advance in temporal phase at low spatial frequencies. The integrated responsivity of the Gaussian center mechanism (K_c) is mainly determined by the peak responsivity of cell. The integrated responsivity of the surround is determined by the relationship between the cell's peak responsivity, the amount of attenuation in responsivity at low spatial frequencies, and the temporal phase of the cell's response at low spatial frequencies relative to its phase at high spatial frequencies. The phase of the model's center mechanism (ρ_c) is determined by the phase of the cell's response at high spatial frequencies. The phase of the surround (ρ_s) is determined by the degree of phase advance as well as responsivity attenuation at low frequencies.

Radii and integrated responsivities of center and surround mechanism (r_c , r_s , K_c , K_s) estimated from the Gaussian fits to each cell were normalized with respect to their values at the highest photopic illuminance (2.5 log cat td in this study). This normalizing takes out the variation in responsivity that might occur over time and the effect eccentricity has on receptive field size. To specify how the properties of the receptive field change with adapting light, we then compared normalized radii and responsivities, center phase, surround phase and the difference between center and surround phase as a function of mean retinal illuminance (log cat td).

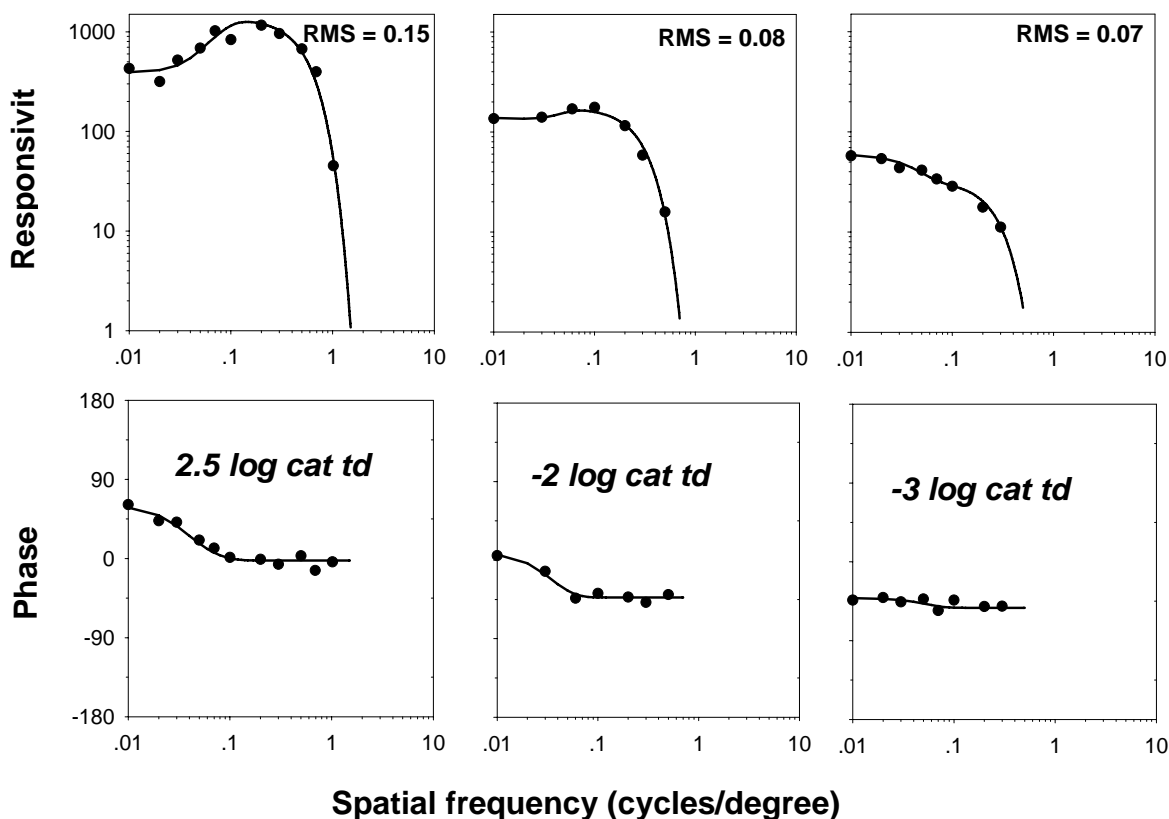


Figure 4-3: Frequency responses (solid circles: responsivity and temporal phase) for sinusoidal gratings of different spatial frequencies of an ON-center Y-cell (J0430) measured at three light levels (2.5, - 2, - 3 log cat td) and fitted with the Gaussian center-surround receptive field model (solid lines). The illuminance and RMS are noted on the responsivity panel of each plot (td: troland; RMS: root mean standard error)

4.2.1 Dependence of center radius on light level

From a number of studies, we know that the radius of the center of the retinal ganglion cell receptive field is invariant at photopic light levels, where cell responses are cone-dominant (Chan et al. 1992; Troy et al., 1993; Troy et al., 1999). A modest expansion in center size under scotopic conditions has been reported in many studies (Barlow et al., 1957;

Cleland & Enroth-Cugell, 1968; Enroth-Cugell et al., 1977; Chan et al., 1992; Troy et al., 1993; Troy et al., 1999). Our data are mostly consistent with these earlier studies at photopic and higher scotopic light levels. Center size is constant at light levels higher than 1.5 log cat td (photopic range), but expands slightly at lower light levels (the mesopic and high scotopic range).

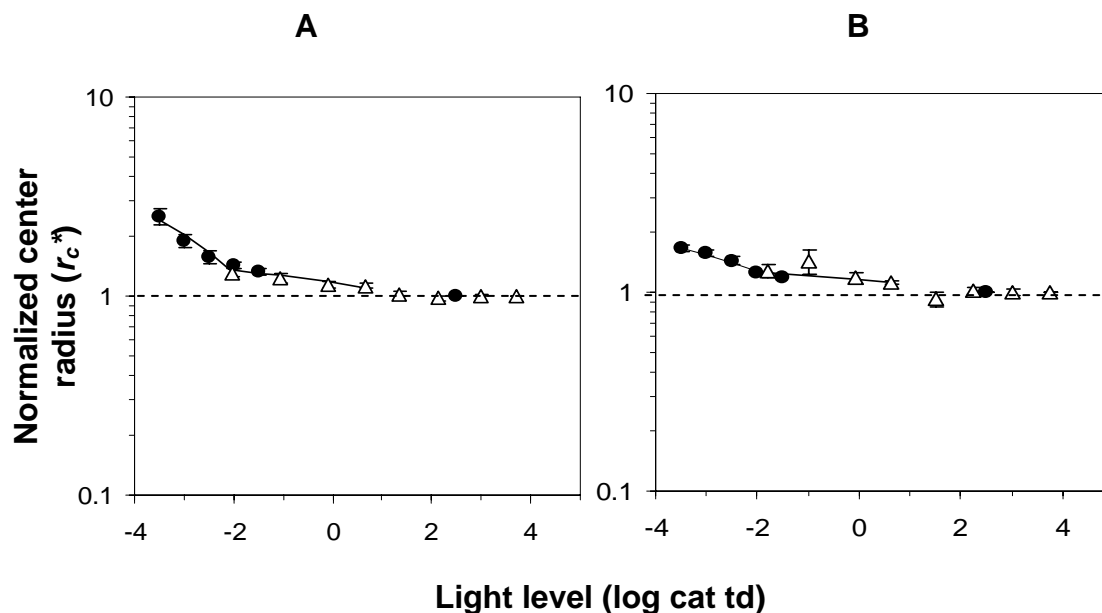


Figure 4-4: Dependence of normalized center radius (r_c^*) upon retinal illuminance. A: Data from ON-X cells; B: Data from ON-Y cells. Open triangles are previous data from the lab (Troy et al., 1993; Troy et al., 1999); Filled circles are new data. Each symbol represents the mean value of r_c^* at that illuminance. Normalized center radius (r_c^*) = center radius at that illuminance (r_c) / center radius at highest light level (2.5 and 3.8 log cat td for new data and previous data respectively). A value > 1 (the horizontal dashed line) indicates an expansion in center radius. Solid lines are the best-fitting lines of regression. The error bar is ± 1 S.E. in length. For most of data points plotted in panels A and B ± 1 S.E. is no larger than the symbol.

However, at lower scotopic light levels (from - 2 to - 3.5 log cat td) we found that center radius expands more significantly than at higher scotopic light levels (Fig. 4-4). The log-log slope of the dependence of r_c upon light level is 0.09 for ON-X cells and 0.05 for ON-

Y cells from 0.5 to $-2 \log \text{cat td}$ and is 0.73 for ON-X cells and 0.27 for ON-Y cells below $-2 \log \text{cat td}$. At the lowest light level ($-3.5 \log \text{cat td}$), the ON-X cell's center radius is 250% its photopic size and the ON-Y cell is 170% its photopic size.

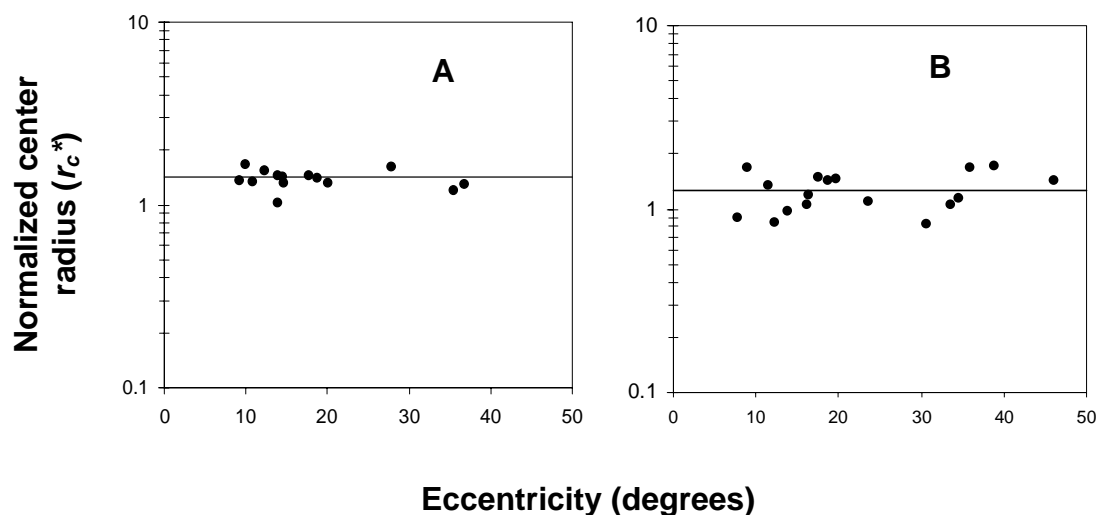


Figure 4-5: Expansion in scotopic center radius is independent of Eccentricity. Plots of normalized center radius as a function of retinal eccentricity at $-2 \log \text{cat td}$ for ON-X cells (A) and ON-Y cells (B). Each symbol represents the value of r_c^* of one cell. The solid lines are the mean value of r_c^* at $-2 \log \text{cat td}$ ($r_{c^* \text{ mean}} = 1.42$ and 1.25 for ON-X and ON-Y cells respectively).

There seems a disagreement in our data (large expansion in center size below $-2 \log \text{cat td}$) and the literature (no or small expansion in center size under scotopic conditions). This discrepancy might be because the range of light levels investigated in this study was rarely explored in previous work. Also, the amount of expansion in center radius under scotopic conditions might correlate with the cone-rod ratio. One assumption is that the retina adjusts the area containing rods feeding a ganglion cell to make combined rod signal that drives the ganglion cell under scotopic conditions proportional to the cone signal which drives it in the

photopic range. Most of our data were collected from cells located over the range $10^\circ \sim 40^\circ$, where the cone-rod ratio is nearly constant, and show that the expansion in center radius is invariant with the retinal location of the cell (Fig. 4-5). It is possible that the extent of center expansion varies with eccentricity over the range $< 10^\circ$, where the cone-rod ratio increases dramatically with decreasing eccentricity.

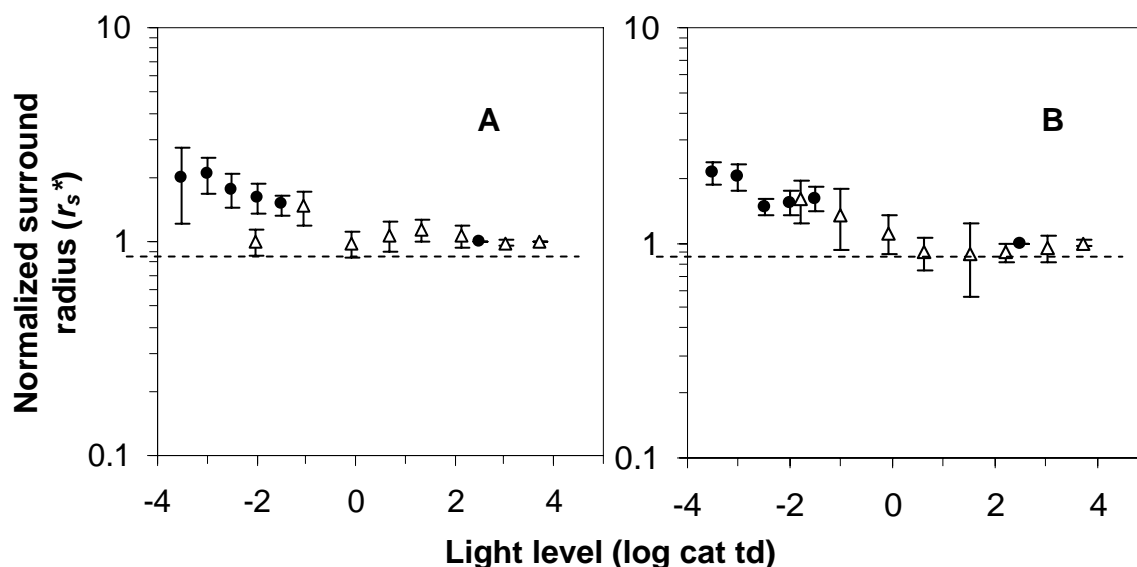


Figure 4-6: Dependence of normalized surround radius (r_s^*) upon retinal illuminance. A: Data from ON-X cells; B: Data from ON-Y cells. Open triangles are previous data from the lab (Troy et al., 1993; Troy et al., 1999); Filled circles are new data. Each symbol represents the mean value of r_s^* at that illuminance. Normalized surround radius (r_s^*) = surround radius at that illuminance (r_s) / surround radius at highest light level (2.5 and 3.8 log cat td for new data and previous data respectively). A value > 1 (the horizontal dashed line) indicates an expansion in surround radius. The error bar is ± 1 S.E. in length.

4.2.2 Dependence of surround radius on light level

Figure 4-6 shows changes in surround radius (r_s) at low light levels (filled circles) (-1.5 ~ -3.5 log cat). Data from earlier studies (open triangles) (Troy et al., 1993; Troy et al.,

1999) are shown for comparison. The extent of expansion in surround radius is similar to that of the center radius (Fig. 4-7). Our data are therefore consistent with the hypothesis that the ratio r_s / r_c for X- and Y-cells is invariant with illuminance within both the photopic and scotopic ranges (-3.5 ~ 4 log cat td).

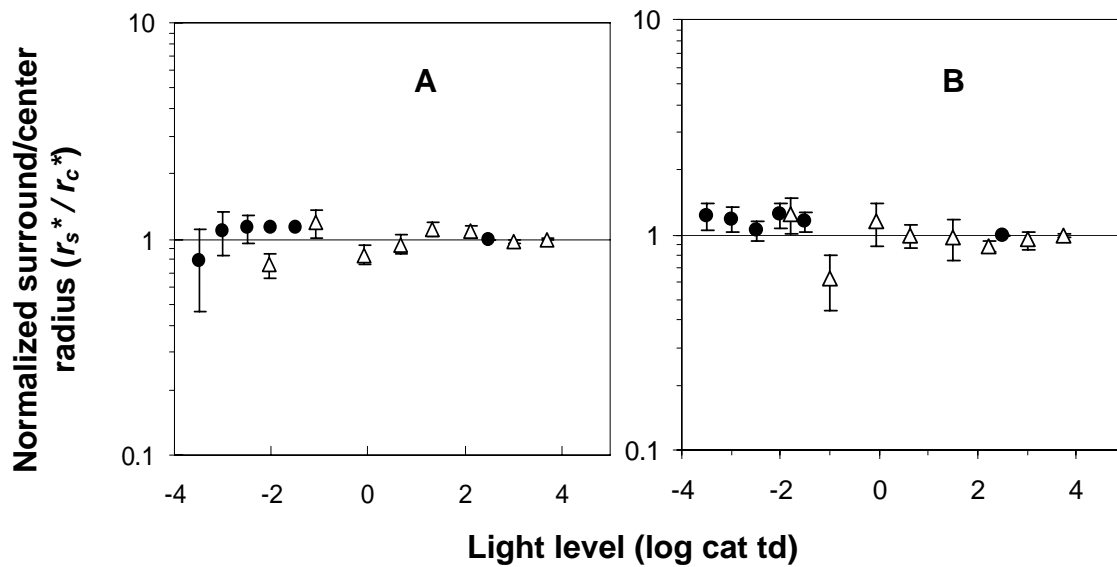


Figure 4-7: The ratio of normalized surround radius to normalized center radius (r_s^* / r_c^*) versus retinal illuminance. A: Data from ON-X cells; B: Data from ON-Y cells. Open triangles are previous data from the lab (Troy et al., 1993; Troy et al., 1999); Filled circles are new data. Each symbol represents the mean value of r_s^* / r_c^* at that illuminance. The error bar is ± 1 S.E. in length.

4.2.3 Dependence of center responsivity on light level

The relationship between the responsivity (Kc) of the retinal ganglion cell's receptive field center and mean light level is plotted in Fig. 4-8. The center responsivity obtained from experiments using sinusoidal grating stimuli is a measure of the integrated strength of the center mechanism (the integral of the red Gaussian in Fig. 2-8). All the data in Fig. 4-8 are

normalized by photopic values so they show the drop in responsivity relative to the photopic norm. The points shown as open triangles are data from earlier studies (Troy et al., 1993; 1999). The points shown as filled circles are new data collected at lower light levels.

From the earlier work in the lab, we have found that there was a clear transition in receptive field properties at a luminance of $\sim 1.5 \log \text{ cat td}$ which can be clearly seen in the figure. For both X- and Y- cells we found that the responsivity is invariant under presumed cone-dominated conditions ($I > 1.5 \log \text{ cat td}$). Below this transition light level, where we believe that ganglion cell responses shifted from cone-dominance to rod-dominance, responsivity was found to decline with retinal illuminance with log-log slopes of 0.24 ± 0.02 for X-cells and 0.27 ± 0.03 for Y-cells. The new data indicate there is another transition at a luminance of $-2 \log \text{ cat td}$. Below this light level the responsivity declines more steeply with log-log slopes of 0.56 ± 0.08 for X-cells and 0.67 ± 0.17 for Y-cells.

In earlier increment threshold studies (Shapley et al., 1972; Enroth-Cugell & Lennie, 1975), small fixed-sized spots of light were used as stimuli. In this case, if spot size were optimized for the photopic condition, as it typically was, it will progressively stimulate the center mechanism sub-optimally as one descends in background luminance through the scotopic range because of center expansion. However with our grating stimuli we can estimate the receptive field center responsivity when fully stimulated. Thus, in order to compare our results with earlier increment threshold studies we need to make allowance for the receptive field center expansion that occurs under scotopic conditions as illustrated above. For this purpose, peak center responsivity (k_c) was calculated in our study, which corresponds to the

height of Gaussian center (the red part in Fig. 2-8). To determine the peak center responsivity (k_c) we need to take into account changes in receptive field center size with light level:

$$k_c = K_c / \pi r_c^2 \quad (10)$$

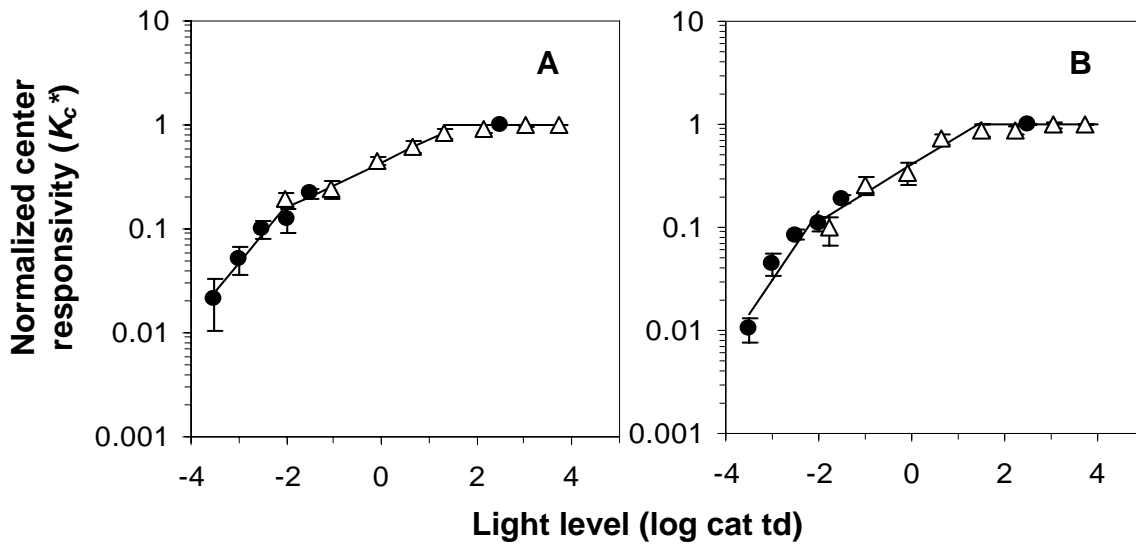


Figure 4-8: Dependence of normalized center responsivity (K_c^*) upon retinal illuminance. A: Data from ON-X cells; B: Data from ON-Y cells. Open triangles are previous data from the lab (Troy et al., 1993; Troy et al., 1999); Filled circles are new data. Each symbol represents the mean value of K_c^* at that illuminance. Normalized center responsivity (K_c^*) = center responsivity at that illuminance (K_c) / center responsivity at highest light level (2.5 and 3.8 log cat td for new data and previous data respectively). Solid lines are the best-fitting lines of regression. The error bar is ± 1 S.E. in length.

As shown in Fig. 4-9, normalized peak responsivity (k_c^*) ($k_c^* = k_c / k_{c,m}$, $k_{c,m}$ is the k_c measured at highest light level) of the Gaussian center mechanism is plotted versus mean retinal illuminance. The points shown as open symbols are data from earlier studies (Troy et al., 1993; Troy et al., 1999). The points shown as filled symbols are the new data collected at

lower light levels. It is clear that the dependence of the peak center responsivity on light level falls into three ranges. As noted above, the center size is constant in the cone dominant range ($1.5 \sim 4 \log \text{ cat td}$) therefore the peak center responsivity is invariant like responsivity itself. The zero slope of the relationship between $\log K_c^*$ and $\log I$ indicates that ganglion cell responses follow Weber's law in the cone-dominated range. Within the rod dominant range ($-3.5 \sim 1.5 \log \text{ cat td}$), there are two distinct parts to the dependency. At light levels below $\sim -2 \log \text{ cat td}$, peak center responsivity rises essentially linearly (with log-log slopes of 1.0 ± 0.1 for ON-center X-cells and 0.95 ± 0.1 for ON-center Y-cells) with mean retinal illuminance. These results are quantitatively consistent with earlier increment threshold studies and the linear law applies therefore in this lower scotopic range. A log-log slope of one on the responsivity vs. illuminance plot (Fig. 4-9) corresponds to a horizontal line on the log increment threshold vs. illuminance plot (Fig. 2-10, left panel). At light levels above $\sim -2 \log \text{ cat td}$, peak center responsivity rises with a shallower slope. The slope lines of these two parts intersect at a light level of $-2.3 \log \text{ cat td}$ for ON-center X-cells and $-2.4 \log \text{ cat td}$ for ON-center Y-cell. This is where each rod captures a photon every 20 seconds. This lower transitional point corresponds well with the background level at which a switch from the linear range to the DeVries-Rose range is seen in increment threshold studies of cat retinal ganglion cells (Enroth-Cugell & Shapley, 1973a, b; Enroth-Cugell & Lennie, 1975; Enroth-Cugell et al., 1977a, b; Harding & Enroth-Cugell, 1978). As might be expected from earlier increment threshold measurements, the relationship between responsivity and retinal illuminance should have a log-log slope of 0.5 as the retina moves into a range of DeVries-Rose Law behavior. However, we found that for both X- and Y- cells the relationship between

k_c^* and I have log-log slopes smaller than 0.5 (0.27 ± 0.02 for X-cells and 0.3 ± 0.04 for Y-cells).

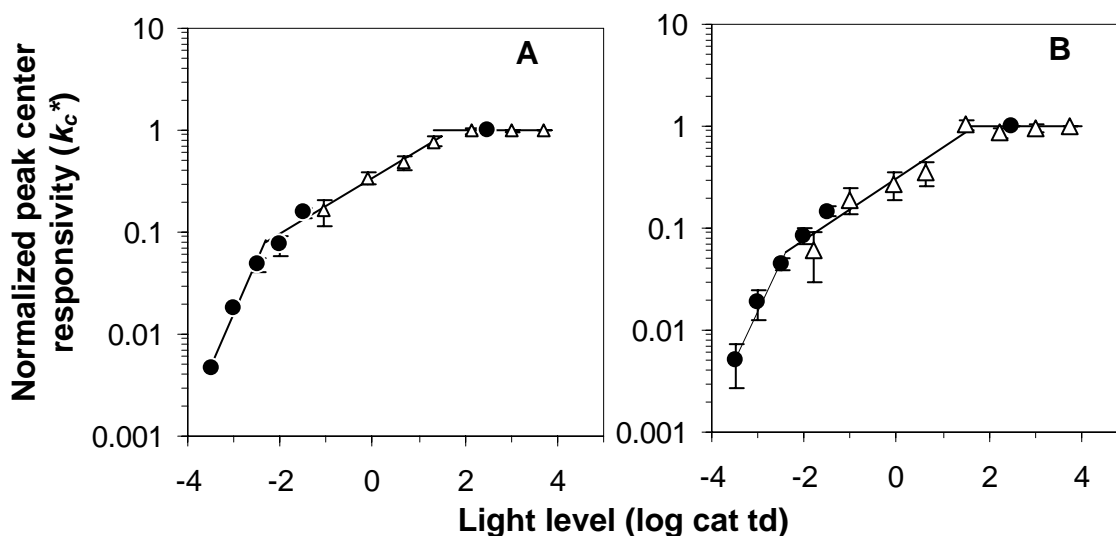


Figure 4-9: Dependence of normalized peak center responsivity (k_c^*) upon retinal illuminance. A: Data from ON-X cells; B: Data from ON-Y cells. Open triangles are previous data from the lab (Troy et al., 1993; Troy et al., 1999); Filled circles are new data. Each symbol represents the mean value of k_c^* at that illuminance. Normalized peak center responsivity (k_c^*) = peak center responsivity at that illuminance (k_c) / peak center responsivity at highest light level (2.5 and 3.8 log cat td for new data and previous data respectively). Solid lines are the best-fitting lines of regression. The error bar is ± 1 S.E. in length.

4.2.4 Dependence of surround responsivity on light level

Previous work found that, while the responsivities of center and surround are reasonably balanced under photopic conditions, surround responsivity declines somewhat more with decreasing mean light level than does center responsivity under scotopic conditions. It has been asserted in the vision literature that the surround disappears under scotopic conditions (Rodieck & Stone, 1965; Maffei et al., 1971; Yoon, 1972; Cleland et al., 1973;

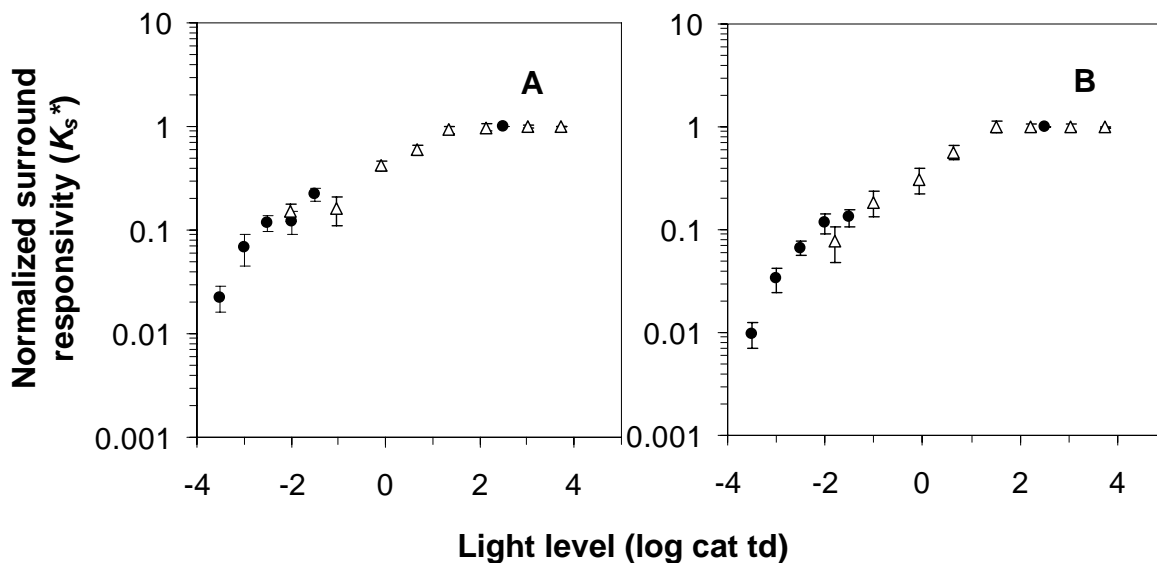


Figure 4-10: Dependence of Normalized surround responsivity (K_s^*) upon retinal illuminance. A: Data from ON-X cells; B: Data from ON-Y cells. Open triangles are previous data from the lab (Troy et al., 1993; Troy et al., 1999); Filled circles are new data. Each symbol represents the mean value of K_s^* at that illuminance. Normalized surround responsivity (K_s^*) = surround responsivity at that illuminance (K_s) / surround responsivity at the highest light level (2.5 and 3.8 log cat td for new data and previous data respectively).

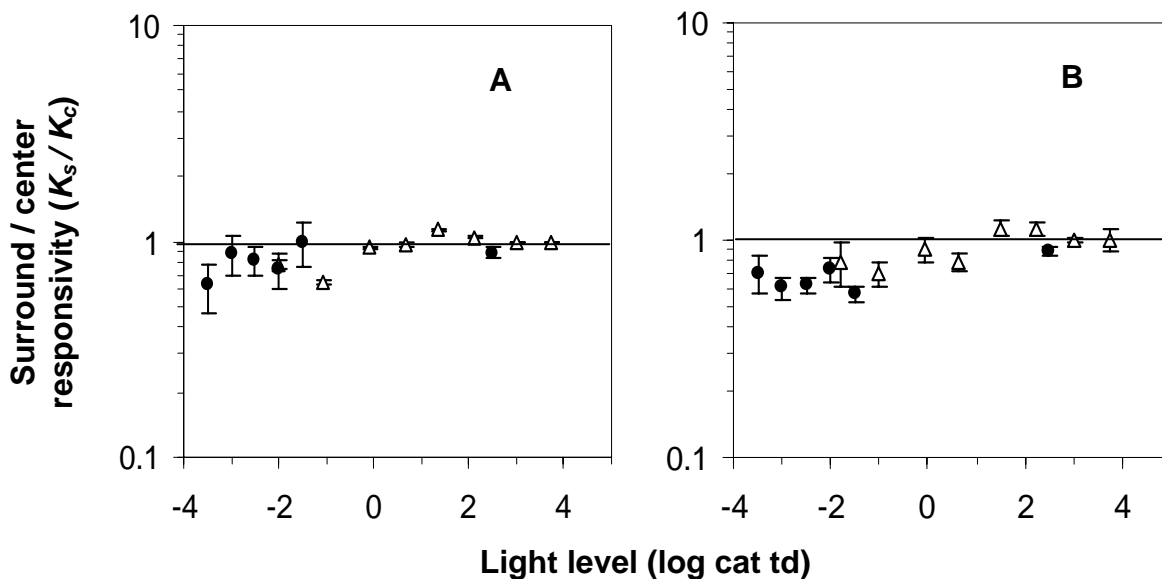


Figure 4-11: The ratio of surround responsivity to center responsivity (K_s / K_c) vs. retinal illuminance. A: Data from ON-X cells; B: Data from ON-Y cells. Open triangles are previous data from the lab (Troy et al., 1993; Troy et al., 1999); Filled circles are new data. Each symbol represents the mean value of K_s / K_c at that illuminance. The error bar is ± 1 S.E. in length.

Barlow & Levick, 1976; Muller & Dacheux, 1997). However our data indicate that the surround remains present throughout the scotopic range (Fig. 4-10). The ratio K_s / K_c is essentially one in the illuminance range 1.5 to 4 log cat td. Below 1.5 log cat td, the ratio has a value significantly less than this and it declines with decreasing light level until - 2 log cat td, below which it remains at a constant level of ~ 0.6 (Fig. 4-11).

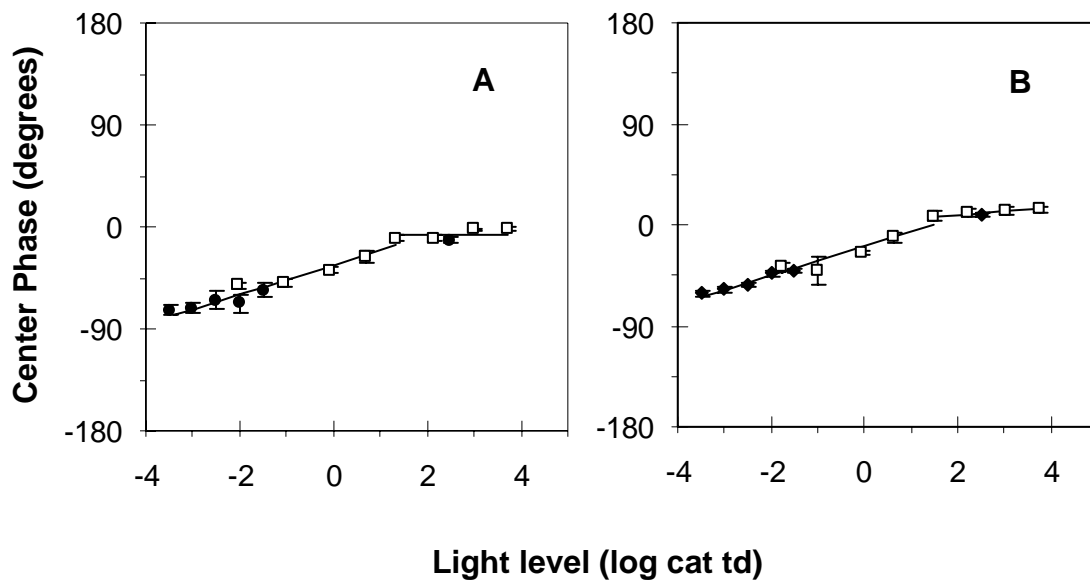


Figure 4-12: Dependence of center phase (ρ_c) upon retinal illuminance. A: Data from ON-X cells; B: Data from ON-Y cells. Open triangles are previous data from the lab (Troy et al., 1993; Troy et al., 1999); Filled circles are new data. Each symbol represents the mean value of ρ_c at that illuminance. Solid lines are the best-fitting lines of regression. The error bar is ± 1 S.E. in length.

4.2.5 Dependence of center and surround phase on light level

Center and surround phase lags increase progressively as light level falls (Figs. 4-12 and 4-13). Open symbols are data from earlier work in the lab (Troy et al., 1993; Troy et al., 1999) and filled symbols are the new data. For the phase of the center mechanism, there

seemed to be two distinct ranges with a transition occurring over the range 1 to 2 log cat td.

The phase lag of the center has a much less pronounced dependence on light level above this transition point but increases significantly more rapidly with decreasing light level below this transition (Fig. 4-12). This abrupt transition in phase lags can be explained by the shift from a response of the cell that receives cone dominated signals to one that receives rod dominated signals. The phase lag of the surround mechanism seemed to be divided into 3 ranges with one transition occurring over a similar range to the one that happened for the center mechanism, but less obviously. The second transition occurs at ~ -1.5 log cat td and was more abrupt (Fig. 4-13), indicating that there might be a change in the circuitry that underlies the surround at this light level.

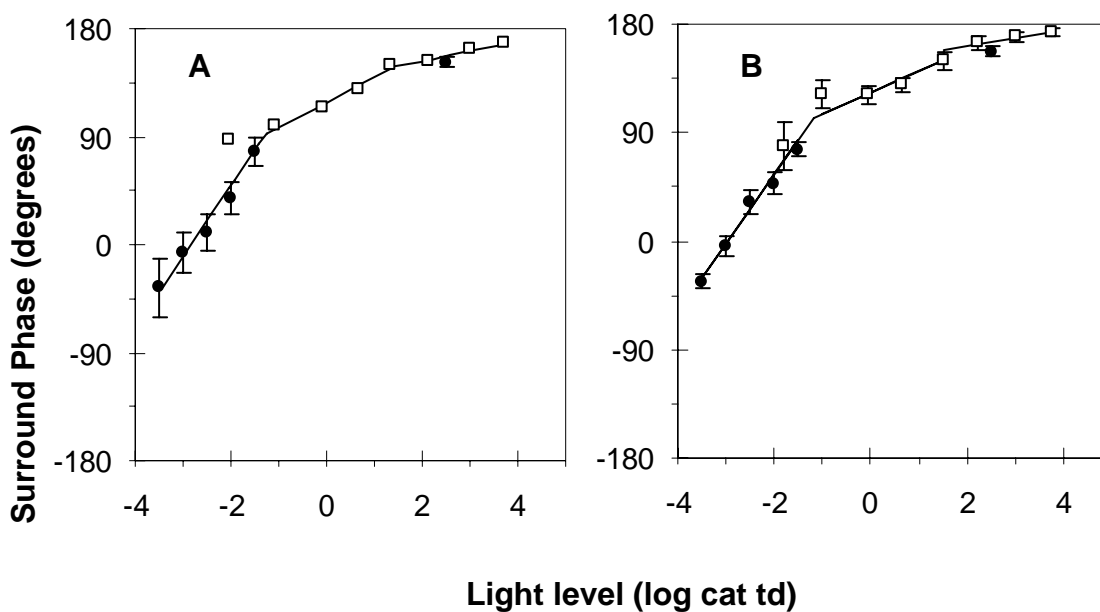


Figure 4-13: Dependence of surround phase (ρ_s) upon retinal illuminance. A: Data from ON-X cells; B: Data from ON-Y cells. Open triangles are previous data from the lab (Troy et al., 1993; Troy et al., 1999); Filled circles are new data. Each symbol represents the mean value of ρ_s at that illuminance. Solid lines are the best-fitting lines of regression. The error bar is ± 1 S.E. in length.

4.2.6 Phase difference between center and surround

Fig. 4-14 shows that the difference in phase between the center and surround mechanisms of X- and Y- cells decreases progressively with decreasing light level. There is one transition occurring at ~ -1.5 log cat td that divided the relationship into two parts. Over the range of illuminances 4 to -1.5 log cat td, the phase difference decreases slightly. From -1.5 to -3.5 log cat td, the phase difference decreases greatly which makes the center and surround signals less antagonistic, even approaching synergy at the lowest scotopic levels. Our result is consistent with the observation of a longer latency difference between the center and surround with decreasing background illuminance reported by Enroth-Cugell and Lennie (1975).

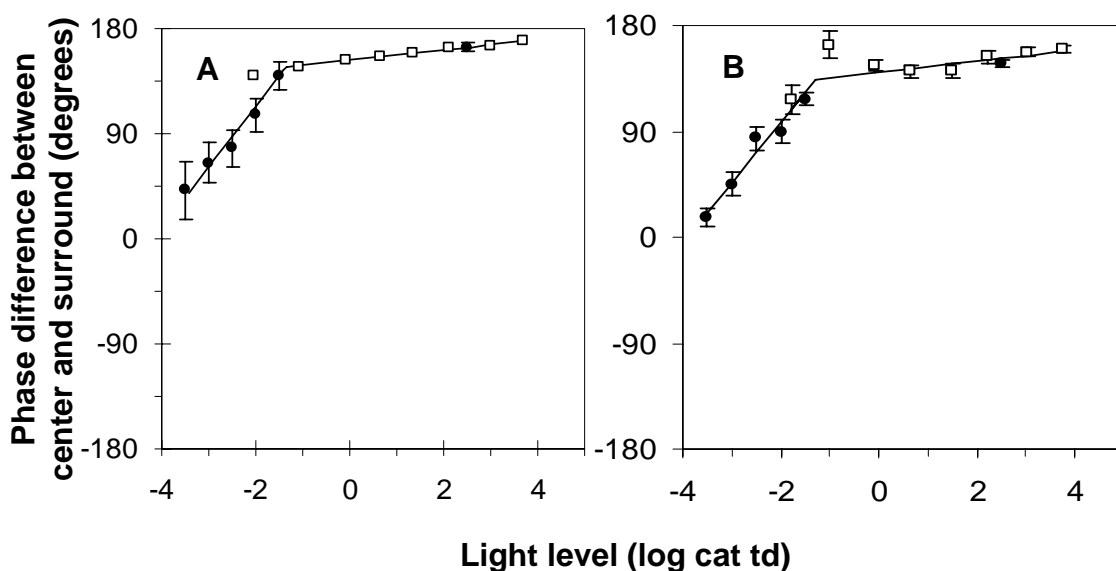


Figure 4-14: Dependence of phase difference between center and surround ($\rho_s - \rho_c$) upon retinal illuminance. A: Data from ON-X cells; B: Data from ON-Y cells. Open triangles are previous data from the lab (Troy et al., 1993; Troy et al., 1999); Filled circles are new data. Each symbol represents the mean value of $\rho_s - \rho_c$ at that illuminance. Solid lines are the best-fitting lines of regression. The error bar is ± 1 S.E. in length.

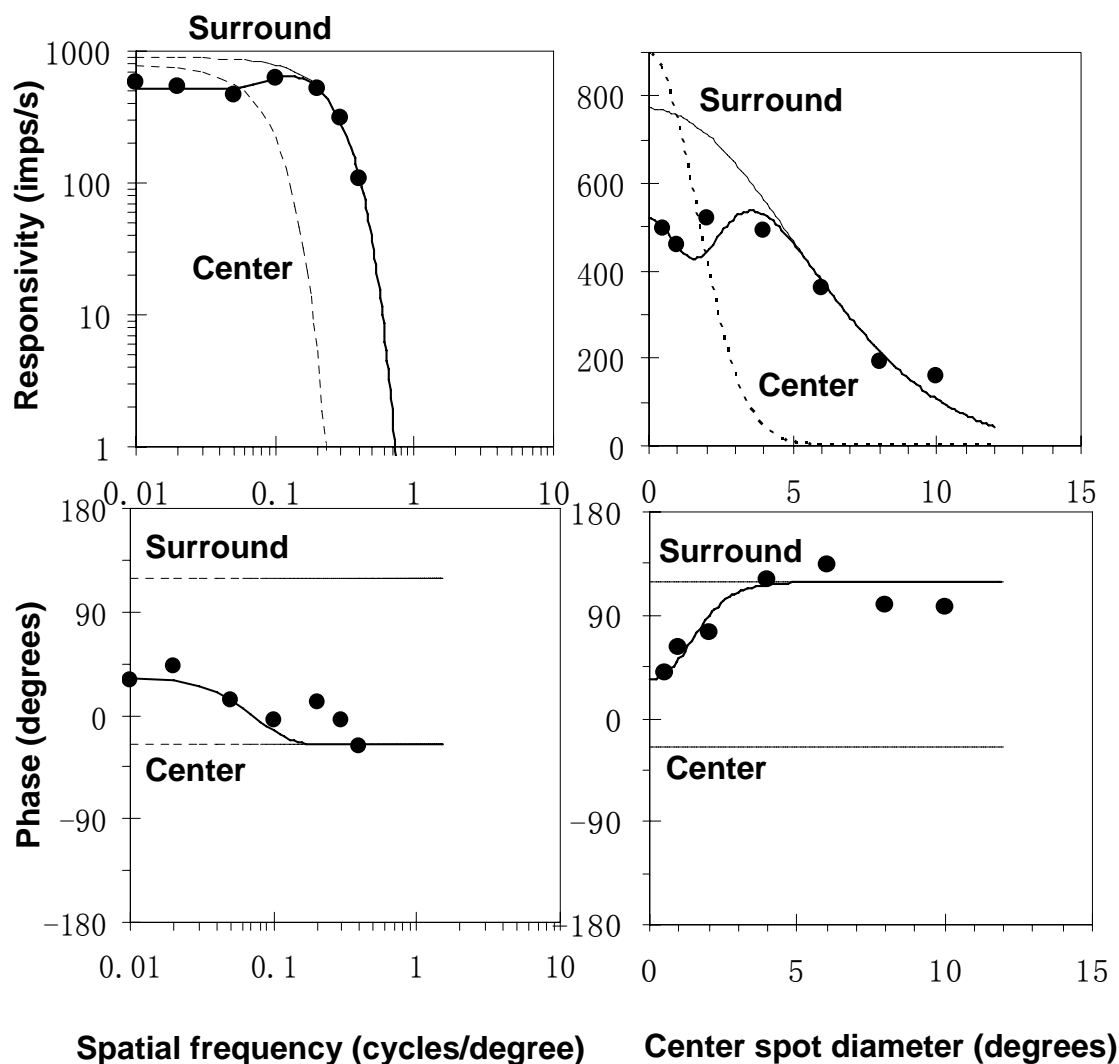


Figure 4-15: Sets of responsivity and phase measurements for spatial-frequency response (left) and responses to the surround-isolating stimuli (right) of an ON-Y cell (J1802) measured at 2.58 log cat td. The smooth curves running through the points represent the prediction of frequency responses for the Gaussian center-surround model which best fit the data. Center spot diameter is the diameter of the center spot of constant luminance of the surround-isolating stimulus. The dashed lines represent the center and surround component predicted by the Gaussian center-surround model.

4.3 Frequency responses and Gaussian center-surround model fits for surround-isolating stimulus

Figure 4-15 and Figure 4-16 show the responsivity (upper panels) and phase (lower panels) for an ON-center Y cell's (J1802) spatial-frequency responses to grating (left panels) and surround-isolating (right panels) stimuli. Figure 4-15 shows the data collected at 2.5 log cat td and Figure 4-16 shows the data collected at -2 log cat td. The responses to the surround-isolating stimuli are very characteristic. As shown in Figure 4-15 and 4-16, the responsivities for the surround-isolating stimuli became smaller as the adapting light level was reduced. There is an obvious tendency for a phase advance for surround-isolating stimuli occurs with increasing center spot diameter is obvious. This phase advance can be explained by the shift from a response of the cell that is the resultant of signals from both center and surround to one that is the result of surround signals alone. The Gaussian center-surround model was fit to the response to the grating stimuli, and a measure of the parameters (r_c , r_s , k_c , k_s , ρ_c , ρ_s) that characterize the receptive field was obtained. Then the responsivities and phases of responses to the surround-isolating stimuli were predicted from the model's parameters obtained with the grating data. As shown in Figures 4-15 and 4-16, the model's prediction and the measured data correspond well (right panels). This verifies that the Gaussian center-surround model can predict responses to other visual stimuli, not just responses to sinusoidal gratings.

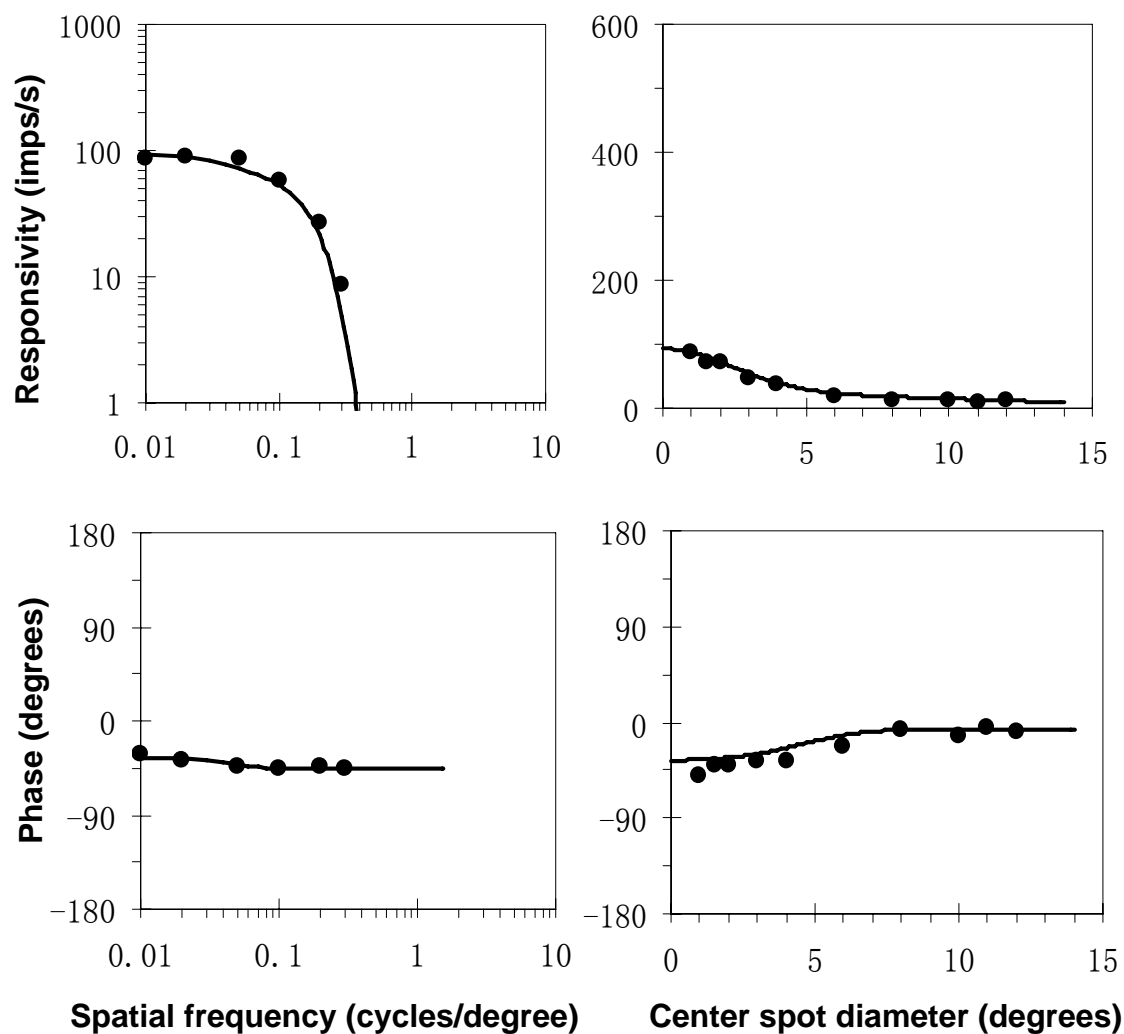


Fig. 4-16: Sets of responsivity and phase measurements for spatial-frequency response (left) and responses to the surround-isolating stimuli (right) of an ON-Y cell (J1802) measured at $-1.92 \log \text{ cat td}$. The smooth curves running through the points represent the prediction of frequency responses for the Gaussian center-surround model which best fit the data in the left hand panels.

Therefore, by fitting the Gaussian center-surround model to the data collected with the surround-isolating stimuli, we are able to obtain the parameters that characterize the receptive field independently from those estimated from measurements made with the grating stimuli. Figure 4-17 shows the center and surround phases measured with the gratings and surround-isolating stimuli respectively. Although the phases measured with surround-isolating stimuli

and gratings were slightly differential from one another, they have similar tendency in change with decreasing background illuminance. The phase difference between the center and surround mechanisms measured with surround-isolating stimuli also decrease dramatically when background illuminance declines from -1.5 to -3.5 log cat td (Fig. 4-18), which is consistent with the phase difference measured with gratings. By comparing the receptive field properties measured with two different stimuli, we further verified the reliability of the data we collected under low scotopic conditions, especially the data for the surround component.

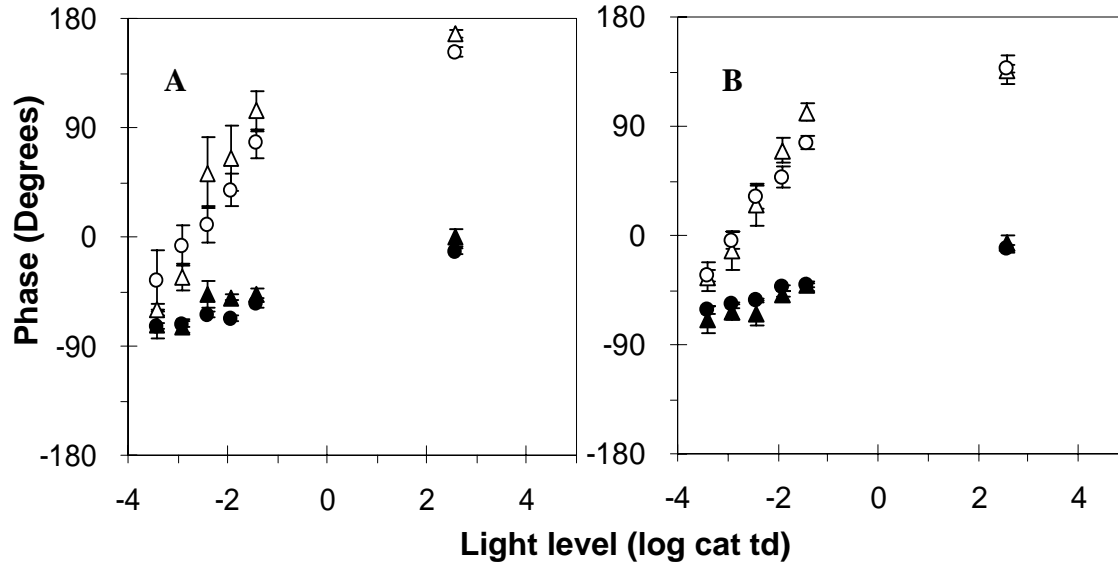


Fig. 4-17: Comparison of center (ρ_c) and surround phase (ρ_s) measured with gratings and surround-isolating stimuli. A: Data from ON-X cells; B: Data from ON-Y cells. Triangles are data from surround-isolating stimuli; Circles are data from grating stimuli. Each filled symbol is the mean value of center phase (ρ_c) at that illuminance; each open symbol is the mean value of surround phase (ρ_s) at that illuminance. The error bar is ± 1 S.E. in length.

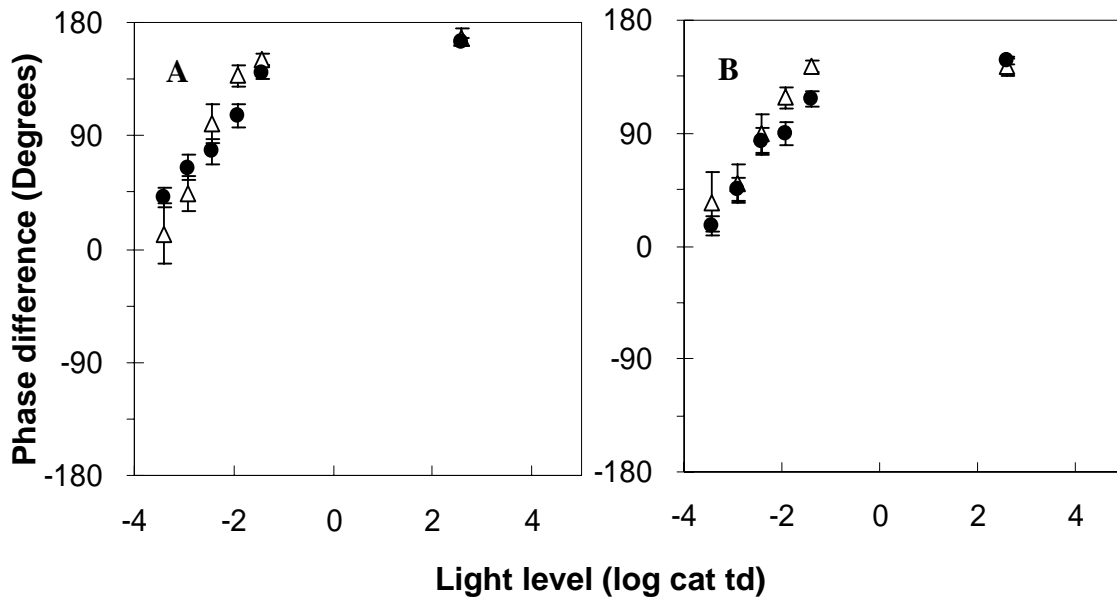


Fig. 4-18: Comparison of phase difference between center and surround ($\rho_s - \rho_c$) measured with gratings and surround-isolating stimuli. A: Data from ON-X cells; B: Data from ON-Y cells. Open triangles are data from surround-isolating stimuli; Filled circles are data from grating stimuli. Each symbol is the mean value of phase difference ($\rho_s - \rho_c$) at that illuminance. The error bar is ± 1 S.E. in length.

V. DISCUSSION

5.1 Expansion of receptive field center at low scotopic levels

There has been considerable interest in whether the size of the receptive-field center of cat retinal ganglion cells is larger under scotopic than photopic lighting. Previous work from our lab suggested that there might be a small step increase in r_c of $13 \pm 1\%$ between 1.5 and 0.5 log cat td followed by a progressive small gradual expansion at lower light levels. Results of a number of other studies have also indicated little or no change in the size of the receptive-field center when going from rod-dominated to cone-dominated conditions (Barlow et al., 1957; Cleland & Enroth-Cugell, 1968; Derrington & Lennie, 1982). At the light level where 1 photon is absorbed by a rod every 10s (-2 log cat td) there was an average expansion of 30% in radius for ON-X cells (Troy et al., 1999). This is similar to the magnitude of average expansion (35%) reported by Ahmed (1981). The center size of Y- geniculate cells at about 1000 and 0.1 photoisomerization/rod/s (corresponding to 2 and -2 log cat td respectively) measured by Kaplan et al. (1979) also indicated that the center radius under low scotopic conditions is 1.4 (median) times greater than under photopic conditions. The results of this study show a similar magnitude of expansion ($42 \pm 5\%$ for X-cells and $24 \pm 5\%$ for Y-cells at -2 log cat td). However, at light levels below -2 log cat td, we found that the expansion of receptive-field center size is more dramatic. The center radii at the lowest light level we explored (-3.5 log cat td) were on average 170% and 250% their photopic sizes for ON-Y and ON-X cells respectively. The great differential expansion of center size in X- and Y- cells ($P_2=0.007$, t-test) might be because the X-cells have much smaller receptive fields. The average photopic center radii for ON center X- and Y- cell were $82 \pm 6 \mu\text{m}$ (0.366 ± 0.027

degree) and $194 \pm 14 \mu\text{m}$ (0.866 ± 0.063 degree) respectively in our study. Thus a Y-cell receptive field center overlaps ~ 6 X-cell receptive field centers. If each X-cell's center radius expands to 250% its photopic size, the Y-cell center would expand to 165% of its center size. This is amazingly consistent with our result.

Actually, our observations might not conflict with the modest expansion in center radius found in the previous studies for the following reasons. Firstly, the stimulation used to measure receptive field size is different between ours and those of some other investigators. We determined the center size by fitting a Gaussian center-surround model to spatial-frequency responses of full screen sinusoidal gratings over a long period of time. However, Barlow et al. (1957) and most of the others cited above determined center size by increasing the size of a spot of light until the cell's response ceased to increase. Considering that the strength of the center at low scotopic levels is much less than that at higher light levels, it is possible that Barlow and others underestimated center size measured with a flashing light. Secondly, the range of light levels investigated could also play an important part. The large expansion in center size we found happens at light levels where a rod captures a photon every $30 \sim 300$ s. But the adaptation levels in most previous studies were higher than in ours. Thirdly, the locations of the cells' receptive fields that were studied might also contribute to the discrepancy in the literature on center expansion under scotopic conditions. Considering that most of our data were collected from cells located between 10 to 25 degree eccentricities, although we found no dependence of center expansion on cell eccentricity in our data, there might be more expansion for cells located in the more central region.

There is good evidence that the light dependence of AII amacrine cell receptive field centers can explain the changes in ganglion cell center radius we report in this study. Troy et al. (1999) calculated that the convergence and dendritic tree size of AII amacrine cells could account for the small expansion in center size when going from cone dominant photopic illuminance to rod dominant scotopic illuminance. A number of studies have shown that AIIs are electrically coupled to other AII cells via gap junctions formed on their distal dendrites in sublamina b of the IPL (Strettoi et al., 1990; Strettoi et al., 1992; Strettoi et al., 1994; Mills et al., 2001). The extent of coupling varies greatly; intercellular movement of biotinylated tracers has showed the network can range from ~ 20 to > 300 coupled cells (Bloomfield et al., 1997). In addition, the extent of coupling can be modulated by dopamine and is dependent upon ambient light conditions (Bloomfield et al., 1997). Changes in AII/AII coupling have been shown to reflect changes in the diameter of the receptive field center of AII cells (Bloomfield & Völgyi, 2004). At light levels higher than $0 \log \text{ cat td}$, AIIs are mostly uncoupled to each other. Below this light level, with decreasing background illuminance, the extent of coupling and, hence receptive field center size of AII cells increases. Bloomfield et al. (2004) reported an $\sim 300\%$ expansion in AII receptive field center size at about $10^{-2} \log \text{ quanta/rod/s}$ ($\sim -3 \log \text{ cat td}$) in rabbit retina. Therefore, coupling between AII cells might be the source of the big expansion of center radius we find for ON center X- and Y- cells at low scotopic light levels. Bloomfield et al., (2004) also reported that AII amacrine cells are completely uncoupled under dark-adapted conditions. However, we did not observed a decrease in center size at lowest light level we explored. Of course, it is impossible to measure center size in the absence of light.

5.2 Presence of the surround under low scotopic conditions

For the past several decades, there has been a controversy over whether or not the surround mechanism of retinal ganglion cell disappears under scotopic conditions. The idea that the surround disappears was proposed by Barlow et al. (1957) and was widely accepted by many subsequent investigators (Rodieck & Stone, 1965; Barlow & Levick, 1976; Kaplan et al., 1979; Peichl & Wässle, 1983). On the other hand, more recent work indicated that the surround is still there under scotopic conditions (Enroth-cugell & Lennie, 1975; Chan et al., 1992; Troy et al., 1993; Troy et al., 1999). Our data show that the surround may still be present under scotopic conditions, all the way down to the dark light level.

The results from spatial frequency response measurements provide good evidence that the surround is present under scotopic light levels. In Figure 4-9, it is clear that the responsivity of the surround decreases progressively all the way down to dark light level (- 3.5 log cat td). If there were no surround under scotopic conditions, the curve would cut off at some point within the scotopic range. Moreover we found that although the responsivity of the surround mechanism weakens more than the center does under scotopic conditions, it is still comparable to the responsivity of the center mechanism. As shown in Figure 4-10 at higher light levels (1.5 to 4 log cat td) the responsivities of center and surround are reasonably balanced ($K_s/K_c \approx 1$). At light levels below 1.5 log cat td, the K_s/K_c decreased with decreasing illuminance until the light level reaches - 2 log cat td. From - 2 log cat td to - 3.5 log cat td (equivalent to the dark light level) K_s/K_c is invariant with illuminance ($K_s/K_c \approx 0.6$).

We also found that in most of the cells, response phase advances with decreasing spatial frequency at low spatial frequencies at low light levels (Fig. 4-1, 4-2), which indicates that the surround is present under scotopic conditions. If there were no surround at low light levels, there would be no change in cell response phase as a function of spatial frequency. The phase advance for low spatial frequencies we observed at low light levels suggests that signals from both center and surround mechanisms are combined to underlie the spatial frequency tuning of the ganglion cell.

Besides the above evidence, we found that, for the data points we collected at low light levels, the RMS error (root-mean-square error) calculated with the Gaussian center-surround model is much lower than that calculated with a single Gaussian function which only represents a center mechanism (a model assuming there is no surround mechanism). For example, at $-3.5 \log \text{ cat td}$ (one photon absorbed every 100 sec), the RMS error for the fits with a double Gaussian model is 0.1 ± 0.01 ($n = 21$), but the RMS error for the fits with a single Gaussian model is 0.16 ± 0.02 ($n = 21$). As shown in Figure 5-1, if we apply a single Gaussian function model to the data (left panels) it gives poorer fits, especially at low spatial frequency, for both responsivity and phase compared to the fits with a double Gaussian model (right panels).

Finally, the phase and strength of the surround mechanism measured with surround-isolating stimuli are very close to those measured with gratings at low light levels.

All the evidence above indicates that the surround mechanism contributes to the cell's response under all scotopic conditions. Thus, how can we explain the historic failure to detect the surround under scotopic conditions? The idea that the surround disappears at low light levels originated from Barlow et al.'s area threshold measurements (1957) on cat ganglion cells. These investigators used spots of light as their stimuli. They found that under photopic conditions, the threshold of an ON-center ganglion cell response decreased as they increased the diameter of the light spot up to some critical size, and beyond this critical size the threshold increased with increasing spot size. This increase in threshold was attributed to antagonism from the surround mechanism of the receptive field. However, under scotopic conditions, they found the same decrease in the threshold of ganglion cell with increasing spot diameter until a critical size was reached, but no significant increase in threshold for larger spots. These results were interpreted as loss of a surround mechanism under scotopic conditions.

Similarly, in our experiments, we found that there was much less responsivity attenuation for low spatial frequency gratings at low light levels than that shown by them at higher light levels. There is little drop or even a slight increase in responsivity (Fig. 4-1, 4-2) at low spatial frequencies, especially at light levels approaching the dark light limit. The responsivity attenuation for low spatial frequency gratings under photopic conditions is equivalent to the increase in the threshold of a ganglion cell for spots larger than some critical size in Barlow et al.'s threshold measurement. Thus the result we observe under scotopic conditions is consistent with Barlow et al.'s measurements but our interpretation is different, because our measurements were more comprehensive. In our experiments, we used full-screen

grating stimuli and averaged retinal ganglion cell's response over a very long period (at - 3.5 log cat td, it took as long as 180s for each data point), so that both center and surround mechanism would be fully stimulated and the signals from both mechanisms, especially from the surround, could be extracted from the noise at low light levels.

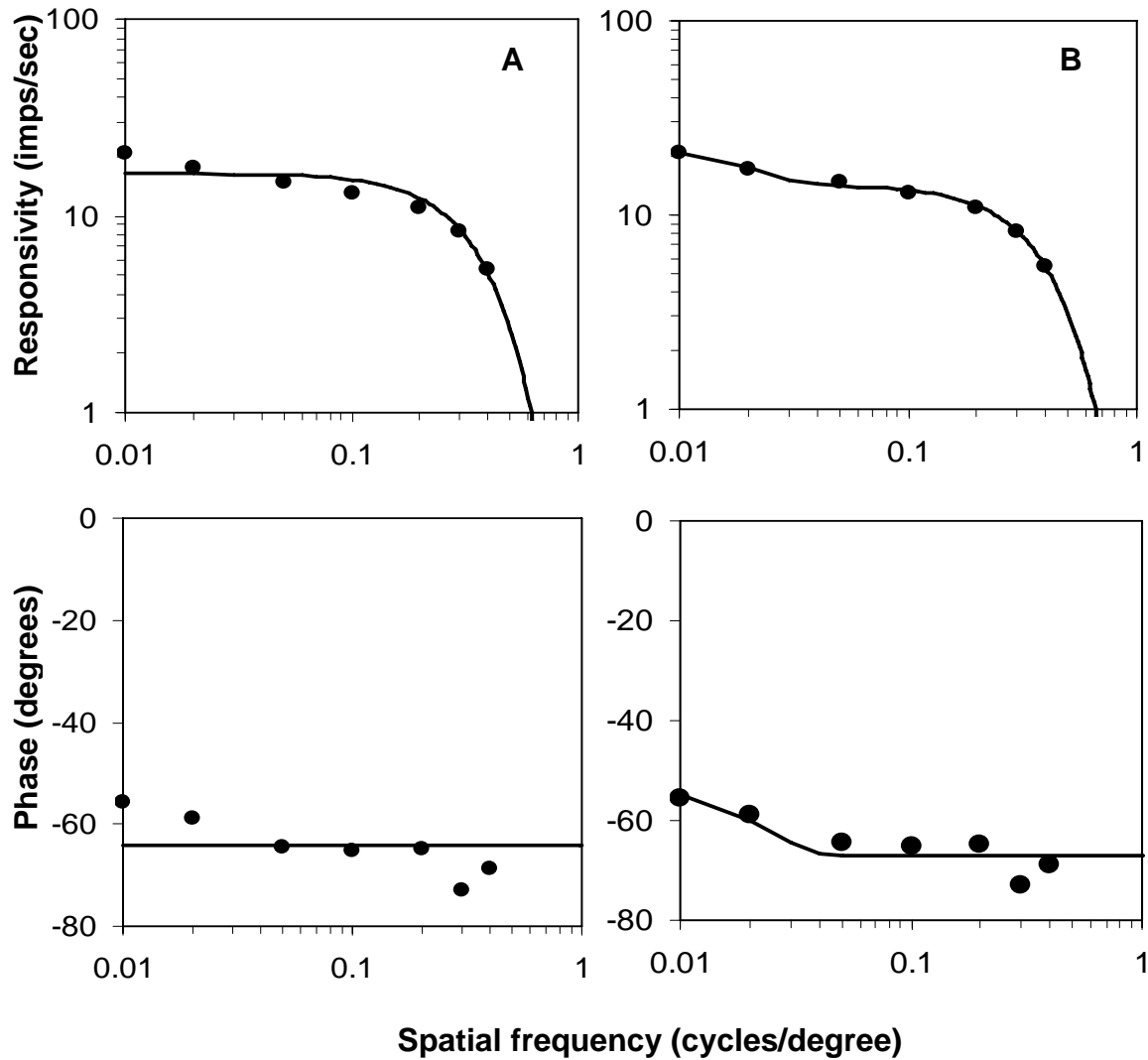


Figure 5-1: Comparison of fits with single Gaussian model and Gaussian center-surround model. Solid circles are data from an ON-Y cell (J1806) measured at - 3.5 log cat td. Solid lines are fits with Gaussian models. A. Fit with single (no surround) Gaussian model. **RMS** = 0.13; B. Fit with Gaussian center-surround model, **RMS** = 0.07

In our data, we noticed there is progressively less phase difference between center and surround mechanisms as light level is reduced. Under photopic conditions, center and surround mechanisms are antagonistic to one another and the phase difference between the two mechanisms close to 180 degrees. While the center and surround phase lags increase progressively as light level falls, the phase difference between these two mechanisms decreases with decreasing light level. As shown in Fig. 4-13, at near dark light levels, signals from center and surround have moved almost into phase with one another, which means that the center and surround mechanisms are no longer antagonistic but more synergistic with respect to one another. The loss of surround antagonism instead of a loss of the surround mechanism might be an alternative interpretation for Barlow et al.'s results and the reason that they failed to detect the surround under scotopic conditions.

The change in the phase of surround mechanisms could be due to either a summation of the classical antagonistic surround and an extra disinhibitory surround, or due to a change in phase of the antagonistic surround itself (Fig. 5-2). The disinhibitory surround, also called outer surround (Ikeda & Wright, 1972; Li et al., 1991; Li et al., 1992) is a extensive disinhibitory (in phase) region (also called outer surround, OS) surrounding the classical inhibitory (out of phase) surround of the retinal ganglion cell receptive field. It is possible that when the strength of the inhibitory surround decreases with decreasing light levels, the effect of the disinhibitory surround becomes more prominent, thus the summed 'surround' becomes more in phase with the center. However, to date, all the data supporting disinhibitory surrounds have been obtained under photopic conditions. It is unknown whether a disinhibitory surround is present under scotopic conditions. For the second reason, since the

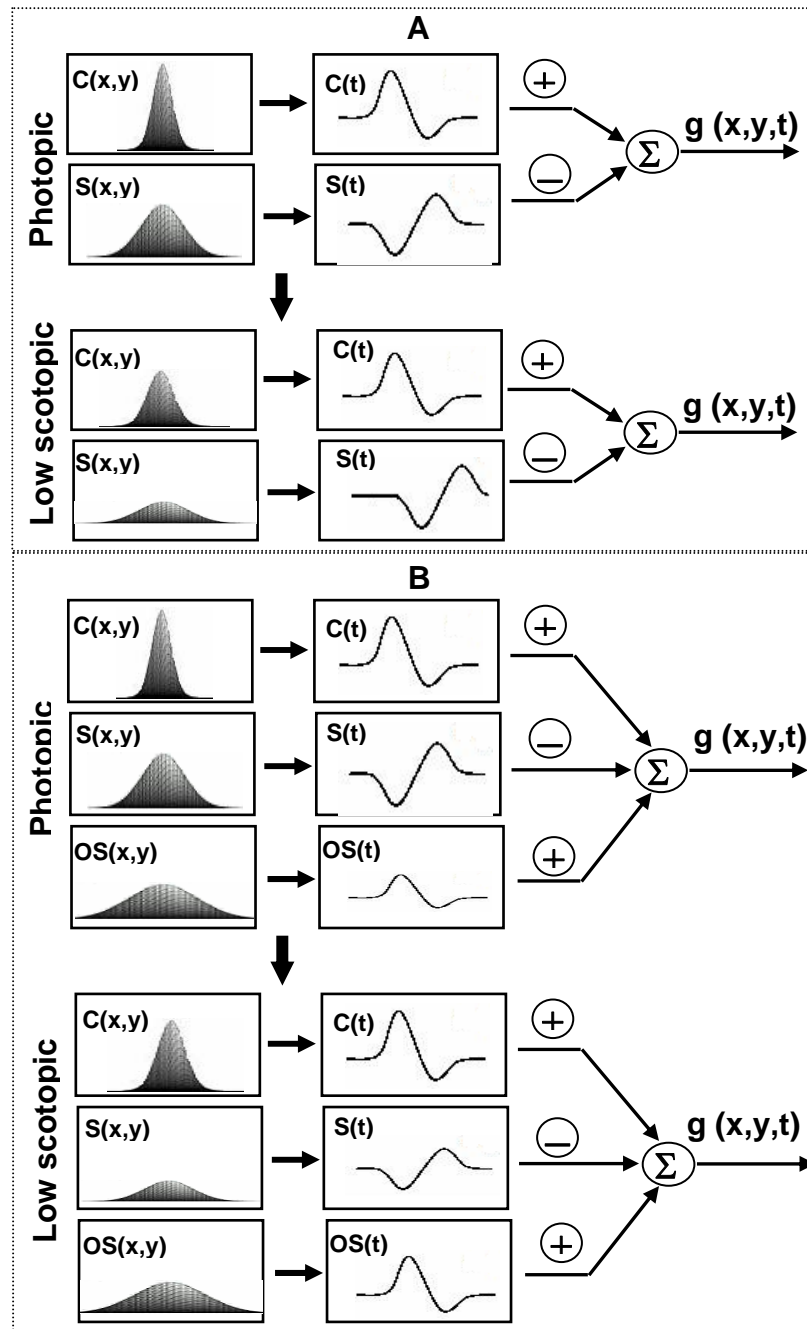


Figure 5-2: Two models that explain the phase change in the surround. A. Gaussian center-surround model. The phase of antagonistic Gaussian surround changes, and the antagonistic Gaussian surround becomes a synergistic surround under low scotopic conditions; B. Gaussian center-surround + outer surround model. The antagonistic Gaussian surround disappears under low scotopic conditions. $C(x,y,t)$: Gaussian center; $S(x,y,t)$: Gaussian surround; $OS(x,y,t)$: Outer (disinhibitory) surround; $g(x,y,t)$: ganglion cell responses.

latency of the center mechanism increases progressively with decreasing light levels, it is no surprise that the latency of surround mechanism increases as well (Enroth-Cugell & Lennie, 1975; Troy et al. 1993; Troy et al., 1999).

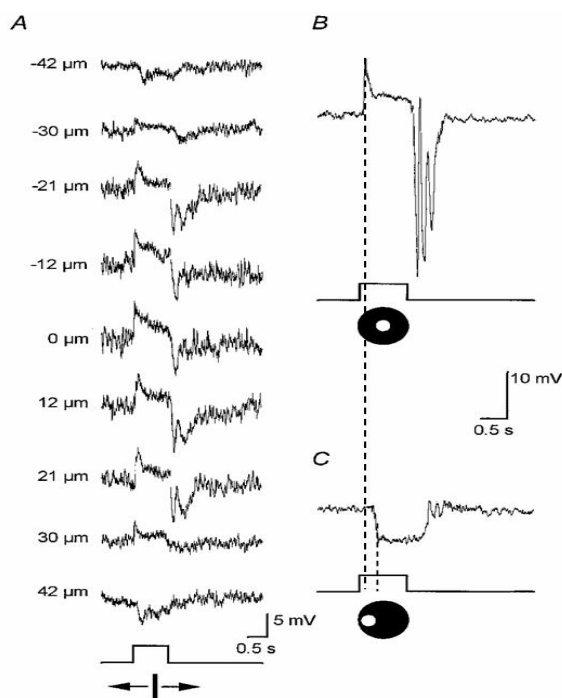


Figure 5-3: Receptive field center and surround responses of dark-adapted AII amacrine cells (modified from Bloomfield & Xin, 2000). Vertical dashed lines line up the beginning of center and surround responses. The time lag between the beginning of two mechanisms is about 200 ms (corresponds to 140 deg phase difference in our study).

Encouragingly, the temporal properties of AII cells seem appropriate to account for the changes in center-surround phase difference at low scotopic light levels. Fig. 5-3 (modified from Bloomfield & Xin, 2000) shows the responses of an AII cells to a 0.5-s rectangular slit of light at about 0.1 photoisomerization/rod/s in rabbits. The difference in the time to peak of the AII cell's on-center response and off-surround response are approximately of the

magnitude needed to account for the center-surround phase difference observed in our data at the corresponding light level ($-2 \log \text{cat td}$). This surround inhibition is thought to be generated by a type of wide-field diffuse amacrine cell, the A17 amacrine cell, through reciprocal, feedback synapses formed with rod bipolar cells in the inner plexiform layer (Sandell et al., 1987, Bloomfield et al., 2000).

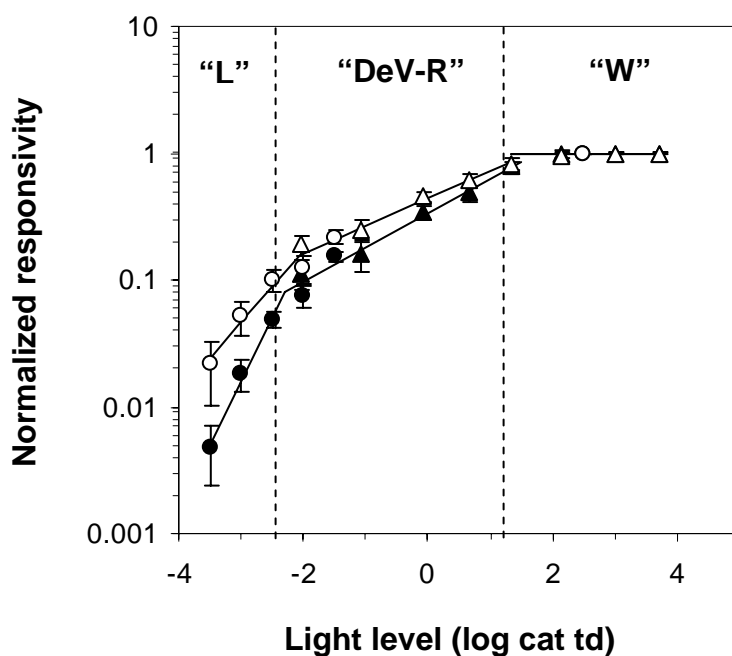


Figure 5-4: Comparison of responsivity with and without center expansion. Filled symbols are the responsivity we measured with gratings; Open symbols are the responsivity we predicted supposing that the center radius were constant. Triangles are previous data from the lab (Troy et al., 1993; Troy et al., 1999); Circles are new data. The dashed vertical lines demarcate the presumed linear, DeVries-Rose, and Weber's ranges.

5.3 Significance of changes in the receptive field center and surround under low scotopic conditions

What is the benefit of having a bigger center and a synergistic surround under low scotopic conditions? Expansion in center size helps to preserve contrast sensitivity and increase signal to noise ratio, albeit at the cost of spatial resolution, because the ganglion cell receives visual signals from larger summed areas. As shown in Fig. 5-3, the attenuation of responsivity is considerably less when account is taken of the expansion of center size under scotopic conditions, especially at the lowest light levels ($0.1 \sim 10^{-2.5}$ photons absorbed/rod/s). Coupling among AII/AII cells has been proposed to be integral to optimizing the signal-to-noise ratio of the AII network (Bloomfield et al., 1997; Bloomfield & Dacheux, 2001) as it allows correlated rod signals to be maintained while uncorrelated noise is decreased (Smith & Vardi, 1995; Vardi & Smith, 1996). An expanded receptive field center expands the 'correlation field' of neighboring ganglion cells. The correlated activity between ganglion cells could improve the brain's ability to discriminate a few absorbed external photons from the high background of spontaneous thermal isomerizations at low scotopic luminances.

A synergistic surround also helps to increase signal-to-noise ratio by providing an additional summing area to the center mechanism. Near dark light, each rod is expected to capture a photon once every 5 minutes. Under such conditions, capturing and making use of every photons is surely the key goal for the visual system. So employing both center and surround mechanisms to sum photons under low scotopic conditions seems potentially advantageous.

Our results are consistent with the optimal coding strategy proposed by Atick & Redlich (1990). In their model, they assumed that the goal of retinal processing is to reduce a ‘generalized redundancy’ subject to a constraint that specifies the amount of average information preserved and takes account of the limit imposed by noise. Under these assumptions, when the signal to noise ratio (S/N) is high, reducing spatial correlations assumes dominance and retinal processing seeks to reduce correlation redundancy. The optimal solution of the spatial filter obtained with high S/N (Fig. 5-4, A) has a small center (excitatory component) and an antagonistic, broader surround (inhibitory component), similar to the Gaussian kernels of X- and Y- ganglion cell receptive fields measured in our experiments under photopic conditions. However, when noise is comparable to the signal and has significant effect on reducing the information in transmitted signals the model leads to a compromise solution in which correlations are increased to reduce the impact of noise on information transmission. Under such circumstances, the model predicts that the size of the center should increase and the surround spread increase too as S/N is decreased (Fig. 5-4, B). This prediction corresponds to our observation that the center and surround radius expand at high scotopic levels. For large enough noise, more spatial correlation is introduced by reversing the inhibitory component into an excitatory component to increase signal to noise ratio (Fig. 5-4, C). Note that the extension of the excitatory component in panel C is similar to the extension of the inhibitory component in panel B. This is consistent with our result under low scotopic conditions.

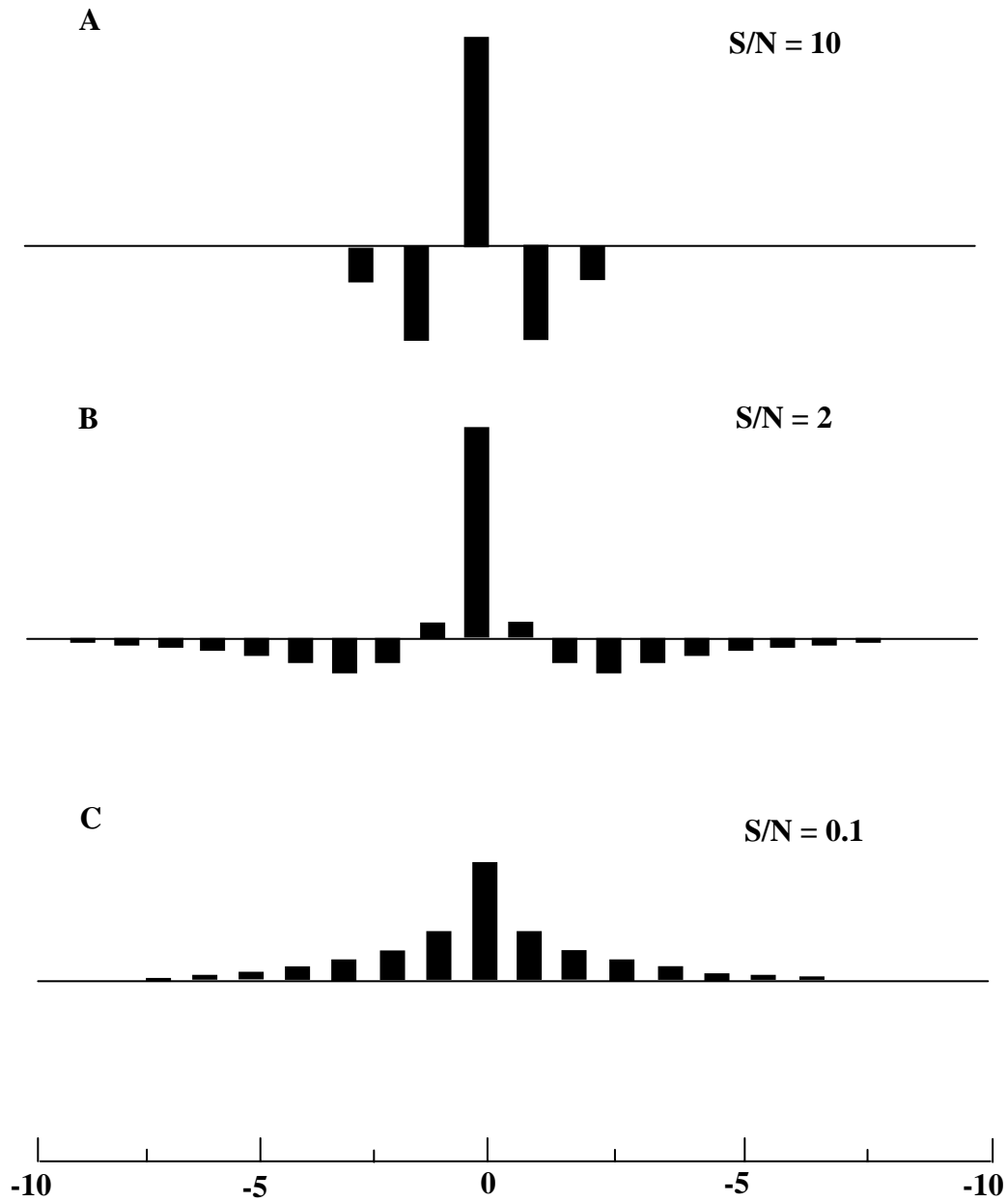


Figure 5-5: Optimal solution of Atick & Redlich's model at different values of S/N (modified from Atick & Redlich, 1990). S/N: signal to noise ratio. The black bars above horizontal lines represent excitatory component of responses; the black bars below horizontal lines represent inhibitory components of responses; Bottom axes indicates arbitrary units.

5.4 Retinal circuitry underlying scotopic vision

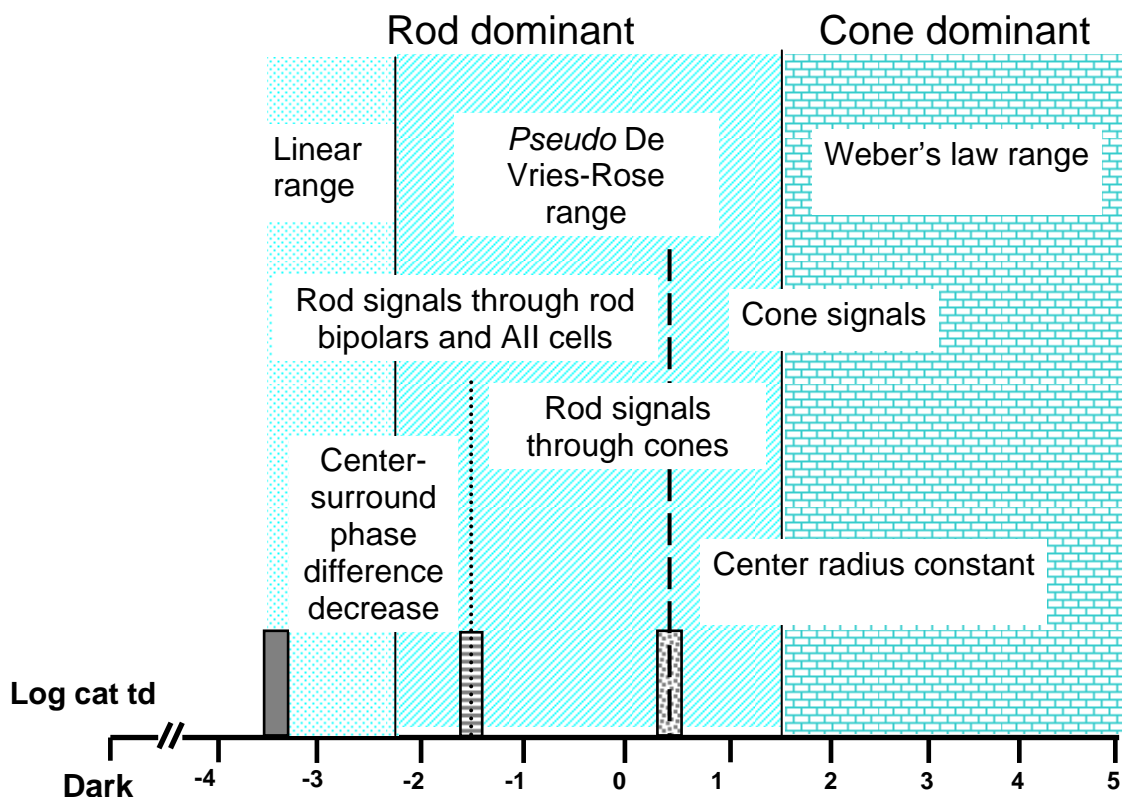


Figure 5-6: Summary of some of the major findings of this and earlier studies and the functional relevance of different light levels for the cat. The solid bar indicates the range of retinal illuminance corresponding to dark light. The range of illuminances above ~ 1.5 log cat td (bricked region) is considered the range over which X- and Y-cell responses are dominated by signals originating in cones. In the range below ~ 1.5 log cat td (hatched and dotted region), X- and Y-cells responses are presumed to be dominated by signals originated in rods. The bar labeled with horizontal stripes marks the light level where we believe the rod signals dominating a ganglion cell's response change from a retinal pathway through the rod bipolar only to one through both rod bipolar and the cone. The bar labeled with dots marks the light level where we believe the rod signals dominating a ganglion cell's response change from a retinal pathway through both rod bipolar and the cone to one through cone only.

Fig. 5-5 summarizes some of the major findings of this study and earlier studies, and relates these results to different functional circuits of the retina. In this figure, 0 log cat td is

equivalent to ~ 70 quanta (560 nm) absorbed/cone/s and ~ 10 quanta (507 nm) absorbed/rod/s (Troy et al., 1993) and the dark light bar is equivalent to 0.0063 ± 0.0036 (95% confidence range) quanta absorbed/rod/s (Troy et al., 1999). The transition from scotopic to photopic responses under our experimental protocol occurred at around 1.5 log cat td (Troy et al., 1999). The rod signals in cones reach semi-saturation at 1.2 ± 0.3 log cat td (Nelson, 1977). Hence, for the range of retinal illuminances above ~ 1.5 log cat td, one can consider retinal ganglion cell responses to be dominated by signals originating in cones and to follow Weber's law. In the range below ~ 1.5 log cat td ganglion cell responses are dominated by signals originating in rods. However the cone signals still contribute to ganglion cell responses in the range of illuminance from 0.5 to 1.5 log cat td (Völgyi et al., 2004).

It is known that there are two paths by which rod signals may reach ON-center ganglion cells in the mammalian retina (Ramón y Cajal, 1892; Steinberg, 1971; Kolb, 1977; Nelson, 1977; Kolb & Nelson, 1983; Nelson & Kolb, 1983; Smith et al., 1986; Sterling et al., 1988; Vaney et al., 1991; Wässle et al., 1995; Vaney, 1997; Völgyi et al., 2004). The first rod pathway, which is called the primary rod pathway, transmits rod signals through rod bipolars, AII amacrine cells and cone bipolars to the ganglion cell. The second rod pathway sends rod signals to ganglion cells through cone and cone bipolars. Recently, Völgyi et al. (2004) reported that ON-center ganglion cells may receive either segregated or convergent inputs from the two rod pathways in mammalian retina. They found there are groups of ON-center ganglion cells whose scotopic inputs derive only from the primary rod pathway and others than are driven from both primary and secondary rod pathways in mice retina. They also reported that the threshold of these two rod pathways are very different, being 0.02 and 0.3

Rh*/rod/s respectively. Although we have found no evidence of segregation of ganglion cells in this way in the vivo cat, these findings fit well with the idea that signals originating in rods reach ganglion cells predominantly through the primary rod pathway under low scotopic conditions ($I < -1.5 \log \text{ cat td}$) (Fig. 5-6), and that impact of the secondary rod pathway takes effect under high scotopic conditions ($-1.5 \log \text{ cat td} < I < 0.5 \log \text{ cat td}$) (Fig. 5-7). Finally under mesopic conditions ($0.5 \log \text{ cat td} < I < 1.5 \log \text{ cat td}$), the ganglion cells receive rod and cone signals from the secondary rod pathway and the cone pathway (Fig. 5-8).

As shown in Fig. 4-11 and Fig. 4-12, at $\sim 0.5 \log \text{ cat td}$ the phases of X- and Y- cell center and surround signals appeared, in parallel, to undergo a sudden change in lag. The dependence of center size on light level seems also to have a discontinuity at this light level (Fig. 4-3). These pieces of evidence indicate that the cone signals are replaced by rod signals and the rod-rod bipolar-AII pathway is activated at $\sim 0.5 \log \text{ cat td}$. It is thought that the surround inhibition through the primary rod pathway is generated by a type of wide-field diffuse amacrine cell, the A17 amacrine cells (corresponding to the S1 amacrine cells of rabbit), through reciprocal, feedback synapses formed with rod bipolar cells in the inner plexiform layer (Sandell et al., 1987, Bloomfield et al., 2000). The delay between center and surround evoked signals for the AII amacrine cell is $\sim 200 \text{ ms}$ (corresponding to 144 degree phase lag at 2 Hz) at an illuminance approximately $-2 \log \text{ cat td}$ in rabbit retina (Bloomfield et al., 2000). The surround inhibition through the secondary rod pathway is provided by the cone connected horizontal cells which should generate a similar center – surround phase difference as the cone pathway. Interestingly, the surround phase and phase difference between center and surround signals appeared to decrease dramatically at $\sim -1.5 \log \text{ cat td}$.

Considering that the delay of the A-type horizontal cell (which we believe provides the surround for the cone pathway) is ~ 120 ms (corresponding to an 85 degree phase lag at 2 Hz) at an illuminance of approximately $-2 \log$ cat td in rabbit retina (Bloomfield et al., 1992), the delay in the surround we measured at low light levels (e.g. 141 ± 14 and 132 ± 9 degree for X-

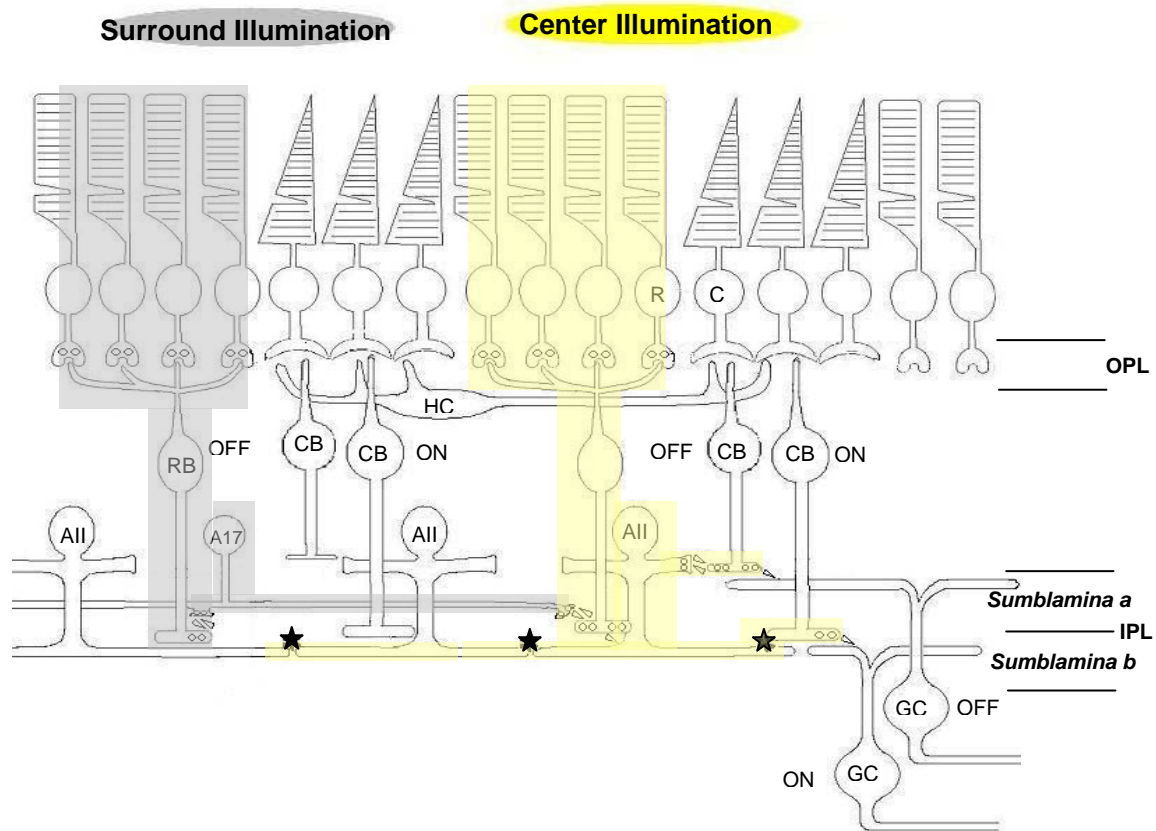


Figure 5-7: Retinal circuitries underlying scotopic vision (I). At low scotopic light levels, rod signals pass through the rod bipolar and AII amacrine to the ganglion cell. The surround is assumed to be provided by A17 amacrine cells. R: rod photoreceptor; C: cone; HC: horizontal cell; RB: rod bipolar; CB: cone bipolar; AII: AII amacrine cell; A17: A17 amacrine cell; GC: ganglion cell; OPL: outer plexiform layer; IPL: inner plexiform layer. Gap junctions between cells are indicated by stars. The presynaptic terminal at a chemical synapse contains schematic synaptic vesicles. Triangle arrows indicate the direction of signal transmission. Activated pathways are indicated by shaded area. The center pathways are shaded yellow and the surround pathways are shaded grey.

and Y-cells at $-2 \log \text{cat td}$) may have originated from sources other than horizontal cells.

We believe that these data lend support to the idea that the primary rod pathway dominates the signals that flow through the retina at light levels below $\sim -1.5 \log \text{cat td}$, and both rod pathways contribute to rod signals transmission within the range from $\sim -1.5 \log \text{cat td}$ to $\sim 0.5 \log \text{cat td}$.

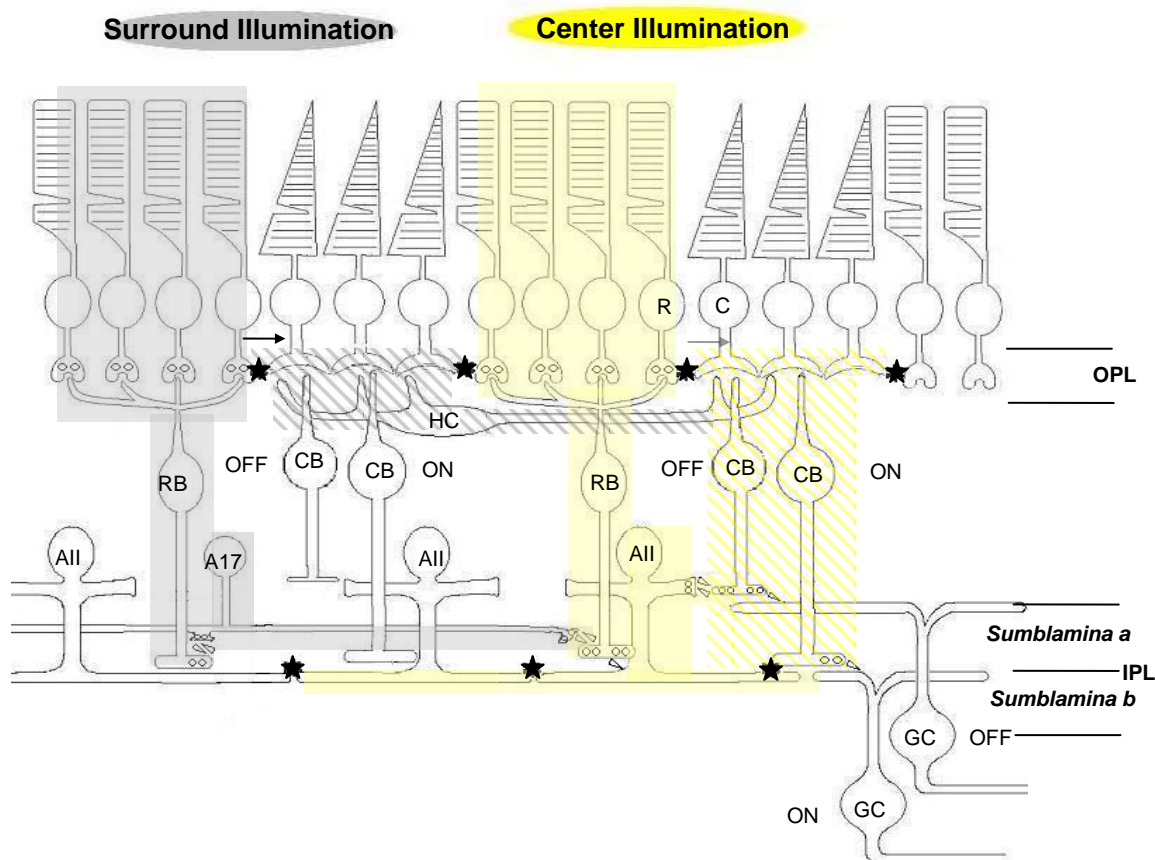


Figure 5-8: Retinal circuitries underlying scotopic vision (II). At high scotopic light levels, rod signals pass through two retinal pathways. One is through rod bipolar and the AII, the other is through rod-cone gap junctions and the cone bipolar. The surround is assumed to be provided by both A17 and horizontal cells. C: cone; HC: horizontal cell; RB: rod bipolar; CB: cone bipolar; AII: AII amacrine cell; A17: A17 amacrine cell; GC: ganglion cell; OPL: outer plexiform layer; IPL: inner plexiform layer. Gap junctions between cells are indicated by stars. The presynaptic terminal at a chemical synapse contains schematic synaptic vesicles. Triangle arrows indicate the direction of signal transmission. Activated pathways are indicated by shaded area. The center pathways are shaded yellow and the surround pathways are shaded grey. The rod pathways are shaded uniformly and the cone pathways are hatched shaded.

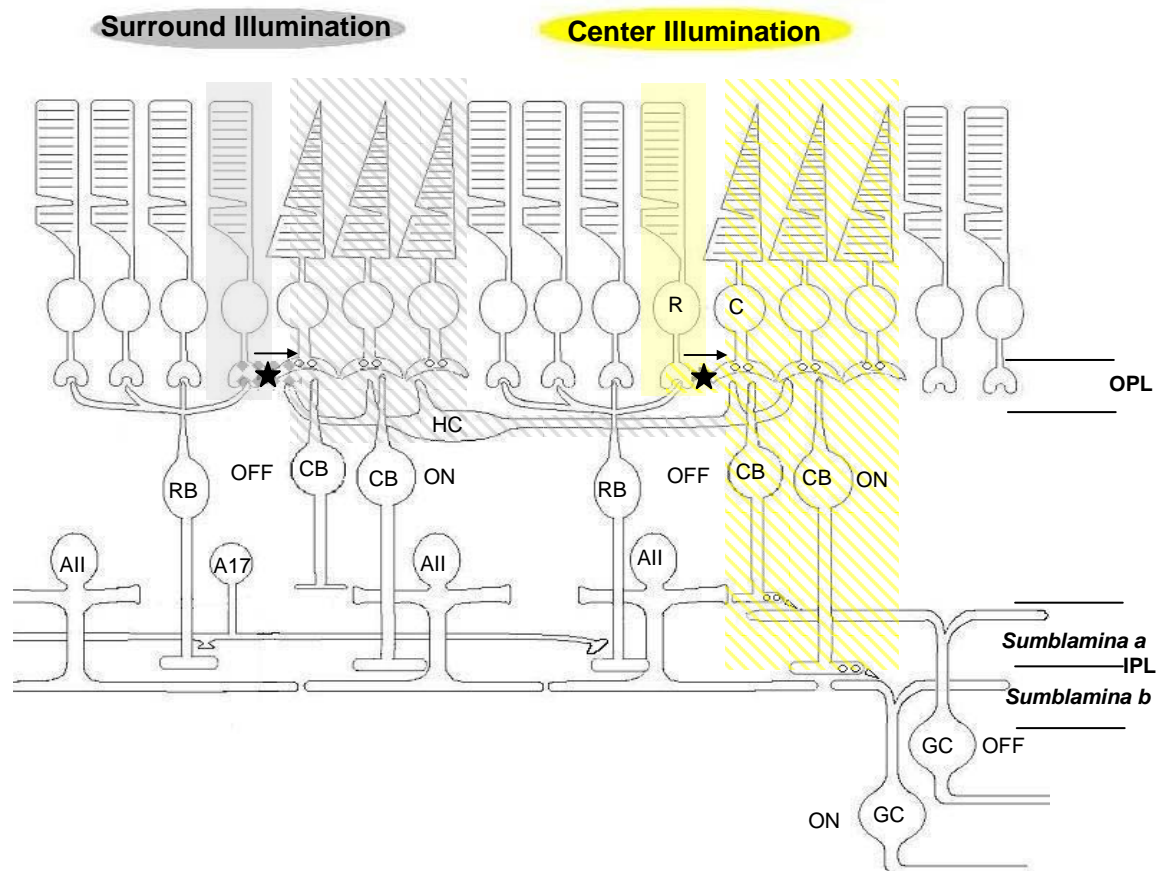


Figure 5-9: Retinal circuitries underlying scotopic vision (III). At mesopic light levels, rod signals pass through rod-cone gap junction and cone bipolar cells and cone signals pass through cone bipolar cells. The surround is assumed to be provided by the horizontal cells. C: cone; HC: horizontal cell; RB: rod bipolar; CB: cone bipolar; AII: AII amacrine cell; A17: A17 amacrine cell; GC: ganglion cell; OPL: outer plexiform layer; IPL: inner plexiform layer. Gap junctions between cells are indicated by asterisks. The presynaptic terminal at a chemical synapse contains schematic synaptic vesicles. Triangle arrows indicate the direction of signal transmission. Activated pathways are indicated by the shaded area. The center pathways are shaded yellow and the surround pathways are shaded grey. The rod pathways are shaded uniformly and the cone pathways are hatched shaded.

VI. REFERENCES

- Ahmed, B. (1981) The size and shape of rod and cone centres of cat retinal ganglion cells. *Experimental Brain Research* **43**: 422-428.
- Andrews, D.P. and Hammond, P. (1970) Suprathreshold spectral properties of single optic tract fibres in cat, under mesopic adaptation: cone-rod interaction. *J Physiol.* **209(1)**: 83-103.
- Archer, S. (1995) Molecular biology of visual pigments. In *"Neurobiology and Clinical Aspects of the Outer Retina"* (Eds. Djamgoz, M.B.A., Archer, S.N. and Vallergera, S.) Chapman & Hall, London, pp. 79-104.
- Atick, J.J. and Redlich, A.N. (1990) Towards a theory of early visual processing. *Neural Computation* **2**: 308-320.
- Atick, J.J. and Redlich, A.N. (1992) What does the retina know about natural scenes? *Neural Computation* **4(2)**: 196 – 210.
- Aubert, H. (1865) *Physiologie der Netzhaut*. Morgenstern, Breslau.
- Barlow, H.B., Fitzhugh R., Kuffler S.W. (1957) Dark adaptation, absolute threshold and Purkinje shift in single units of the cat's retina. *J Physiol.* **137(3)**: 327-37.
- Barlow, H.B. (1958) Temporal and spatial summation in human vision at different background. *J Physiol.* **141(2)**: 337-50.
- Barlow, H.B. and Levick, W.R. (1969) Changes in the maintained discharge with adaptation level in the cat retina. *J Physiol.* **202(3)**: 699-718.
- Barlow, H.B., Levick, W.R., Yoon, M. (1971) Responses to single quanta of light in retinal ganglion cells of the cat. *Vision Res.* **3**: 87-101.

- Barlow, H.B. and Levick, W.R. (1976) Threshold setting by the surround of cat retinal ganglion cells. *J Physiol.* **259(3)**: 737-57.
- Baylor DA, Matthews G, Yau KW. (1980) Two components of electrical dark noise in toad retinal rod outer segments. *J Physiol.* **309**: 591-621.
- Baylor, D.A., Hunn, B.J. and Schnapf, J.L. (1984) The photocurrent noise and spectral sensitivity of rods of the monkey *Macaca fascicularis*. *J Physiol.* **357**: 575-607.
- Blakemore, C.B. and Rushton, W.A. (1965a) Dark adaptation and increment threshold in a rod monochromat. *J Physiol.* **181(3)**: 612-28.
- Blakemore, C.B. and Rushton, W.A. (1965b) The rod increment threshold during dark adaptation in normal and rod monochromat. *J Physiol.* **181(3)**: 629-40.
- Bloomfield, S.A. and Xin, D. (2000) Surround inhibition of mammalian AII amacrine cells is generated in the proximal retina. *J Physiol.* **523(3)**: 771-83.
- Bloomfield, S.A. (1996) Effect of spike blockade on the receptive-field size of amacrine and ganglion cells in the rabbit retina. *J Neurophysiol.* **75(5)**: 1878-93.
- Bloomfield, S.A. (1992) A unique morphological subtype of horizontal cell in the rabbit retina with orientation-sensitive response properties. *J Comp Neurol.* **320**: 69-85.
- Bloomfield, S.A., Xin D., Osborne T. (1997) Light-induced modulation of coupling between AII amacrine cells in the rabbit retina. *Vis Neurosci.* **14(3)**:565-76.
- Bloomfield, S.A. and Dacheux, R.F. (2001) Rod vision: pathways and processing in the mammalian retina. *Prog Retin Eye Res.* **20(3)**: 351-84. Review.
- Bloomfield, S.A and Völgyi, B. (2004) Function and plasticity of homologous coupling between AII amacrine cells. *Vision Res.* **44(28)**: 3297-306.

- Bohnsack D.L., Diller L.C., Yeh T., Jenness J.W. and Troy J.B. (1997) Characteristics of the Sony Multiscan 17se Trinitron color graphic display. *Spat Vis.* **10(4)**: 345-51.
- Boycott, B.B. and Wässle, H. (1974) The morphological types of ganglion cells of the domestic cat's retina. *J Physiol.* **240(2)**: 397-419.
- Boycott, B.B. and Wässle, H. (1991) Morphological Classification of Bipolar Cells of the Primate Retina. *Eur J Neurosci.* **3(11)**: 1069-1088.
- Cajal, S. Ramón y. (1890) A quelle époque apparaissent les expansions des cellules nerveuses de la moëlle épinière du poulet? *Anat. Anz.* **5 (Nr. 21 and 22)**: 609-613, 631-639.
- Cajal, S. Ramón y. (1892) La rétine des vertébrés. *La Cellule* **9**: 121-133.
- Chan, L.H., Freeman, A.W., and Cleland, B.G. (1992) The rod-cone shift and its effect on ganglion cells in the cat's retina. *Vision Res.* **32(12)**: 2209-19.
- Cleland, B.G and Enroth-Cugell, C. (1968) Quantitative aspects of sensitivity and summation in the cat retina. *J Physiol.* **198(1)**: 17-38.
- Cleland, B.G and Enroth-Cugell, C. (1970) Quantitative aspects of gain and latency in the cat retina. *J Physiol.* **206(1)**: 73-91.
- Cleland, B.G. and Levick, W.R. (1974a) Brisk and sluggish concentrically organized ganglion cells in the cat's retina. *J Physiol.* **240(2)**: 421-56.
- Cleland, B.G. and Levick, W.R. (1974 b) Properties of rarely encountered types of ganglion cells in the cat's retina and an overall classification. *J Physiol.* **240(2)**: 457-92.
- Cleland, B.G., Levick, W.R., Sanderson, K.J. (1973) Properties of sustained and transient ganglion cells in the cat retina. *J Physiol.* **228(3)**: 649-80.
- Connaughton, V. P., and Nelson, R. (2000). Axonal stratification patterns and glutamate-gated conductance mechanisms in zebrafish retinal bipolar cells. *J Physiol.* **524**:135-146.

- Croner, L.J., Purpura, K., Kaplan, E. (1993) Response variability in retinal ganglion cells of primates. *Proc Natl Acad Sci U S A.* **90(17)**: 8128-30.
- Daitch, J.M and Green, D.G. (1969) Contrast sensitivity of the human peripheral retina. *Vision Res.* **9(8)**: 947-52.
- Daw, N.W and Ariel, M. (1981) Effect of synaptic transmitter drugs on receptive fields of rabbit retinal ganglion cells. *Vision Res.* **21(11)**: 1643-7.
- Derrington, A.M and Lennie, P. (1982) The influence of temporal frequency and adaptation level on receptive field organization of retinal ganglion cells in cat. *J Physiol.* **333**: 343-66.
- DeVries, S.H. and Schwartz, E.A. (1999) Kainate receptors mediate synaptic transmission between cones and 'Off' bipolar cells in a mammalian retina. *Nature.* **397(6715)**: 157-60.
- DeVries, S.H. (2000) Bipolar cells use kainate and AMPA receptors to filter visual information into separate channels. *Neuron.* **28(3)**: 847-56.
- Enroth-Cugell, C. and Robson, J.G. (1966) The contrast sensitivity of retinal ganglion cells of the cat. *J Physiol.* **187(3)**: 517-52.
- Enroth-Cugell, C. and Shapley, R.M. (1973a) Adaptation and dynamics of cat retinal ganglion cells. *J Physiol.* **233(2)**: 271-309.
- Enroth-Cugell, C. and Shapley, R.M. (1973b) Flux, not retinal illumination, is what cat retinal ganglion cells really care about. *J Physiol.* **233(2)**: 311-26.
- Enroth-Cugell, C. and Lennie, P. (1975) The control of retinal ganglion cell discharge by receptive field surrounds. *J Physiol.* **247(3)**: 551-78.
- Enroth-Cugell, C., Hertz, B.G., Lennie, P. (1977a) Cone signals in the cat's retina. *J Physiol.* **269(2)**: 273-96.

- Enroth-Cugell, C., Hertz, B.G., Lennie, P. (1977b) Convergence of rod and cone signals in the cat's retina. *J Physiol.* **269(2)**: 297-318.
- Enroth-Cugell, C., Robson, J.G., Schweitzer-Tong, D.E, Watson AB. 1983 Spatio-temporal interactions in cat retinal ganglion cells showing linear spatial summation. *J Physiol.* **341**: 279-307.
- Euler, T., Schneider, H., and Wässle, H. (1996). Glutamate responses of bipolar cells in a slice preparation of the rat retina. *J Neurosci.* **16**: 2934-44.
- Famiglietti, E.V. Jr. and Kolb, H. (1975) A bistratified amacrine cell and synaptic circuitry in the inner plexiform layer of the retina. *Brain Res.* **84(2)**: 293-300.
- Famiglietti, E.V. Jr. and Kolb, H. (1976) Structural basis for ON-and OFF-center responses in retinal ganglion cells. *Science.* **194(4261)**: 193-5.
- Field, G.D. & Rieke, F. (2002) Nonlinear signal transfer from mouse rods to bipolar cells and implications for visual sensitivity. *Neuron* **34**: 773-785.
- Flores-Herr, N., Protti, D.A., Wässle, H. (2001) Synaptic currents generating the inhibitory surround of ganglion cells in the mammalian retina. *J Neurosci.* **21(13)**: 4852-63.
- Frishman, L.J. and Linsenmeier, R.A. (1982) Effects of picrotoxin and strychnine on non-linear responses of Y-type cat retinal ganglion cells. *J Physiol.* **324**: 347-63.
- Frishman, L.J. and Levine, M.W. (1983) Statistics of the maintained discharge of cat retinal ganglion cells. *J Physiol.* **339**: 475-94.
- Frishman, L.J., Freeman, A.W., Troy, J.B., Schweitzer-Tong, D.E., Enroth-Cugell, C. (1987) Spatiotemporal frequency responses of cat retinal ganglion cells. *J Gen Physiol.* **89(4)**: 599-628.

- Fukuda, Y. and Stone, J. (1974) Retinal distribution and central projections of Y-, X-, and W-cells of the cat's retina. *J Neurophysiol.* **37(4)**: 749-72.
- Fukuda, Y., Hsiao, C.F., Watanabe, M., Ito, H. (1984) Morphological correlates of physiologically identified Y-, X-, and W-cells in cat retina. *J Neurophysiol.* **52(6)**: 999-1013.
- Hack, I., Peichl, L., Brandstatter, J.H. (1999). An alternative pathway for rod signals in the rodent retina: rod photoreceptors, cone bipolar cells, and the localization of glutamate receptors. *Proc Natl Acad Sci U S A.* **96(24)**: 14130-5.
- Hammond, P. (1974). Cat retinal ganglion cells: size and shape of receptive field centres. *J Physiol.* **242(1)**: 99-118.
- Hampson, E.C., Vaney, D.I., Weiler, R. (1992) Dopaminergic modulation of gap junction permeability between amacrine cells in mammalian retina. *J Neurosci.* **12(12)**: 4911-22.
- Harding, T.H and Enroth-Cugell, C. (1978) Absolute dark sensitivity and center size in cat retinal ganglion cells. *Brain Res.* **153(1)**: 157-62.
- Hargrave, P.A. and McDowell, J.H. (1992) Rhodopsin and phototransduction. *Internat Rev Cytol.* **137B**: 49-97. Review.
- Hartline, H.K. (1940) The receptive fields of optic nerve fibers. *Am. J. Physiol.* **130**: 690-699.
- Hecht, S., Schlaer, S., Pirenne, M. H. (1942) Energy, quanta and vision. *J. Gen. Physiol.* **25**: 819-840.
- Hochstein, S. and Shapley, R.M. (1976a) Quantitative analysis of retinal ganglion cell classifications. *J Physiol.* **262(2)**: 237-64.
- Hochstein, S. and Shapley, R.M. (1976b) Linear and nonlinear spatial subunits in Y cat retinal ganglion cells. *J Physiol.* **262(2)**: 265-84.

- Ikeda, H. and Wright, M.J. (1972) The outer disinhibitory surround of the retinal ganglion cell receptive field. *J Physiol.* **226(2)**: 511-44.
- Kaneko, A. (1971) Electrical connexions between horizontal cells in the dogfish retina. *J Physiol.* **213(1)**: 95-105.
- Kaplan, E., Marcus, S., So, Y.T. (1979) Effects of dark adaptation on spatial and temporal properties of receptive fields in cat lateral geniculate nucleus. *J Physiol.* **294**: 561-80.
- Kirby, A.W. and Schweitzer-Tong, D.E. (1981) Gaba-antagonists alter spatial summation in receptive field centres of rod- but not cone-drive cat retinal ganglion Y-cells. *J Physiol.* **320**: 303-308.
- Kolb, H. and Famiglietti, E.V. (1974) Rod and cone pathways in the inner plexiform layer of cat retina. *Science.* **186(4158)**: 47-9.
- Kolb, H. (1977) The organization of the outer plexiform layer in the retina of the cat: electron microscopic observations. *J Neurocytol.* **6(2)**: 131-53.
- Kolb, H. (1979) The inner plexiform layer in the retina of the cat: electron microscopic observations. *J Neurocytol.* **8(3)**: 295-329.
- Kolb, H., Nelson, R., Mariani, A. (1981) Amacrine cells, bipolar cells and ganglion cells of the cat retina: a Golgi study. *Vision Res.* **21(7)**: 1081-1114.
- Kolb, H. and Nelson, R. (1983) Rod pathways in the retina of the cat. *Vision Res.* **23(4)**: 301-12.
- Kolb, H., Cuenca, N., Wang, H.H., Dekorver, L. (1990) The synaptic organization of the dopaminergic amacrine cell in the cat retina. *J Neurocytol.* **19(3)**: 343-66.
- Kolb, H., Linberg, K.A., Fisher, S.K.(1992) Neurons of the human retina: a Golgi study. *Journal of Comparative Neurology.* **318(2)**: 147-87.

- Kuffler, S.W. (1952) Neurons in the retina; organization, inhibition and excitation problems. *Cold Spring Harb Symp Quant Biol.* **17**: 281-92.
- Kuffler, S.W. (1953) Discharge patterns and functional organization of mammalian retina. *J Neurophysiol.* **16(1)**: 37-68.
- Kuffler, S.W., FITZHUGH, R., BARLOW, H.B. (1957) Maintained activity in the cat's retina in light and darkness. *J Gen Physiol.* **40(5)**: 683-702.
- Levick, W.R. (1972) Another tungsten microelectrode. *Med Biol Eng.* **10(4)**: 510-5.
- Levick, W.R. and Thibos, L.N. (1983) Analysis of orientation bias in cat retina. *J Physiol.* **329**: 243-61.
- Li, C.Y., Pei, X., Zhou, Y.X., von-Mitzlaff, H.C. (1991) Role of the extensive area outside the X-cell receptive field in brightness information transmission. *Vision Res.* **31(9)**: 1529-40.
- Li, C.Y., Zhou, Y.X., Pei, X., Qiu, F.T., Tang, C.Q., Xu, X.Z. (1992) Extensive disinhibitory region beyond the classical receptive field of cat retinal ganglion cells. *Vision Res.* **32(2)**: 219-28.
- Li, W., Keung, J.W., Massey, S.C. (2004) Direct synaptic connections between rods and OFF cone bipolar cells in the rabbit retina. *J Comp Neurol.* **474(1)**: 1-12.
- Linsenmeier, RA, Frishman, L.J., Jakiela, H.G., Enroth-Cugell, C. (1982) Receptive field properties of x and y cells in the cat retina derived from contrast sensitivity measurements. *Vision Res.* **22(9)**: 1173-83.
- Maffei, L., Fiorentini, A., Cervetto, L. (1971) Homeostasis in retinal receptive fields. *J Neurophysiol.* **34(4)**: 579-87.

- Mariani, A.P (1984) The neuronal organization of the outer plexiform layer of the primate retina. *Int Rev Cytol.* **86**: 285-320. Review.
- Mariani, A.P. (1985) Multiaxonal horizontal cells in the retina of the tree shrew, *Tupaia glis*. *J Comp Neurol.* **233(4)**: 553-63.
- Mariani, A.P. (1990) Amacrine cells of the rhesus monkey retina. *J Comp Neurol.* **301(3)**: 382-400.
- Masu, M., Iwakabe, H., Tagawa, Y., Miyoshi, T., Yamashita, M., Fukuda, Y., Sasaki, H., Hiroi, K., Nakamura, Y., Shigemoto, R., Takada, M., Nakamura, K., Nakao, K., Katsuki, M. & Nakanishi, S. (1995) Specific deficit of the ON response in visual transmission by targeted disruption of the mGluR6 gene. *Cell* **80**: 757-765.
- McMahon, M.J., Packer, O.S., Dacey, D.M. (2004) The classical receptive field surround of primate parasol ganglion cells is mediated primarily by a non-GABAergic pathway. *J neurosci.* **24(15)**: 3736-3745.
- Mills, S.L. and Massey, S.C. (1991) Labeling and distribution of AII amacrine cells in the rabbit retina. *J Comp Neurol.* **304(3)**: 491-501.
- Mills, S.L. and Massey, S.C. (1994) Distribution and coverage of A- and B-type horizontal cells stained with Neurobiotin in the rabbit retina. *Vis Neurosci.* **11(3)**: 549-60.
- Mills, S.L. and Massey, S.C. (1995) Differential properties of two gap junctional pathways made by AII amacrine cells. *Nature.* **377(6551)**: 734-7.
- Mills, S.L. and Massey, S.C. (1999) AII amacrine cells limit scotopic acuity in central macaque retina: A confocal analysis of calretinin labeling. *J Comp Neurol.* **411(1)**: 19-34.
- Mills, S.L., O'Brien, J.J., Li, W., O'Brien, J., Massey, S.C. (2001) Rod pathways in the mammalian retina use connexin 36. *J Comp Neurol.* **436(3)**: 336-50.

- Muller, J.F and Dacheux, R.F. (1997) Alpha ganglion cells of the rabbit retina lose antagonistic surround responses under dark adaptation. *Vis Neurosci.* **14(2)**: 395-401.
- Nawy, S. (1999). The metabotropic receptor mGluR6 may signal through G(o), but not phosphodiesterase, in retinal bipolar cells. *J Neurosci*, **19**: 2938-44.
- Nelson, R. and Kolb, H. (1983). Synaptic patterns and response properties of bipolar and ganglion cells in the cat retina. *Vision Res.* **23(10)**: 1183-95.
- Nelson, R. and Kolb, H. (1985) A17: a broad-field amacrine cell in the rod system of the cat retina. *J Neurophysiol.* **54(3)**: 592-614.
- Nelson, R. (1977) Cat cones have rod input: a comparison of the response properties of cones and horizontal cell bodies in the retina of the cat. *J Comp Neurol.* **172(1)**: 109-35.
- Nelson, R., Famiglietti, E.V. Jr., Kolb, H. (1978) Intracellular staining reveals different levels of stratification for on- and off-center ganglion cells in cat retina. *J Neurophysiol.* **41(2)**: 472-83.
- Passaglia, C.L. and Troy, J.B. (2004) Impact of noise on retinal coding of visual signals. *J Neurophysiol.* **92(2)**: 1023-33.
- Pasternak, T. and Merigan, W.H. (1981) The luminance dependence of spatial vision in the cat. *Vision Res.* **21(9)**: 1333-9.
- Peichl, L. and Wässle, H. (1983) The structural correlate of the receptive field centre of alpha ganglion cells in the cat retina. *J Physiol.* **341**: 309-24.
- Pettigrew, J.D., Cooper, M.L., Blasdel, G.G. (1979) Improved use of tapetal reflection for eye-position monitoring. *Invest Ophthalmol Vis Sci.* **18(5)**: 490-5.

- Raviola, E. and Gilula, N.B. (1973) Gap junctions between photoreceptor cells in the vertebrate retina. *Proc Natl Acad Sci U S A.* **70(6)**: 1677-81.
- Rodieck, R.W. (1965) Quantitative analysis of cat retinal ganglion cell response to visual stimuli. *Vision Res.* **5(11)**: 583-601.
- Rodieck, R.W. and Stone, J. (1965) Analysis of receptive fields of cat retinal ganglion cells. *J Neurophysiol.* **28(5)**: 833-49.
- Rodieck, R.W. (1967) Maintained activity of cat retinal ganglion cells. *J Neurophysiol.* **30(5)**: 1043-71.
- Rose, A. (1948) The sensitivity performance of the human eye on an absolute scale. *J Opt Soc Amer.* **38**: 196-208.
- Roska, B., Nemeth, E., Orzo, L., Werblin, F.S. (2000) Three levels of lateral inhibition: A space-time study of the retina of the tiger salamander. *J Neurosci.* **20(5)**: 1941-51.
- Sandell, J.H., Masland, R.H., Raviola, E. and Dacheux, R.F. (1989) Connections of indoleamine-accumulating cells in the rabbit retina. *J. Comp. Neurol.* **283**: 303-313.
- Schneeweis, D.M and Schnapf, J.L. (1995) Photovoltage of rods and cones in the macaque retina. *Science.* **268(5213)**: 1053-6.
- Schwartz EA. (1973) Organization of on-off cells in the retina of the turtle. *J Physiol.* **230(1)**:1-14.
- Shapley, R., Enroth-Cugell, C., Bonds, A.B., Kirby, A. (1972) Gain control in the retina and retinal dynamics. *Nature.* **236(5346)**: 352-3.
- Shapley, R.M. and Enroth-Cugell, C. (1984) Visual adaptation and retinal gain controls. *Progress in Retinal Research.* **3**: 263-346.

- Slaughter, M.M and Miller, R.F. (1983) Bipolar cells in the mudpuppy retina use an excitatory amino acid neurotransmitter. *Nature*. **303(5917)**: 537-8.
- Smith, R.G., Freed, M.A., Sterling, P. (1986) Microcircuitry of the dark-adapted cat retina: functional architecture of the rod-cone network. *J Neurosci*. **6(12)**: 3505-17.
- Smith, R.G. and Vardi, N. (1995) Simulation of the AII amacrine cell of mammalian retina: functional consequences of electrical coupling and regenerative membrane properties. *Vis Neurosci*. **12(5)**: 851-60.
- Srinivasan, M.V., Laughlin, S.B., Dubs, A. (1982) Predictive coding: a fresh view of inhibition in the retina. *Proc R Soc Lond B Biol Sci*. **216(1205)**: 427-59.
- Steinberg, R.H. (1971) Incremental responses to light recorded from pigment epithelial cells and horizontal cells of the cat retina. *J Physiol*. **217(1)**: 93-110.
- Sterling, P. (1983) Microcircuitry of the cat retina. *Annu Rev Neurosci*. **6**:149-85.
- Sterling, P., Freed, M.A., Smith, R.G. (1988) Architecture of rod and cone circuits to the on-beta ganglion cell. *J Neurosci*. **8(2)**: 623-42.
- Stone, J. and Fukuda, Y. (1974) Properties of cat retinal ganglion cells: A comparison of W-cells with X- and Y-cell. *J Neurophysiol*. **37(4)**: 722-48.
- Strettoi et al., 1990 Synaptic connections of rod bipolar cells in the inner plexiform layer of the rabbit retina. *J Comp Neurol*. **295(3)**: 449-66.
- Strettoi, E., Dacheux, R.F., Raviola, E. (1992) Synaptic connections of rod bipolar cells in the inner plexiform layer of the rabbit retina. *J Comp Neurol*. **295(3)**: 449-66.
- Strettoi, E., Dacheux, R.F., Raviola, E. (1994) Cone bipolar cells as interneurons in the rod pathway of the rabbit retina. *J Comp Neurol*. **347(1)**: 139-49.
- Svaetichin, G. (1953) The cone action potential. *Acta Physiol. Scand*. **29**: 565-599.

- Svaetichin, G. and Macnichol, E.F. JR. (1958) Retinal mechanisms for chromatic and achromatic vision, *Ann. New York Acad. Sc.*, **74**: 385.
- Taylor, W.R. (1999) TTX attenuates surround inhibition in rabbit retinal ganglion cells. *Vis Neurosci.* **16(2)**: 285-90.
- Teranishi T, Negishi K, Kato S. (1983) Dopamine modulates S-potential amplitude and dye-coupling between external horizontal cells in carp retina. *Nature* **301(5897)**:243-6.
- Troy, J.B. and Lennie, P. (1987) Detection latencies of X and Y type cells of the cat's dorsal lateral geniculate nucleus. *Exp Brain Res.* **65(3)**: 703-6.
- Troy, J.B. and Robson, J.G. (1992) Steady discharges of X and Y retinal ganglion cells of cat under photopic illuminance. *Vis Neurosci.* **9(6)**: 535-53.
- Troy, J.B. and Enroth-Cugell, C. (1993) X and Y ganglion cells inform the cat's brain about contrast in the retinal image. *Exp Brain Res.* **93(3)**: 383-90.
- Troy, J.B., Oh, J.K., Enroth-Cugell, C. (1993) Effect of ambient illumination on the spatial properties of the center and surround of Y-cell receptive fields. *Vis Neurosci.* **10(4)**: 753-64.
- Troy, J.B. and Lee, B.B. (1994) Steady discharges of macaque retinal ganglion cells. *Vis Neurosci.* **11(1)**: 111-8.
- Troy, J.B., Bohnsack, D.L., Diller, L.C. (1999) Spatial properties of the cat X-cell receptive field as a function of mean light level. *Vis Neurosci.* **16(6)**: 1089-104.
- Troy, J.B. and Shou, T. (2002) The receptive fields of cat retinal ganglion cells in physiological and pathological states: where we are after half a century of research. *Prog Retin Eye Res.* **21(3)**: 263-302.

- Vaney, D.I. (1985) The morphology and topographic distribution of AII amacrine cells in the cat retina. *Proc R Soc Lond B Biol Sci.* **224(1237)**: 475-88.
- Vaney, D.I., Gynther, I.C., Young, H.M. (1991) Rod-signal interneurons in the rabbit retina: 2. AII amacrine cells. *J Comp Neurol.* **310(2)**: 154-69.
- Vaney, D.I. (1991) Many diverse types of retinal neurons show tracer coupling when injected with biocytin or Neurobiotin. *Neurosci Lett.* **125(2)**: 187-90.
- Vaney, D.I. (1997) Neuronal coupling in rod-signal pathways of the retina. *Invest Ophthalmol Vis Sci.* **38(2)**: 267-73. Review.
- Vardi, N. and Smith, R.G. (1996) The AII amacrine network: coupling can increase correlated activity. *Vision Res.* **36(23)**: 3743-57.
- Voigt, T. and Wässle, H. (1987) Dopaminergic innervation of A II amacrine cells in mammalian retina. *J Neurosci.* **7(12)**: 4115-28.
- Völgyi, B., Xin, D., Bloomfield, S.A. (2002) Feedback inhibition in the inner plexiform layer underlies the surround-mediated responses of AII amacrine cells in the mammalian retina. *J Physiol.* **539(Pt 2)**: 603-14.
- Völgyi, B., Deans, M.R., Paul, D.L., Bloomfield, S.A. (2004) Convergence and segregation of the multiple rod pathways in mammalian retina. *J Neurosci.* **24(49)**: 11182-92.
- Wässle, H., Peichl, L., Boycott, B.B.(1981a) Morphology and topography of on- and off-alpha cells in the cat retina. *Proc R Soc Lond B Biol Sci.* **212(1187)**: 157-75.
- Wässle, H., Boycott, B.B., Illing, R.B. (1981b) Morphology and mosaic of on- and off-beta cells in the cat retina and some functional considerations. *Proc R Soc Lond B Biol Sci.* **212(1187)**: 177-95.

- Wässle, H., Grunert, U., Rohrenbeck, J. (1993) Immunocytochemical staining of AII-amacrine cells in the rat retina with antibodies against parvalbumin. *J Comp Neurol.* **332(4)**:407-20.
- Wässle, H., Grunert, U., Chun, M.H., Boycott, B.B. (1995) The rod pathway of the macaque monkey retina: identification of AII-amacrine cells with antibodies against calretinin. *J Comp Neurol.* **361(3)**: 537-51.
- Werblin, F.S. and Dowling, J.E. (1969) Organization of the retina of the mudpuppy, *Necturus maculosus*. II. Intracellular recording. *J Neurophysiol.* **32(3)**: 339-55.
- Werblin, F.S. (1991) Synaptic connections, receptive fields, and patterns of activity in the tiger salamander retina. *Invest. Ophthalm. Vis. Sci.* **32**, 459-483.
- Witkovsky, P. and Deary, A. (1992) Functional roles of dopamine in the vertebrate retina. In: *Progress in retinal research (Osborne NN, Chader GJ, eds)*, pp 247-292. Oxford: Pergamon.
- Wu, S. M., Gao, F., and Maple, B. R. (2000). Functional architecture of synapses in the inner retina: segregation of visual signals by stratification of bipolar cell axon terminals. *J Neurosci.* **20**: 4462-70.
- Xin, D. and Bloomfield, S.A. (1999) Comparison of the responses of AII amacrine cells in the dark- and light-adapted rabbit retina. *Vis Neurosci.* **16(4)**: 653-65.
- Yoon, M. (1972) Influence of adaptation level on response pattern and sensitivity of ganglion cells in the cat's retina. *J Physiol.* **221**: 537-551.